Nano-Micro Letters

ISSN 2311-6706
e-ISSN 2150-5551
CN 31-2103/TB

REVIEW

https://doi.org/10.1007/s40820-020-0407-5

Cite as
Nano-Micro Lett.
(2020) 12:71

Received: 3 December 2019
Accepted: 2 February 2020

Gas Sensors Based on Chemi-Resistive Hybrid Functional Nanomaterials

Yingying Jian[1], Wenwen Hu[2], Zhenhuan Zhao[1], Pengfei Cheng[2], Hossam Haick[1,3] ✉, Mingshui Yao[4] ✉, Weiwei Wu[1] ✉

Yingying Jian and Wenwen Hu contributed equally to this review.

✉ Hossam Haick, hhossam@technion.ac.il; Mingshui Yao, mingshuiyao@gmail.com; Weiwei Wu, wwwu@xidian.edu.cn

[1] School of Advanced Materials and Nanotechnology, Interdisciplinary Research Center of Smart Sensors, Xidian University, Xi'an 710071, People's Republic of China

[2] School of Aerospace Science and Technology, Xidian University, Xi'an 710071, People's Republic of China

[3] Department of Chemical Engineering, Russell Berrie Nanotechnology Institute, Technion-Israel Institute of Technology, 3200003 Haifa, Israel

[4] Institute for Integrated Cell-Material Sciences (WPI-iCeMS), Kyoto University Institute for Advanced Study, Kyoto University, Yoshida Ushinomiya-cho, Sakyo-ku, Kyoto 606-8501, Japan

HIGHLIGHTS

- This review gives a thinking based on the generic mechanisms rather than simply dividing them as different types of combination of materials, which is unique and valuable for understanding and developing the novel hybrid materials in the future.
- The hybrid materials, their sensing mechanism, and their applications are systematically reviewed. Critical thinking and ideas regarding the orientation of the development of hybrid material-based gas sensor in the future are also discussed.

ABSTRACT Chemi-resistive sensors based on hybrid functional materials are promising candidates for gas sensing with high responsivity, good selectivity, fast response/recovery, great stability/repeatability, room-working temperature, low cost, and easy-to-fabricate, for versatile applications. This progress report reviews the advantages and advances of these sensing structures compared with the single constituent, according to five main sensing forms: manipulating/constructing heterojunctions, catalytic reaction, charge transfer, charge carrier transport, molecular binding/sieving, and their combinations. Promises and challenges of the advances of each form are presented and discussed. Critical thinking and ideas regarding the orientation of the development of hybrid material-based gas sensor in the future are discussed.

KEYWORDS Gas sensor; Hybrid; Chemi-resistor; Functional nanomaterials

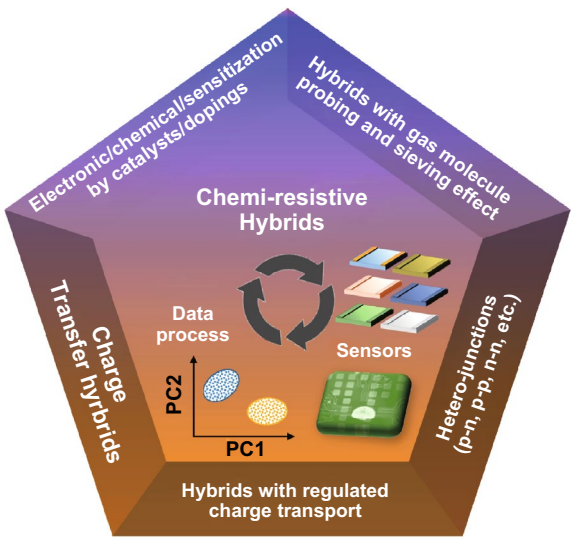

Published online: 11 March 2020

1 Introduction

Monitoring and recording chemical stimulus or variations in the environment are increasingly important in future production and daily life of human health [1]. Achieving this goal relies on the availability of high-performance sensor units that are capable of detecting gas analytes, such as volatile/semi-volatile organic compounds (VOCs/SVOCs) highly rich regarding critical information for the detection, monitoring and closed-loop control in many fields, including medicine, food industry, environmental monitoring, public security, and agricultural production [2, 3].

An ideal gas sensor requires high responsivity, good selectivity, fast response/recovery, great stability/repeatability, room-working temperature, low cost, and easy-to-fabricate for practical applications [4–6]. To meet those requirements, many types of gas sensors with different transduction forms, e.g., chemi-resistor, field-effect transistor (FET), solid-state electrochemical sensor (SSES), quartz-crystal microbalance (QCM), gas capacitor, surface acoustic wave (SAW), have been well studied and developed. Among them, since the 1960s [7], a chemi-resistor that contains an active sensing layer bridging a pair of electrodes became a promising candidate due to its advantages [4–6, 8–12] including easy-to-fabricate, use of very small quantity (milligram level) active materials, wide adoption of sensitive materials, and simple sensing data, which ensure its success in certain commercialization opportunities [13–15]. However, it is rare to find chemi-resistors that can meet these specific requirements.

An emerging approach in chemi-resistors to meet these needs relies on hybrid materials, viz. materials that integrate 2+ single constituents at the nanometer or molecular level [16–36], to achieve new and/or enhanced sensing properties. In this progress report, we review the advances of the hybrid material-based gas sensors concisely and comprehensively. The hybrid materials-based chemi-resistive gas sensors are distinguished, understood, and introduced based on the generic mechanisms rather than simply dividing them as different types of combination of materials. Then, the report, in detail, focuses on the research and development (R&D) aspects of hybrid gas sensors, while presenting and discussing the sensing performances of different types of hybrid materials, and associated enhanced sensing mechanisms. Promises and challenges toward the future development of each elements are deeply thought and discussed. Critical thinking and ideas regarding the orientation of the development of hybrid material-based gas sensor in the future are also discussed.

2 The Need for Hybrid Functional Nanomaterials for Sensing Applications

Chemi-resistors for gas sensing include three main processes: diffusion/molecule capture unit, surface reaction unit (including charge transfer), and charge carrier transport unit (Fig. 1a) [37]. To date, most of these sensors and/or sensor arrays utilize sensing elements that are based on single material or transduction mechanism, of which intrinsic sensing activity or additional thermal/photonic energy are usually employed as the driving force to stimulate the sensing effects of target gases (Fig. 1b). The hindrances are unavoidable at several levels: (i) not satisfying long-term stability and sensitivity of organic chemi-resistors due to the high affinity of conductive polymers (CP), such as polyaniline (PANI), polypyrrole (PPy), and polythiophene (PTh), toward volatile organic compounds (VOCs) and humidity existed in the atmosphere; (ii) high operating temperatures (usually > 200 °C), baseline drift, limited selectivity, and oxidation/decomposition of VOCs in the case of inorganic materials (especially metal oxide materials, e.g., ZnO, SnO, TiO_2, SnO_2)-based chemi-resistor. A reliable solution for these drawbacks is the design and utilization of new gas sensitive materials based on hybrid inorganic–inorganic [8], organic–organic [12], and inorganic–organic materials [8, 9, 12, 16–36].

Using hybrid materials as sensitive transducer offers several obvious advantages, compared with the single constituent. First, the inexhaustible abundance of hybrid materials (in both the complex constituents and novel nanostructures) makes it possible to involve an almost infinite continuum of variable factors (surface-dependent factor, interface-dependent factor, and structure-dependent factor) to generate new sensing behaviors (Fig. 1c) [38–49]. Second, with hybrid material, more chemical/physical processes with different enhanced mechanisms could be introduced to precisely design, regulate, and enhance the sensing performance mainly through catalytic reaction with analyte [50–58], charge transfer [59–63], charge carrier transport [64–66] manipulation/construction of heterojunctions [39,

https://doi.org/10.1007/s40820-020-0407-5

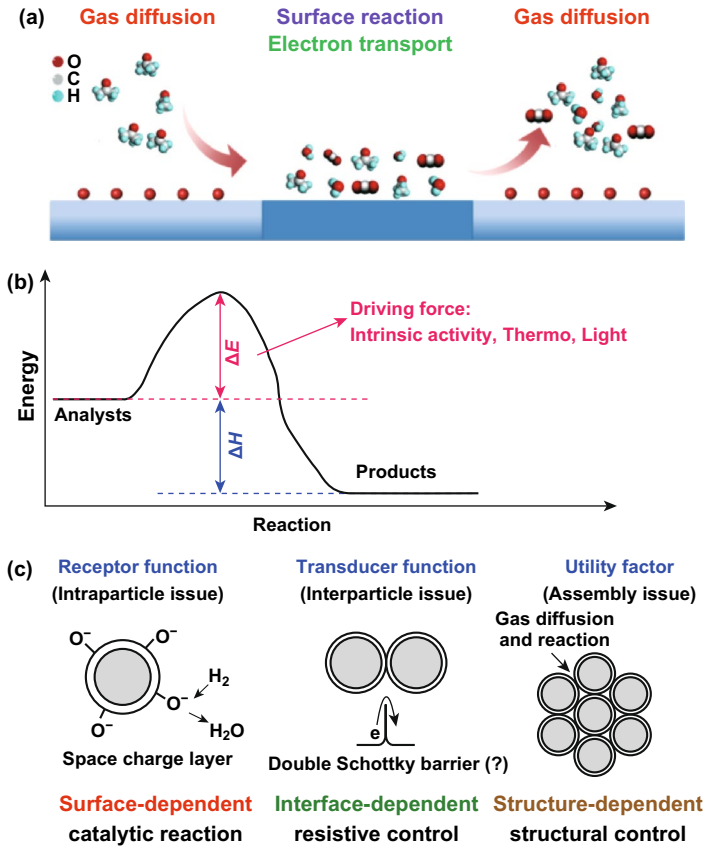

Fig. 1 Schematic illustration of **a** three gas-sensing units and **b** sensing reactions. **c** The enhanced gas-sensing mechanisms for hybrid chemi-resistive nanomaterials. The upper part of **c** was modified from reference. Reproduced with permission [38]. Copyright 2009, Elsevier

67], molecular binding/sieving [68–73], and their combinations [74–77].

3 Hybrid Chemi-Resistive Gas Sensors

Hybrid materials can perform improved sensing characteristics via one or a combination from five typical hybridizing forms which are categorized into three sensing-dependent factors (Fig. 2a). The first combination relies on catalysis reactions (normally noble metal catalysts, e.g., Pt [78], Pd [79], Au [50], and Ag [51]) between analyte gas and decorated catalysts on host semi-conductive materials (categorized as surface-dependent factor). The second relies on a fast charge transfer process, viz carrier withdrawal or donation, electron acceptor or acceptor between guest additives and the host material (e.g., carbon nanotubes (CNTs)), reduced graphene oxide (rGO) (categorized as interface-dependent factor) [63]. The third relies on regulating the charge carrier transport in a conductive/semi-conductive materials (e.g., single-wall carbon nanotube (SWCNT)-metallo-supramolecular polymer (MSP), gold nanoparticles (GNPs)-thiols, *N*,*N*'-diphenyl perylene tetracarboxylic diimide (PTCDI-Ph)/para-sexiphenyl (p-6P)) upon exposure to gas analytes (categorized as interface- and structure-dependent factor) [66, 80, 81]. The fourth relies on manipulation/construction of the heterojunctions such as n–n, p–n, p–p, p–n–p heterogeneous semi-conductive materials (categorized as interface-dependent factor) [39]. The last one relies on semiconductors coated by gas molecular sieving/binding layers or ligands/complexes for selective gas detection (categorized as surface- and structure-dependent factor) [72, 76, 82]. In the following section, we provide more details on each of these combinations. It should be noted that, according to the understanding of authors on chemi-resistors (1. measuring the resistors directly; 2. measuring the current when the device is applied a constant bias voltage; 3. measuring the partial voltage on the device in parallel

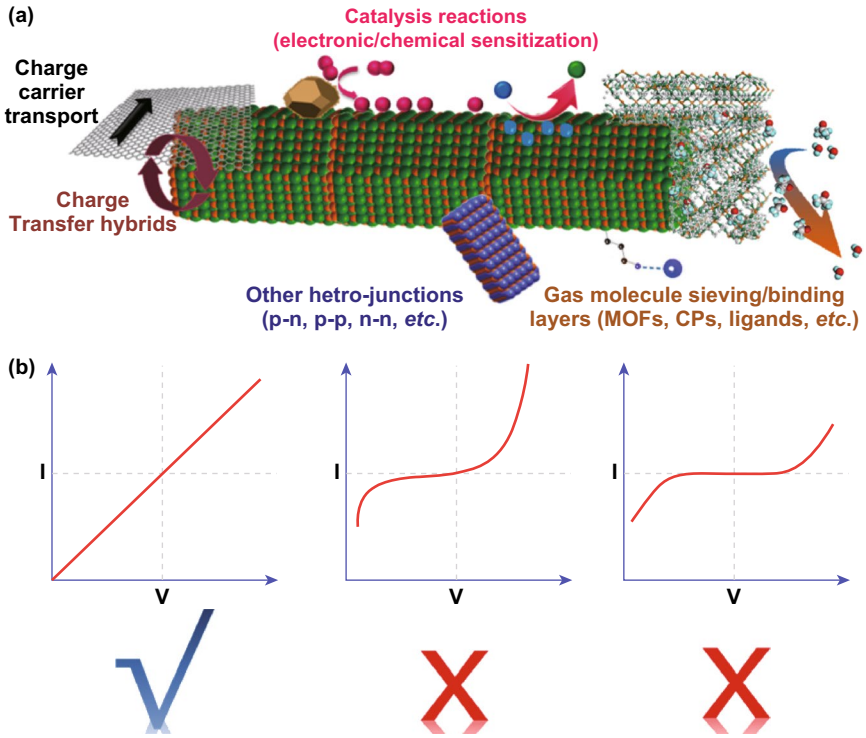

Fig. 2 **a** Schematic illustration of five typical forms of hybrid functional nanomaterials for chemi-resistive gas sensing; **b** typical *I–V* curves of different sensors under DC bias (from left to right, chemi-resistors, chemical diodes, and proton/ions types)

with a constant resistance when the resistance and device is applied a constant bias voltage), we will review here only resistive-change sensing devices in which the contact of sensitive materials and electrodes is ohmic (good linearity of *I–V* curves under DC bias, Fig. 2b); therefore, we exclude devices in which the *I–V* curves under DC bias are nonlinear despite that they exhibit similar resistance changes (e.g., chemical diodes, proton/ions types).

3.1 Hybrid Gas Sensors Based on Catalytic Effects

Catalytic effects of hybrid functional nanomaterials contribute to high response, fast speed, and low operating temperature via chemical/electronic sensitization, which is usually accompanied by synergistic effects, complementary behavior, and porous structures [50, 52, 83–86]. In addition, the exposed facets (morphologies) of matrix nanograins (facet-dependent chemical activity) and catalytic additives can greatly enhance the sensing properties of hybrid nanomaterials [87, 88]. For example, introduction of Cr dopants to WO_3 polydedra can not only control the specific exposed facets and activation energy, but bring catalytic effects to the matrix [50]. The combining effects led to improved sensitivity and reduced operating temperature. Further hybridization with catalytic Au nanocrystals—to form Au/Cr–WO_3 hybrids—contributed to high sensitivity, fast speed, and reduced working temperature to acetone and benzene due to Au/Cr co-catalysts-enhanced surface reaction (Fig. 3a, b). The advantages of co-catalysts can improve even further the hybrid materials. A recent example of this approach is Pd/Sb nanocrystals modification of SnO_2 that Sb and Pd functioned as anti-humidity and catalytic sites, respectively, which remarkably reduced humidity interference and improved responses toward H_2 (Fig. 3c) [89, 90].

The catalytic effects of loaded catalysts on host-sensitive materials are associated with the contact between catalyst and gas. A gas diffusion-favoured structure can provide additional exposed surface areas and fast speed via a combination of surface- and structure-dependent factors. The introduction of catalytic Ag NCs via *e*-beam evaporation and calcination into quasi-1D heterostructures significantly enhances the response and selectivity to ethanol (Fig. 3d) [51, 91]. For even further performance, quasi-1D nanostructures with

 https://doi.org/10.1007/s40820-020-0407-5

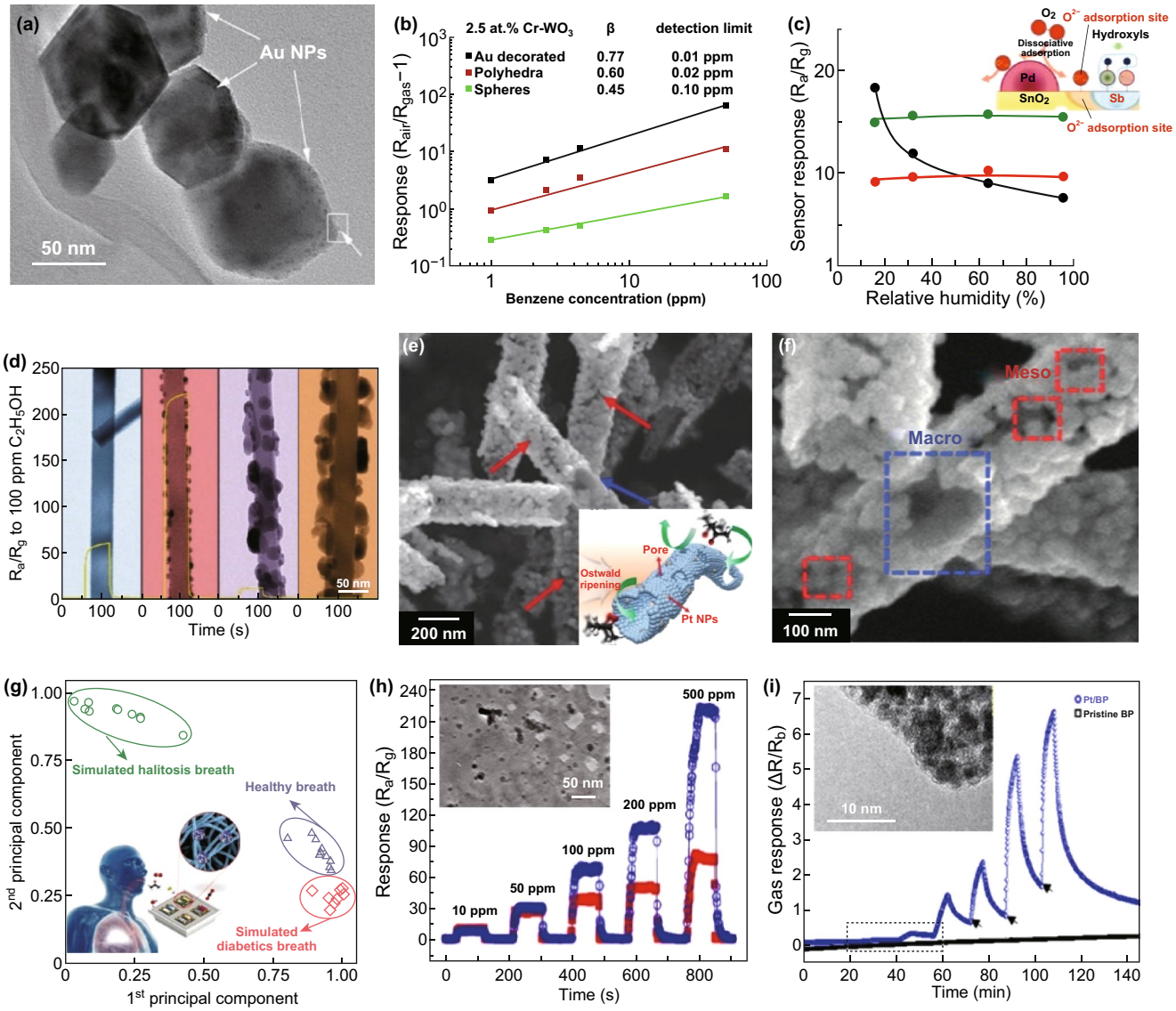

Fig. 3 **a** SEM images of WO_3 octahedron, **b** 2.5 at.% Cr–WO_3 truncated octahedron and 10.0 at.% Cr–WO_3 cuboid. Reproduced with permission [50]. Copyright 2015, American Chemical Society. **c** Humidity dependence of sensor response to 200 ppm hydrogen at 350 °C, using (black) undoped SnO_2, (red) 0.1 mol % Sb-doped SnO_2, and (green) 0.1 mol.% Pd-loaded and Sb-doped SnO_2 nanoparticles. Reproduced with permission [89]. Copyright 2016, American Chemical Society. **d** TEM images of pure SnO_2, 5Ag–SnO_2, 10Ag–SnO_2, and 50Ag–SnO_2 NW after heating at 450 °C for 2 h and the corresponding response-recovery curves to ethanol gas. Reproduced with permission [51]. Copyright 2011, American Chemical Society. **e, f** SEM images of Pt–PS–SnO_2 NTs (the inset is a schematic illustration). Reproduced with permission [52]. Copyright 2016, Wiley–VCH. **g** Pattern recognition by PCA using dataset from sensor arrays of PtM-decorated meso-WO_3 NFs evaluating real and simulated (diabetes and halitosis) breath. Reproduced with permission [53]. Copyright 2017, Wiley–VCH. **h** TEM image of Pd nanoparticles@ZnO NSs and the corresponding response-recovery curves to acetone gas (red ZnO NSs). Reproduced with permission [54]. Copyright 2012, American Chemical Society. **i** Gas response of Pt/BP and pristine BP to various H_2 concentrations (the inset shows the TEM images of Pt/BP). Reproduced with permission [55]. Copyright 2017, American Chemical Society. (Color figure online)

both porosity and sensitive nanobuilding blocks, namely mesoporous 1D nanofibers/tubes (meso-NF/NTs), have been reported [41, 92–94]. By introducing sacrificial polymeric colloids and protein-templated catalysts to the solutions, meso- and macro-porous Pt-decorated SnO_2 NTs have been fabricated by electrospinning and sintering in sequence (Fig. 3e, f) [52]. The combined effects of porous nanostructures, fully depleted sensing areas and uniformly distributed Pt nanocatalysts on SnO_2 NTs allow a highly selective detection of acetone (R5ppm = 192). Similarly, bimetallic PtM

(M = Pd, Rh, and Ni) catalysts can be introduced to meso-WO_3 NFs that are then highly selective detectors of acetone and H_2S gas [53]. Sensors array combined with pattern recognition methods (so-called e-nose) based on three different PtM-decorated meso-WO_3 NFs can accurately detect and discriminate the breath of a simulated biomarker through principal component analysis (PCA, Fig. 3g).

On the basis of intensive works on porous 2D ZnO nanostructures [37, 95, 96], Pd NCs have been deposited on porous 2D ZnO nanoplates (host materials) transformed by $Zn_5(CO_3)_2(OH)_6$ nanoplates to form 2D Pd/ZnO hybrid nanoplates (Fig. 3h); these acquire enhanced sensing properties [54]. Similarly, catalytic Pt can be used to decorate the surface of BP, which enables RT detection of H_2 by Pt/BP at RT (Fig. 3i) [55]. When the structure of the host materials is further upgraded to 3D hierarchical porous (hp) nanostructures, a good gas diffusion platform is obtained with a large loading area of catalysts. By taking the advantage of the opals/polymeric beads or mesoporous silica/carbon/polymers templating method, hp-MOX thin films (3D hp nanostructures) with certain additives (catalysts) have been developed [97–102]. In this simple approach, hp-SnO_2-inverted opal thin films loaded with mono-dispersed Pt catalyst (of uniform size of ~5 nm) were prepared (Fig. 4a) [103]. The improved sensing responses of Pt-doped SnO_2-inverted opal thin films were achieved due to increased porosity, electronic sensitization, and synergism (Fig. 4b). Similarly, hp–Pt–WO_3 or hp–Cr–WO_3-inverted opal thin films have been successfully

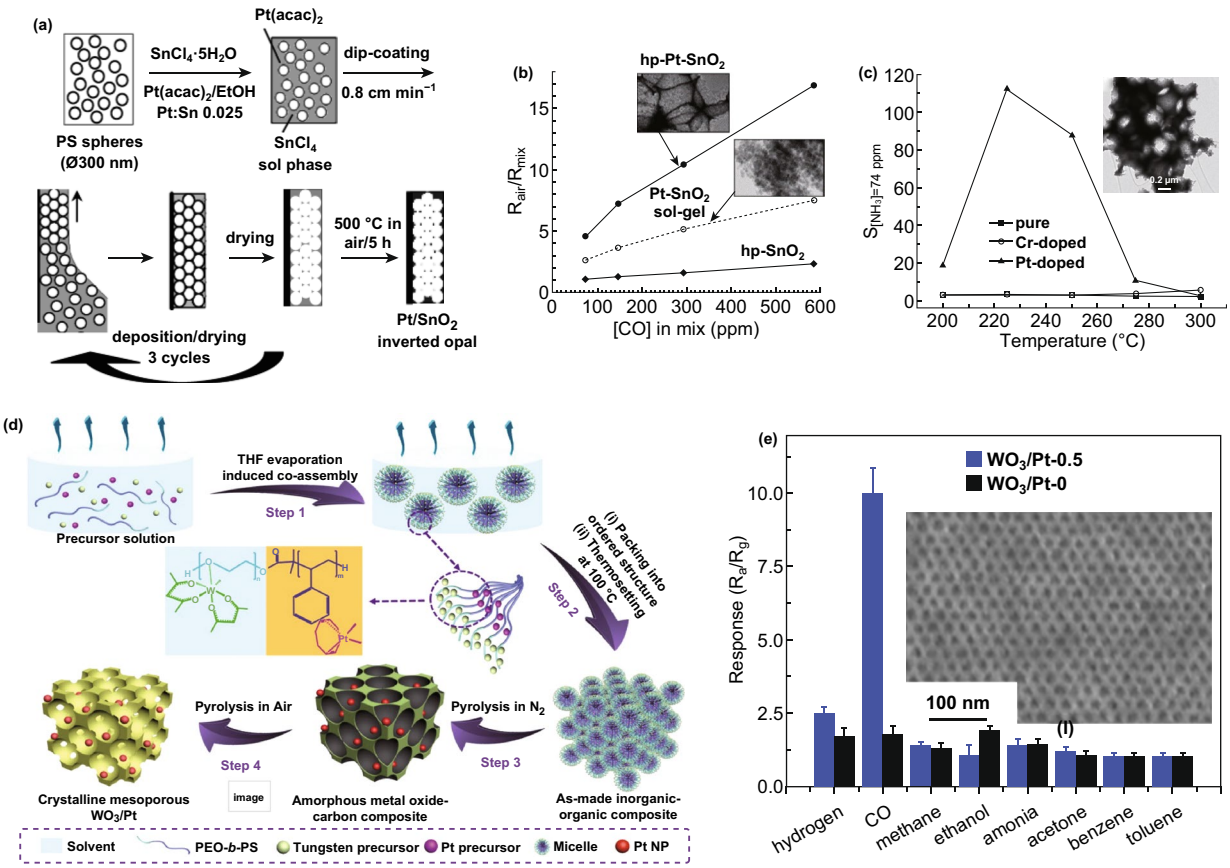

Fig. 4 **a** Schema of the one-step preparation of Pt-doped SnO_2-inverted opal films, and **b** responses comparison of different sensors as a function of CO concentration at 350 °C (insets are the corresponding HRTEM micrographs). Reproduced with permission [103]. Copyright 2010, American Chemical Society. **c** Responses comparison of different sensors as a function of working temperature to 74 ppm NH_3 gas (the inset is the corresponding HRTEM micrograph of Pt-WO_3-inverted opal films). Reproduced with permission [104]. Copyright 2011, American Chemical Society. **d** Synthesis of ordered mesoporous WO_3/Pt hybrids. **e** Gas response of WO_3/Pt-0.5 and WO_3/Pt-0 to different gases (hydrogen, CO, methane, ethanol, ammonia, acetone, benzene, and toluene) at 100 ppm and 125 °C in 55–60% RH (the inset is an FESEM image of the crystalline WO_3/Pt-0.5 viewed from the top surface). Reproduce with permission [56]. Copyright 2018, Wiley–VCH

https://doi.org/10.1007/s40820-020-0407-5

prepared (Fig. 4c) [104]. Due to the catalytic activation of N–H bond dissociation and effective gas diffusion within the macro-porous structures, excellent NH_3 responses were obtained for the hp–Pt–WO_3 sensor. As another example, well-controlled self-assembly of block copolymers such as poly(ethylene oxide)-blockpolystyrene (PEO–b–PS) could generate a perfect template with a highly ordered structure. Mesoporous WO_3/Pt with a highly ordered and porous structure (inset of Fig. 4e) could be obtained by using this template and a 2-step pyrolysis process (Fig. 4d, including first treated in inert atmosphere and finally calcinated in air) [56]. Contributed to high surface areas (112–128 m^2 g^{-1}), large pore size (13 nm), and well-dispersed catalytic Pt NCs (~4 nm), the WO_3/Pt-0.5 sensor had the highest response and fastest response-recovery speeds (Fig. 4e). Another category of nanostructures of host materials is multi-shell, yolk–shell, and multi-yolk–shell with hollow nanochamber [83–86]. With the hollow host nanochamber (SnO_2) loading catalytic Pd through spray pyrolysis (Fig. 5a) [57], and showing the formation of double-shelled Pd–SnO_2@Pd–SnO_2@Pd–SnO_2 yolk–shell spheres (Fig. 5b) [57], both sensitivity and selectivity were enhanced due to the unique hierarchical porous structure and uniformly exposed Pd catalysts. The representative works are summarized in Table 1.

As aforementioned, greatly improved sensitivity and speed have been realized by well design on the dispersion of catalysts/co-catalysts and gas diffusion-favored structures of hybrid gas sensors based on catalytic effects. The remaining problems of operating temperature and selectivity might be resolved by further combination with charge

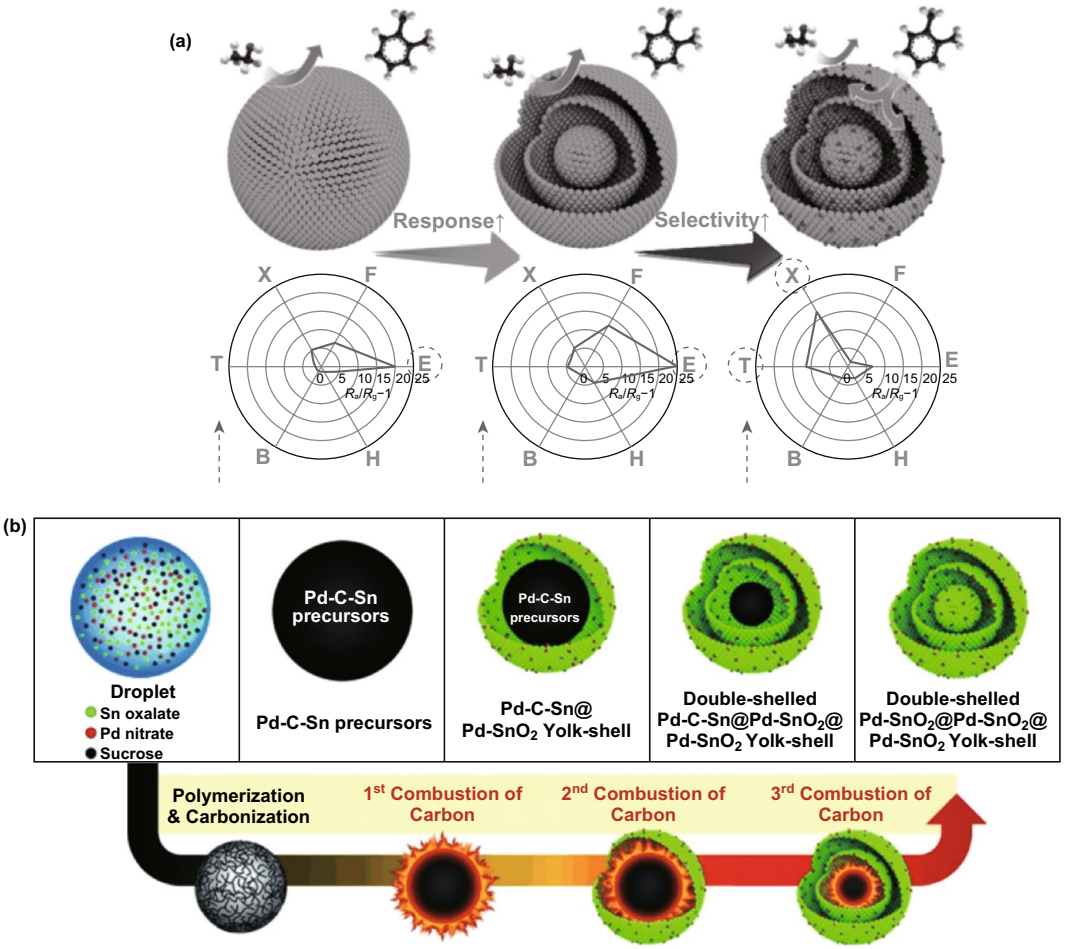

Fig. 5 **a** Gas responses of dense SnO_2 spheres, SnO_2 yolk–shell spheres, and Pd-loaded SnO_2 yolk–shell spheres to various analytical gases at 350-450 °C (B: benzene, H: H_2, E: C_2H_5OH, F: HCHO, X: o-xylene, T: toluene). **b** Scheme showing the formation of double-shelled Pd-SnO_2@Pd-SnO_2@Pd-SnO_2 yolk–shell spheres. Reproduced with permission [57]. Copyright 2014, The Royal Society of Chemistry

Table 1 Representative works based on catalytic effects

Materials	Gas detection	Detection range	Work temperature	Refs.
WO_3/Pt	CO	100–500 ppm	125 °C	[56]
SiO_2/In_2O_3	NOx	970 ppb–97 ppm	RT	[220]
Pd/WO_3	Acetone	50 ppb–500 ppm	300 °C	[221]
PdO/$ZnFe_2O_4$	Acetone	5–300 ppm	275 °C	[222]
Au/$LaFeO_3$	Acetone	2.5–40 ppm	100 °C	[223]
Au NPs/ZnO	Athanol	5–60 ppm	RT	[224]
Sm_2O_3/SnO_2	Acetone	0.1–200 ppm	250 °C	[225]
Pd/SWNT	CH_4	6–100 ppm	RT	[226]
Pt/SnO_2 NTs	CH_3COCH_3	10–100 ppb	350 °C	[52]
Pd@SnO_2	H_2S	5–100 ppm	290 °C	[227]
CuO/Pd	H_2S	1–100 ppm	20-100 °C	[228]

transfer (Sect. 3.2) and molecule sieving layers (Sect. 3.5), respectively. Moreover, the newly developed single atomic metal and/or metal cluster-based catalysts with better catalytic effect might bring new understandings and chance in such areas [105–108].

3.2 Hybrid Gas Sensors Based on Charge Transfer Effects

Charge transfer happens between decorations and the host materials (good conductivity), which could vary the conductivity of the hybrid materials. This process improves sensitivity to the analysts at low temperature or even at room temperature (RT), accompanying fast response and recovery properties [4]. Discrete and uniform SnO_2 NCs-decorated multi-walled CNTs (MWCNTs) (Fig. 6a) [59] gave high performances (response of ~ 180% to 100 ppm of NO_2) at RT due to the abundance of active sites and easy electron transfer under the assistance of the well-matched work functions of SnO_2 and MWCNTs. Liu et al. [109] used rGO instead of the carbon nanotubes. This researcher successfully synthesized SnO_2 QDs/rGO hybrids by a one-step solvent thermal reaction at 180 °C (oleic acid and oleylamine as capping agents) (Fig. 6b) [109]. Due to co-effects of excellent gas adsorption of QDs, effective charge transfer between SnO_2–rGO interfaces and the superb transport capability of rGO, the sensor responses in 2 s with fully recovery properties upon exposure to 33 to 50 ppm of H_2S at RT (Fig. 6c). Meanwhile, the SnO_2/rGO-based sensor showed an obvious enhanced response compared with the responses of pure SnO_2- or rGO-based sensors toward H_2S at 22 °C, in which the rGO acted as a host transducer material. By combining both advantages, 2D MoS_2 sheets were hybridized with 2D graphene to form rGO/MoS_2 aerogel with large surface areas, porous structure, and high electrical conductivity (Fig. 6d) [61]. Efficient and rapid charge transfer across the interface ensured enhancement and fast detection of NO_2 than bare rGO or MoS_2 (Fig. 6e). Ascribing to the high specific surface area of porous Cu_2O nanowires networks and improved conductivity via effective charge transfer, rGO–Cu_2O mesocrystals had much higher sensitivity to NO_2 at RT, surpassing the performance of stand-alone systems of Cu_2O and rGO sheets (Fig. 6f) [62].

CPs could also be applied in charge transfer hybrids by replacing the inorganic components. For instance, graphene was combined with PANI to form a hybrid thin film that had improved, reversible, and stable NH_3 sensing (Fig. 6g, h). The fast electron transfer between hybrids and NH_3, assisted by π–π interactions of PANI and rGO with low electron transfer energy barrier, led to more electrons transfer from PANI to rGO; this effectively improved the responsivity and response time (Fig. 6i) [63]. Up to date, the detecting gases are limited to strong reducing/oxidizing molecules such as NO_2, NH_3, and H_2S, which hinders the widely application of such hybrid gas sensors. The critical points to overcome this shortcoming may be depicted as: (1) the chemical/electronic modification of the reported charge transfer based hybrids to improve the sensitivity and expand the types of detectable gases (i.e., Pt–SnO_2/rGO, details in Sect. 3.6); (2) the development on the new candidate of chemi-resistive decorations with desired absorption–desorption process and well-tailored energy level/energy band gap structure, which always shows low thermal activation energy (< 0.5 eV, i.e., electronic conductive metal–organic frameworks (EC-MOFs), for details see Sect. 3.5). The representative works are summarized in Table 2.

3.3 Hybrid Gas Sensors Based on Regulation of Charge Transport

Different from charge transfer that simply uses high charge transport capability of the highly conductive component, hybrid gas sensors based on regulation of charge carrier

https://doi.org/10.1007/s40820-020-0407-5

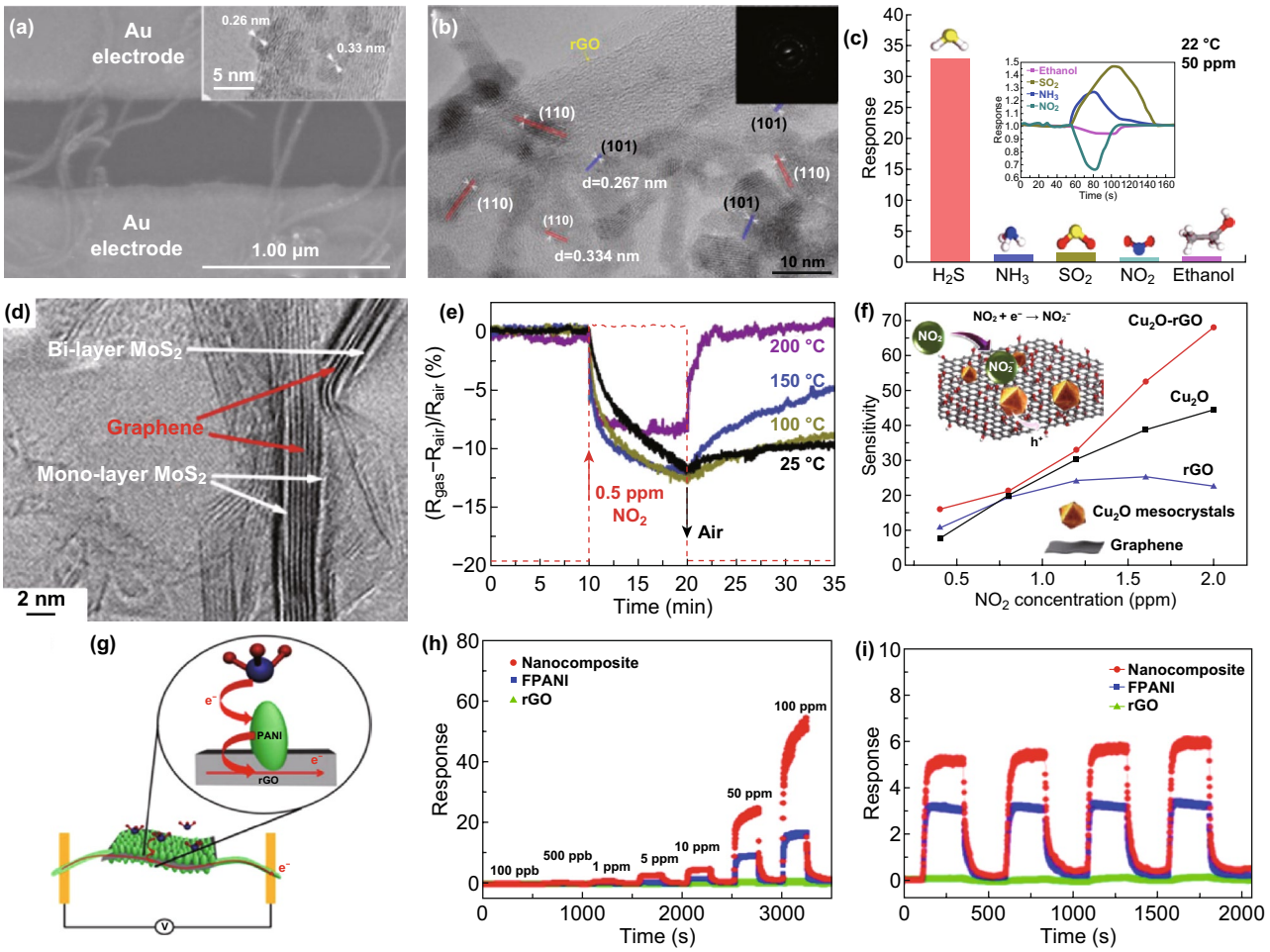

Fig. 6 **a** SEM image of the sensor after assembly of SnO_2 nanocrystals onto the MWCNTs (inset is the HRTEM image of a MWCNT uniformly coated with SnO_2 nanocrystals). Reproduced with permission [59]. Copyright 2009, Wiley–VCH. **b** TEM image of SnO_2 QDs/rGO hybrids; and **c** sensor responses to 50 ppm of different gas at RT. Reproduced with permission [109]. Copyright 2016, American Chemical Society. **d** Enlarged TEM image demonstrating the MoS_2 coating of the few-layer graphene scaffold. **e** Sensor response to 0.5 ppm NO_2 at different microheater temperatures, improving response and recovery time. Reproduced with permission [61]. Copyright 2016, Wiley–VCH. **f** Sensitivities of NO_2 sensor for the three devices (inset is a schema of the mechanism of NO_2 sensing of rGO-Cu_2O). Reproduced with permission [62]. Copyright 2012, American Chemical Society. **g** Schema of the sensing mechanism of rGO-PANI hybrids. **h** NH_3 responses of PANI, rGO and their hybrids at different concentrations. **i** Repeated NH_3 responses of PANI, rGO and their hybrids at 10 ppm. Reproduced with permission [63]. Copyright 2016, Royal Society Chemistry

transport can manipulate the sensing properties by changing carrier concentrations, transportation mode, and/or pathways of charge transport.

A simple and effective way of enhancing responsivity relies on controlling the charge transport by tuning carrier concentrations. For example, a PTCDI-Ph/p-6P ultrathin film was fabricated with a thickness of only 6 nm, of which 5 nm was attributed to (p-6p/p type) asymmetric thickness and 1 nm to (PTCDI-Ph/*n* type) (Fig. 7a) [64]. Electrons in the PTCDI-Ph were deprived by NO_2, which simultaneously released the restricted hole in p-6p, and thus influenced the transportation of p-6p; this generated a NO_2 sensing signal at RT (Fig. 7b). Chi et al. [64] thermal-deposited a high-quality crystalline terrace-like TIPS-pentacene film on p-6P that can easily be positively charged (Fig. 7c). The efficient charge transport ability and low original carrier concentration gave superb NO_2 sensing in terms of both response/recovery speed (Fig. 7d) and responsivity/sensitivity (Fig. 7e) [64]. Impressively, when the transport direction of charge carriers changes from horizontal to vertical in a vertical diode

Table 2 Representative works based on charge transfer effects

Materials	Gas detection	Detection range	Work temperature	Refs.
CuxO/multilayer graphene	NO_x	97 ppb–97 ppm	RT	[229]
rGO/NiO	NO_2	0.25–60 ppm	RT	[230]
ZnO QDs/graphene	HCHO	25–100 ppm	RT	[231]
SnO_2/rGO	H_2S	10–100 ppm	RT	[109]
Graphite/polyaniline	NH_3	50–1600 ppm	RT	[232]
SnO_2/graphene	CH_4	1000–10,000 ppm	150 °C	[233]
SnO_2 CQD/MWCNT	H_2S	3.3–100 ppm	70 °C	[234]
rGO/TiO_2–Nb	CO	100–1000 ppm	380 °C	[235]
Fe_3O_4@RGO	NO_2	50 ppb–50 ppm	RT	[236]

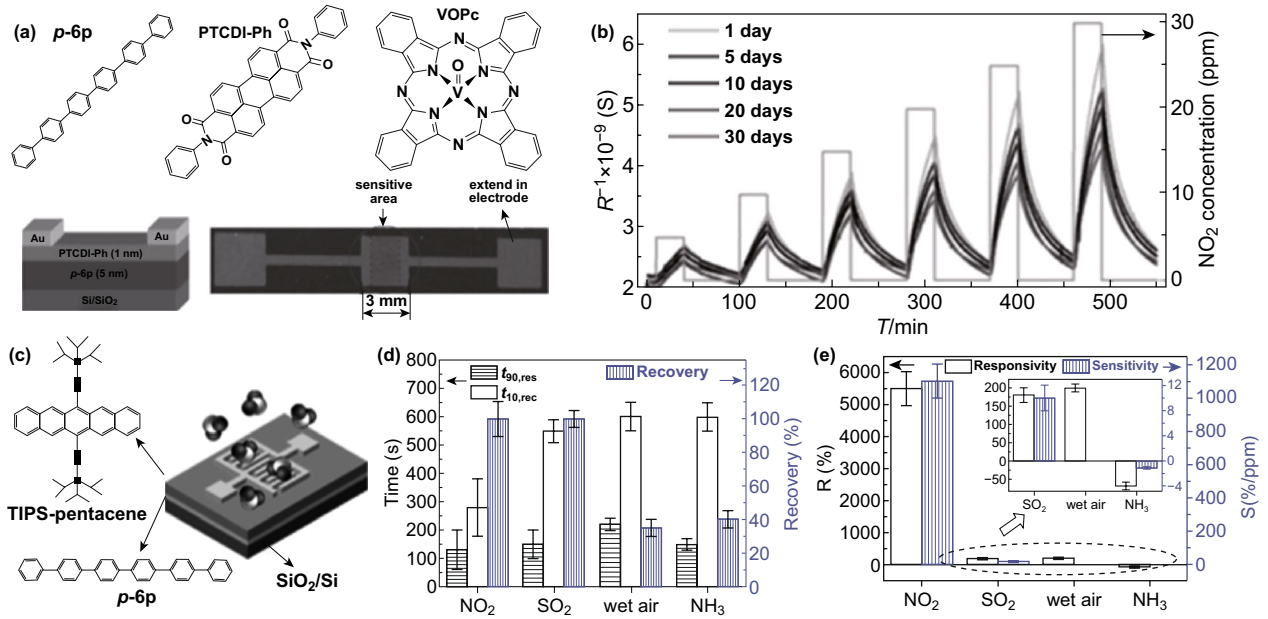

Fig. 7 **a** Sensor device configuration and molecular structures of the materials. **b** The relative response of 1 nm PTCDI-Ph/5 nm p-6P film to NO_2 pulses. The relative response curve is plotted as a function of time as the devices become exposed to different NO_2 concentrations. Reproduced with permission [66]. Copyright 2013, Wiley–VCH. **c** Sensor device configuration and molecular structures of the materials. **d** The $t_{90,res}$, $t_{10,rec}$ and relative recovery after 10-min N_2 pulse of the responses to different gases. **e** Responsivity (R) and sensitivity (S) to different gases. Reproduced with permission [64]. Copyright 2017, Wiley–VCH

(containing top/down electrodes and VOPc/F16CuPc layers, Fig. 8a), the sensor responded remarkably well to 0.5–5 ppm NO_2 at RT (Fig. 8c), with an acceptable sensing stability (Fig. 8b) and wide linear working region [65]. More interestingly, when the voltage bias is raised from 0.2 to 1.5 V, the sensing ability weakened dramatically (Fig. 8d), being ascribed to the transportation change from ohmic to space charge limited current (SCLC) mode (Fig. 8e) [65], which may give guidance as to how to choose the bias to control the charge transportation for gas sensors to get them to work under the best conditions.

Another strategy to manipulate the properties of sensors based on charge transport is by regulating the conductive pathways of conductive-insulate hybrid materials via physical cracks, chemical bindings, or the phase of the component. More specifically, this approach relies indeed on regulating the electron hopping barrier, the interspace between conductive materials, phase-change or their combination. Insulating polymers can be combined with sensitive

https://doi.org/10.1007/s40820-020-0407-5

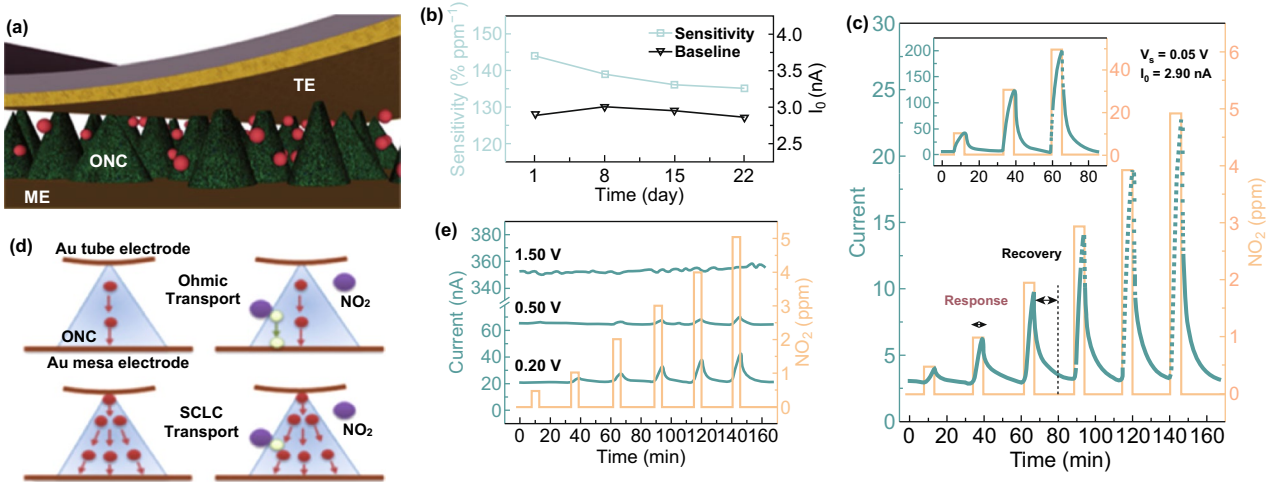

Fig. 8 **a** Schema of the cross section of the tube/organic/mesa structure. VOPc nanopyramids (green cones) provide sufficient space for NO_2 gas molecules to penetrate the structure. The red particles denote NO_2 gas molecules. **b** Stability test in ambient atmosphere: sensitivity (left axis) and baseline (right axis) over time. **c** Response of periodic NO_2 exposure. The device is operated under 0.05 V bias applied to the tube electrode. **d** Schematic diagram of charge transport and response to NO_2 under ohmic transport (upper panel) and SCLC transport (lower panel) conditions. **e** Response of organic nanocrystal diode sensor (device 1) at 0.20, 0.50, and 1.50 V bias applied to the tube electrode. Reproduced with permission [65]. Copyright 2018, Wiley–VCH. (Color figure online)

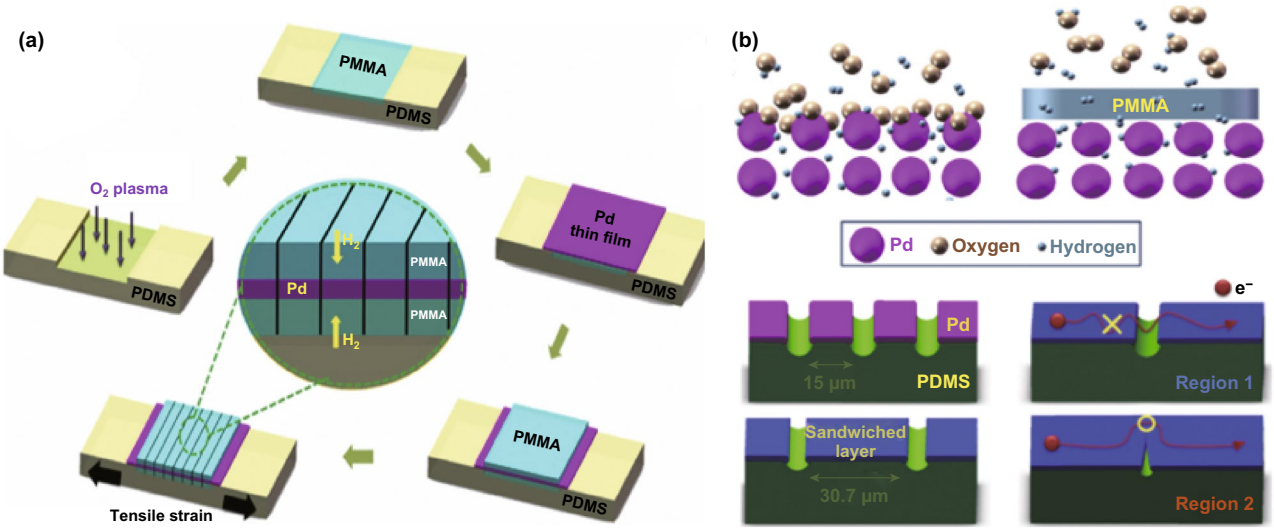

Fig. 9 **a** Schematic diagram of the fabrication of nanogap sensors using PMMA/Pd/PMMA trilayer films on a PDMS substrate. **b** Schematic diagrams indicating the origins of the difference between the H_2 detection limits of the Pd nanogap and the PMMA/Pd/PMMA hybrid nanogap sensors. Reproduced with permission [110]. Copyright 2014, Elsevier

inorganic materials to fabricate highly sensitive and selective chemi-resistors (Fig. 9a). Hybrid thin films as sandwiched PMMA/Pd/PMMA (PMMA = poly(methyl methacrylate)) were prepared on a flexible substrate using sputtering and spin coating in sequence (Fig. 9a) [110]. Hybrid thin films with nanogaps formed by 25% mechanical stretching have very selectivity and sensitivity in detecting H_2 against O_2, ascribed to the selective penetration of H_2 in PMMA membranes and the density reduction of the cracks formed in the trilayer of the hybrid thin films (Fig. 9b). Adoption of similar principles, but with higher effects, relies on films of GNPs coated with monolayers of thiols [111]. These structures were a good solution for VOCs sensing due to the swelling and shrinkage of molecular chains interacting with

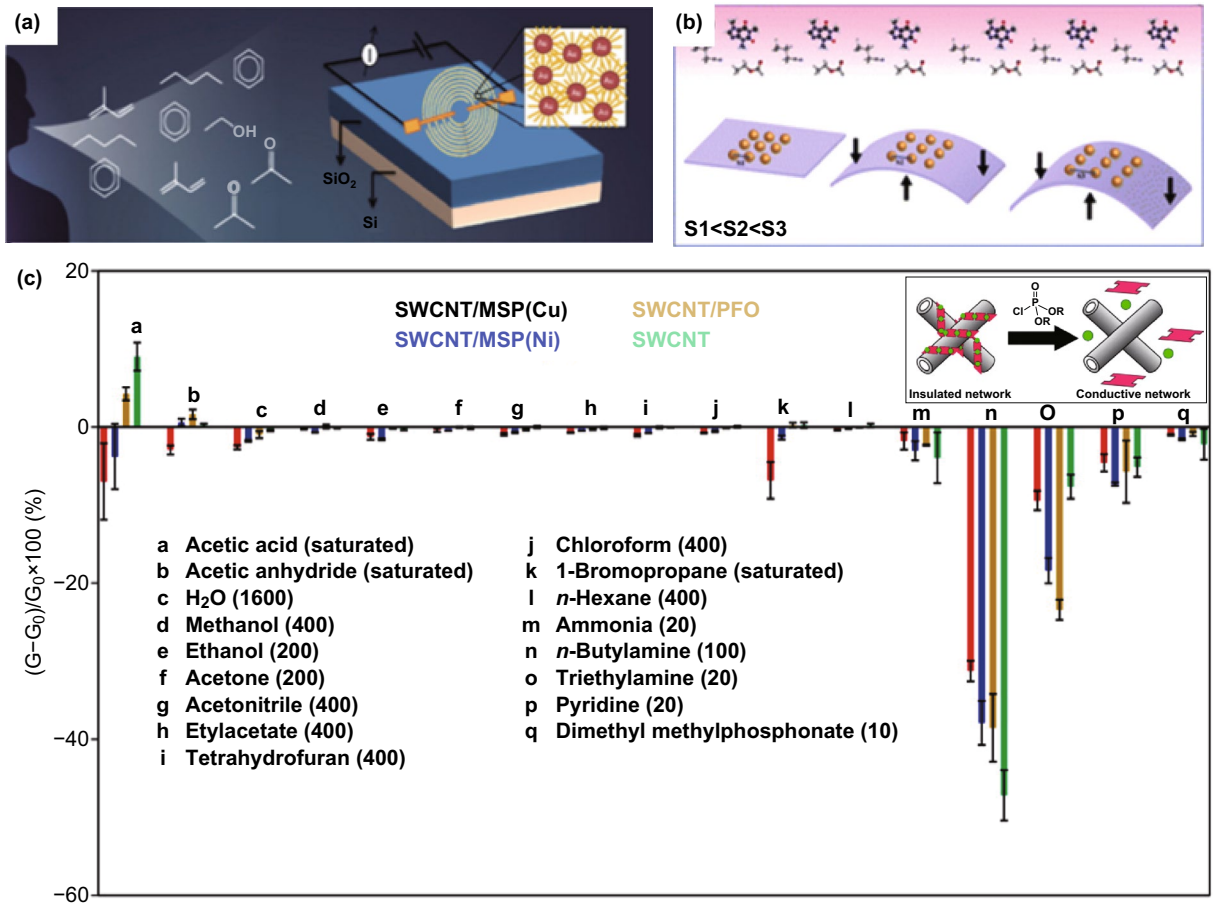

Fig. 10 **a** Schema of the working principles of gold NPs thiol-coated thiols gas sensor. Reproduced with permission [81]. Copyright 2014, Elsevier. **b** Schema of a strain regulated gold NPs-based gas sensor. Reproduce with permission [112] . Copyright 2015, American Chemical Society. **c** Response of SWCNT-based chemi-resistive sensors after 50-s exposure to different vapors in N_2 (concentration in ppm in parentheses). The inset is the schema of the working mechanism. Reproduced with permission [80]. Copyright 2015, American Chemical Society

VOCs (Fig. 10a) [81]. Assembly of the GNP-based chemi-resistors with a wide variety of functional groups creates sensor arrays with different resistances that can be further varied after interacting with VOCs [81]. The transport of electrons, expressed in electrical resistance, can be dually regulated by controlling the interspaces between GNPs after applying strain to the GNPs-based film, which further influence sensitivities (Fig. 10b) [112]. CNTs are also used as the host with the surface coverage of molecular (MSPs) (inset of Fig. 10c) [80]. Such MSPs could create sensory devices with a dosimetric (time- and concentration-integrated) increase in electrical conductivity triggered by electrophilic chemical substances (Fig. 10c).

In summary, for cases where the resistance decreased upon exposure to target gas, the depression of the off current via carrier concentrations reduction, transportation mode changes and/or physical cracks might be the most effective way to realize high sensitivity. Simultaneously, as presented above, the component used for the controlling charge transport of host materials can further contribute to improved speed, long-term stability, and excellent selectivity. The representative works are summarized in Table 3.

3.4 Hybrid Gas Sensors Based on Heterojunctions

Heterojunction is defined as the interface between two dissimilar semiconductors (one is the host, and the other one is the guest) that form a junction (n–n, p–p, p–n) linked with energy band structure due to the alignment of their fermi level. Notably, although the broad definition of

https://doi.org/10.1007/s40820-020-0407-5

Table 3 Representative works based on regulation of charge transport

Materials	Gas detection	Detection range	Work temperature	Refs.
TIPS-pentacene	NO_2	0.2–20 ppm	RT	[64]
PMMA/Pd/PMMA	H_2	600–6000 ppm	RT	[110]
PANI/SWCNT	NH_3	1–100 ppm	RT	[237]
Oleylamine/Pt	Organic contamination	< 0.3 ppm	RT	[238]
Ionic liquids/CNT	Heptanal	200 ppm	RT	[239]
	Toluene	1000 ppm		
	Ethanol	1000 ppm		
CNTs/hexa-peri-hexabenzocoronene bilayers	Decane	~ 10 ppb	RT	[240]
	Octane	~ 15 ppb		
	Hexane	~ 10 ppb		
	Ethanol	~ 10 ppb		
GNPs	Nonanal, styrene, ethanol, propionitrile	50–1000 ppb	RT	[112]

heterojunctions covers all types of composites forming a junction in the interface, it is not clear enough for the well understanding of the complicated sensing mechanisms of composites sensing materials. Therefore, in this work, the narrow definition of manipulating/constructing heterojunctions is used, which excludes cases of catalytic effects, charge transfer, and charge carrier transport. According to the definition, the junction changes the interface potential energy barriers and regulates the transfer and/or injection of electrons and holes in a precise manner when it interacts with gas analytes. For example, n–n heterojunctions made of In_2O_3 hollow spheres (acetone-sensitive host) coated with CeO_2 nanoparticles (humidity-sensitive guest) were synthesized and characterized as a chemi-resistive film. Exposing the layer to various gas analytes has shown selective detection of acetone in the presence of water, taking advantage of the chemical interaction between CeO_2, In_2O_3, and water vapor, which greatly reduces the interfering effects of humidity (Fig. 11a) [113]. By modulating interface potential energy barrier between n–n junctions, as in the case of Fe_2O_3/TiO_2 tube-like quasi-1D nanostructures synthesized through a multi-step hydrolysis (Ostwald ripening & thermal reduction), the corresponding sensing performance could be greatly improved (Fig. 11b) [114]. Combining modulation of electron transfer over the energy barrier at the perfect SnO_2/ZnO heterojunction—fabricated by atomic layer deposition—and UV light generated electron–hole pairs, the sensitivity to NO_2 could be improved using the SnO_2/ZnO core-sheath nanowires (Fig. 11c) [115]. By introducing narrow band gap into the junction, such as in the case of In_2O_3 NCs to ZnO, a good response at visible-light conditions to gas analytes (e.g., formaldehyde) at RT (R100 ppm = 419%) [54] was attainable.

The unique morphology (good compatibility with the devices), nanoscale thickness, and high surface area of 2D nanostructures make them promising as the host materials for chemi-resistive gas sensors. Hybrids of SnO_2 NCs-decorated MoS_2 nanosheet (MoS_2/SnO_2) were synthesized via hydrolysis-pyrolysis processes (Fig. 11d) with air stability [116]. The SnO_2 NCs not only enhanced the stability of MoS_2 nanosheets in dry air, but served as strong dopants for MoS_2, leading to the changes of conduction channels in the MoS_2 nanosheets (Fig. 11e). For further improvements in the sensing performance, introduction of porosity, such as in the case of WO_3 lamella-based films loaded with mono-dispersed SnO_2 QDs (~ 4 nm) (Fig. 11f), could reach high levels [117]. Experimental results show that the porous lamellar-structured WO_3–SnO_2 hybrid films could achieve high response to NO_2 gas, ascribing the effective insertion of QDs into lamella stacks as a strong electronic sensitization.

Compared with n–n heterojunctions, p–n heterojunctions provide a stronger manipulation on interface potential energy barriers, build-in electric field and additional catalytic effects in some unique cases. For example, exposing p–CuO nanoparticles loaded on CuO–SnO_2 p–n nanowires to H_2S transformed it to highly conductive CuS (Fig. 12a) [67], resulting in depleted region change (the p–n junction breakup) and second-order effects (the oxidation of H_2S by absorbed oxygen) after p-CuO was reversibly generated and removed on the SnO_2 surface. Without generating

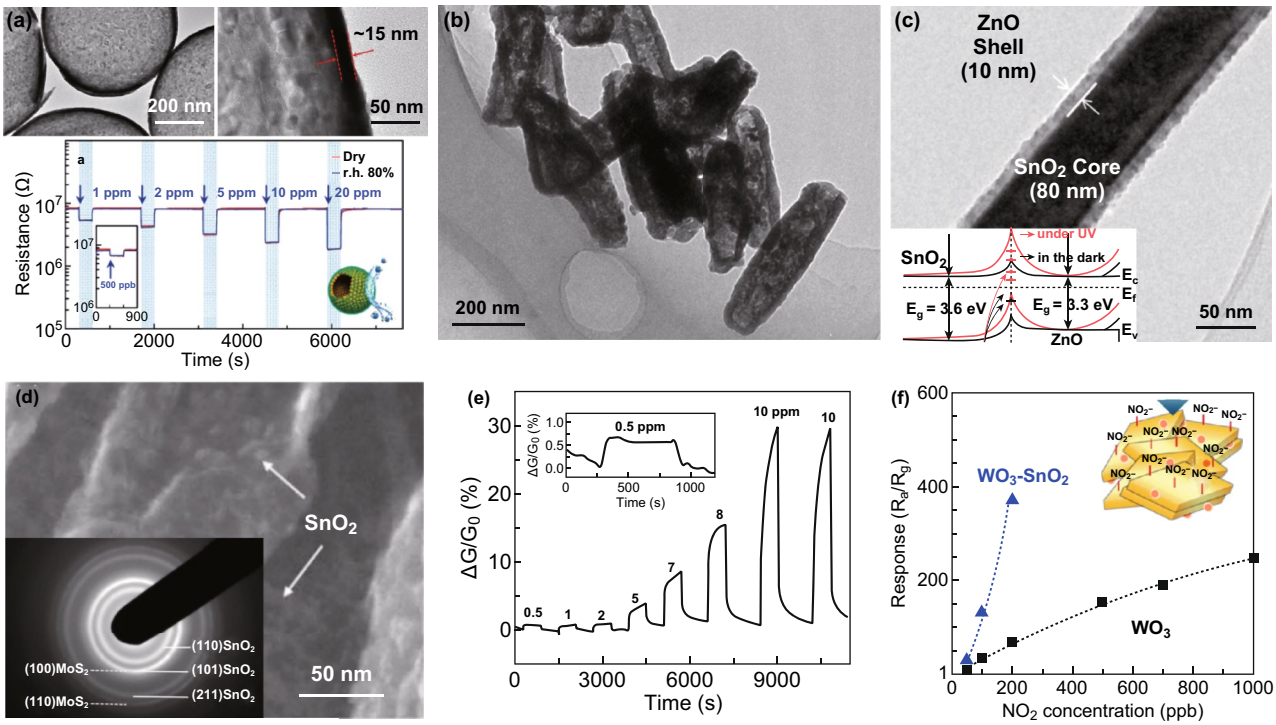

Fig. 11 **a** TEM images and dynamic sensing transients of Ce–In_2O_3 hollow spheres exposed to 0.5–20 ppm of acetone at 450 °C in dry (red) and RH 80% (blue). Reproduced with permission [113]. Copyright 2016, Wiley–VCH. **b** TEM image of 1D Fe_2O_3/TiO_2 tube-like nanostructures. Reproduced with permission [114]. Copyright 2012, American Chemical Society. **c** Low-magnification TEM image of SnO_2/ZnO core–shell nanowires (the inset is the corresponding energy band diagram of the SnO_2/ZnO system with/without UV light). Reproduced with permission [115]. Copyright 2013, American Chemical Society. **d** High-resolution SEM image showing that SnO_2 NCs decorate on the MoS_2 nanosheets (the inset is the corresponding SAED patterns), and **e** dynamic sensing response of the MoS_2/SnO_2 nanohybrids to different NO_2 concentrations (the inset is the enlarged sensing response curve for 0.5 ppm NO_2). Reproduced with permission [116]. Copyright 2012, Wiley–VCH. **f** Schematic of the sensing mechanism of WO_3–SnO_2 nanoplates and the corresponding responses comparison toward NO_2 gas. Reproduced with permission [117]. Copyright 2014, American Chemical Society. (Color figure online)

new chemical compounds, simply tuning the thickness of in situ oxidation layer, rich Te–Te or TeO_2/TeO_2 bridging point contacts and additional p–n heterojunctions (Te/SnO_2) contributed to further excellent sensing performances (to CO and NO_2) of the brush-like heterostructures (Fig. 12b) [118]. The nanorods of *p*-type coating layer can be replaced by continuous layer to form core-sheath hybrids processing radial modulation of potential energy barriers, for instance, both n-ZnO/p-CoPc (cobalt phthalocyanines, Fig. 12c) [119] and n-SnO_2/p-Cu_2O (Fig. 12d) [120]. Core-sheath NRs have better sensitivity of the target gases.

Conductive polymers (CPs, e.g., PPy, poly(3,4-ethylenedioxythiophene) (PEDOT), PANI) that are p-type components of diverse types of p-n heterojunctions can work at RT or low operating temperature with different working principles. First, PPy-ZnSnO4, p–n hybrid nanoparticles, can enhance the NH_3 sensing performance (3–4 times higher) compared with pure PPy and $ZnSnO_4$ (Fig. 13a) [121]. The concentration of NH_3 can be quantitatively detected (Fig. 13b) with shorter time of response (26 s) and recovery (24 s) (Fig. 13c). The overall improved performance has been ascribed to the p–n heterojunction, in which the holes at high concentration in PPy and the electrons in Zn_2SnO_4 diffuse into each other to form a built-in electric field of a depletion layer (Fig. 13d). Interaction between Zn_2SnO_4–PPy and NH_3 broadens the depletion layer, which determines the response, and the speed of response/recovery. When the p–n junction was reinforced as dual p–n junctions (p–n–p) in the hybrids of the hollow In_2O_3 nanofibers (NFs) and PANI (Fig. 13e), the performances were further enhanced (Fig. 13f) [122]. For CP-based chemi-resistive heterojunctions, unsatisfied sensitivity (response) and long-term stability will be two challenging issues for researchers.

https://doi.org/10.1007/s40820-020-0407-5

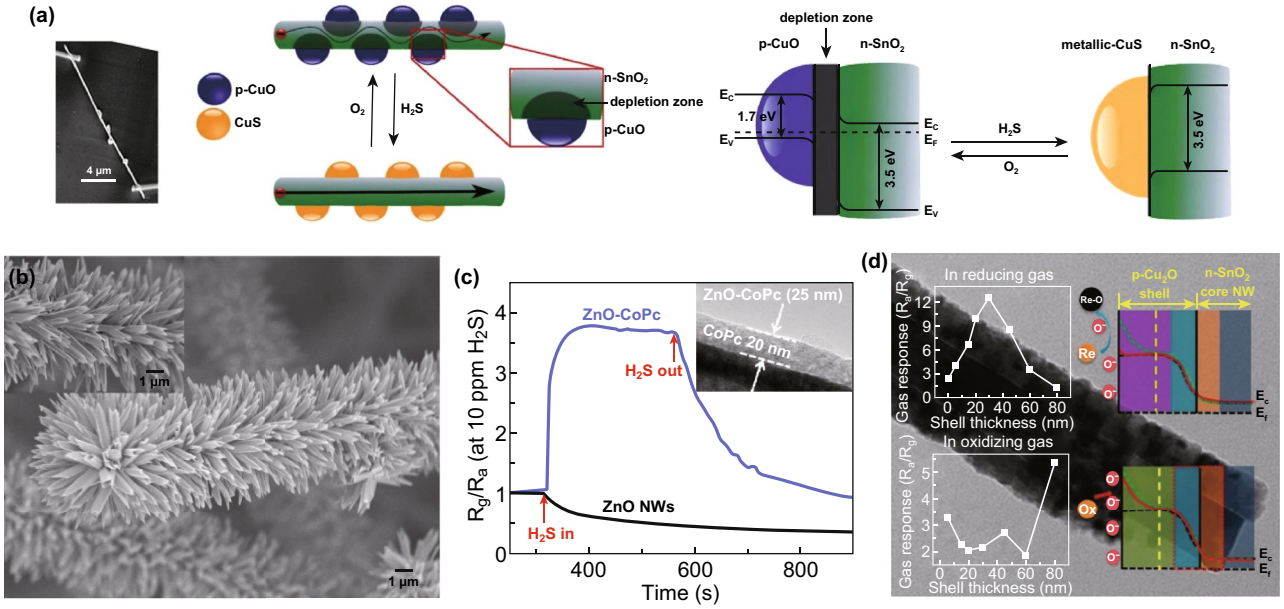

Fig. 12 **a** SEM image of a single hybrid NW and the schematic illustration of gas-sensing mechanism of CuO–SnO_2 p–n nanowires. Reproduced with permission [67]. Copyright 2013, Elsevier. **b** SEM images of the as-grown Te-coated SnO_2 brush-like products prepared at source temperatures of 560 °C. Reproduced with permission [118]. Copyright 2014, American Chemical Society. **c** The dynamic response-recovery curves for ZnO and n-ZnO/p-CoPc to 10 ppm of H_2S (the inset is the TEM image of n-ZnO/p-CoPc). Reproduced with permission [119]. Copyright 2015, American Chemical Society. **d** TEM image of 1D SnO_2/CuO nanostructures (left insets are responses to reducing and oxidizing gas as a function of shell thickness, respectively; right insets are the corresponding sensing mechanism). Reproduced with permission [120]. Copyright 2015, American Chemical Society

Obvious advantages of heterojunction-type chemi-resistive hybrids-based gas sensor can be summarized as: (1) higher sensitivity due to manipulations of the potential energy barrier formed by band bending of different components (e.g., Fe_2O_3/TiO_2 tube-like quasi-1D nanostructures (n–n) [114], n-ZnO/p-CoPc [119], and n-SnO_2/p-Cu_2O [120] core-sheath NRs); (2) improved selectivity to some gases (e.g., CuO–SnO_2 p–n nanowires to H_2S [67]); (3) promising, although limited so far, to anti-interference gas (e.g., CeO_2–In_2O_3 hollow spheres with anti-humidity properties [113]); (4) avoiding UV-introduced ozone and performance degradation (for example, when narrow-band guest material hybrids with semi-conductive host materials, e.g., CdS-ZnO [123, 124], ZnO-CdS [125], CdSe-ZnO [126], the room operation temperature can be achieved by the visible-light-driven gas sensing). The representative works are summarized in Table 4.

In summary, the critical points to achieve better performance in heterojunction-based gas sensor are depicted as: (1) maximum effective contact areas of the interfaces via surface and structure design; (2) matched band structure to facilitate the manipulation of potential energy barrier; (3) additional capability of catalysis of guest additives to host materials; (4) visible-light-driven photocatalytic abilities and good charge carriers separations for light-driven n–n or n–p hybrids; (5) selectivity-improvement-purposed heterojunction design based on specific interaction (e.g., Pd–H_2, CuO–H_2S, PPy–NH_3) or n–p response-type reversion (Co_3O_4–SnO_2 p–n junctions for H_2) [127].

3.5 Hybrid Gas Sensors Enhanced by Molecular Probing and Sieving Effect

Functionalization, coating or doping in/on the sensing materials, i.e., introduction of the sensing probe, was demonstrated as an effective way of improving the selectivity and specificity through a one-lock one-key binding or structure similarity-based combination. Both the inorganic and organic probes have been well developed. The sieving of interferon, especially the humidity in the environment, is an alternative way of improving specificity.

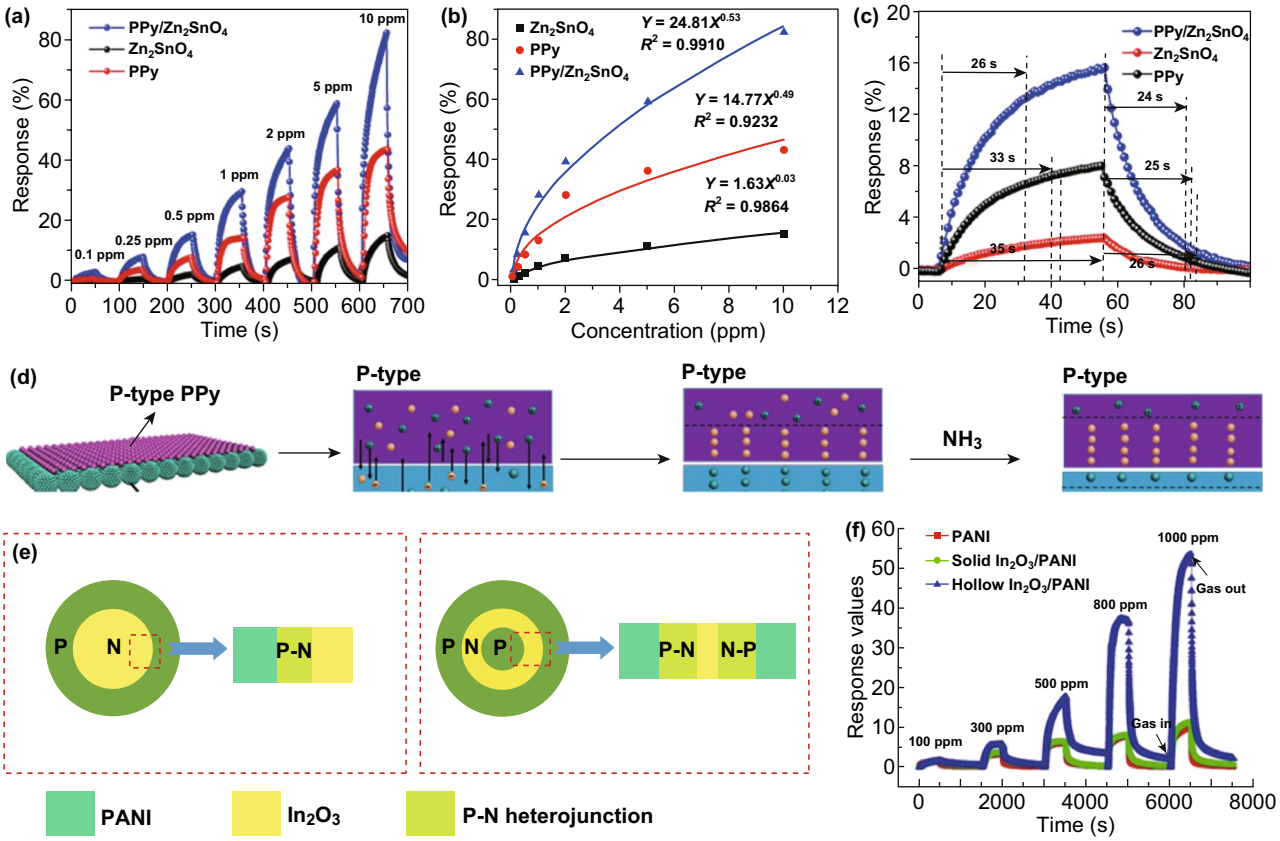

Fig. 13 **a** NH_3 response to PPy-Zn_2SnO_4, PPy, and Zn_2SnO_4. **b** Curve of concentration versus response. **c** Curve of a single response and recovery to NH_3. **d** Schema of sensing mechanism. Reproduced with permission [121]. Copyright 2018, Elsevier. **e** Schema of sensing mechanism. **f** Gas response of PANI, solid In_2O_3/PANI and hollow In_2O_3/PANI. Reproduced with permission [122]. Copyright 2016, Springer

Table 4 Representative works based on heterojunctions

Materials	Gas detection	Detection range	Work temperature	Refs.
α-Fe_2O_3/SnO_2	Acetone	10–2000 ppm	250 °C	[241]
ZnO/SnO_2	NO_2	200–2000 ppb	RT	[242]
SnO_2/SnS_2	NO_2	1–8 ppm	80 °C	[243]
SnO_2/α-Fe_2O_3	Ethanol	20–100 ppm	225 °C	[244]
ZnO/$ZnFe_2O_4$	Acetone	5–700 ppm	250 °C	[245]
α-Fe_2O_3/NiO	Toluene	5–100 ppm	300 °C	[246]
SnO_2/SnS_2	NH_3	10–500 ppm	RT	[247]
TiO_2 QDs/NiO	NO_2	5–60 ppm	RT	[248]
ZnO/MoS_2	Acetone	10–500 ppb	350 °C	[249]
ZnO/$ZnCo_2O_4$	Acetone	50–300 ppm	175 °C	[250]
Si/SnO_2	H_2S	10–50 ppm	100 °C	[251]
SnO_2@PANI	NH_3	10 ppb–100 ppm	RT	[252]
NiO@SnO_2	H_2S	0.1–50 ppm	250 °C	[253]
SnS_2/SnS	NO_2	0.125–8 ppm	RT	[254]
SnO_2/Sn_3O_4	NO_2	20 ppb–50 ppm	150 °C	[255]
ZnO/$ZnCo_2O_4$	Acetone	10–100 ppm	275 °C	[256]
In_2O_3/ZnO	HCHO	5–100 ppm	RT	[257]

https://doi.org/10.1007/s40820-020-0407-5

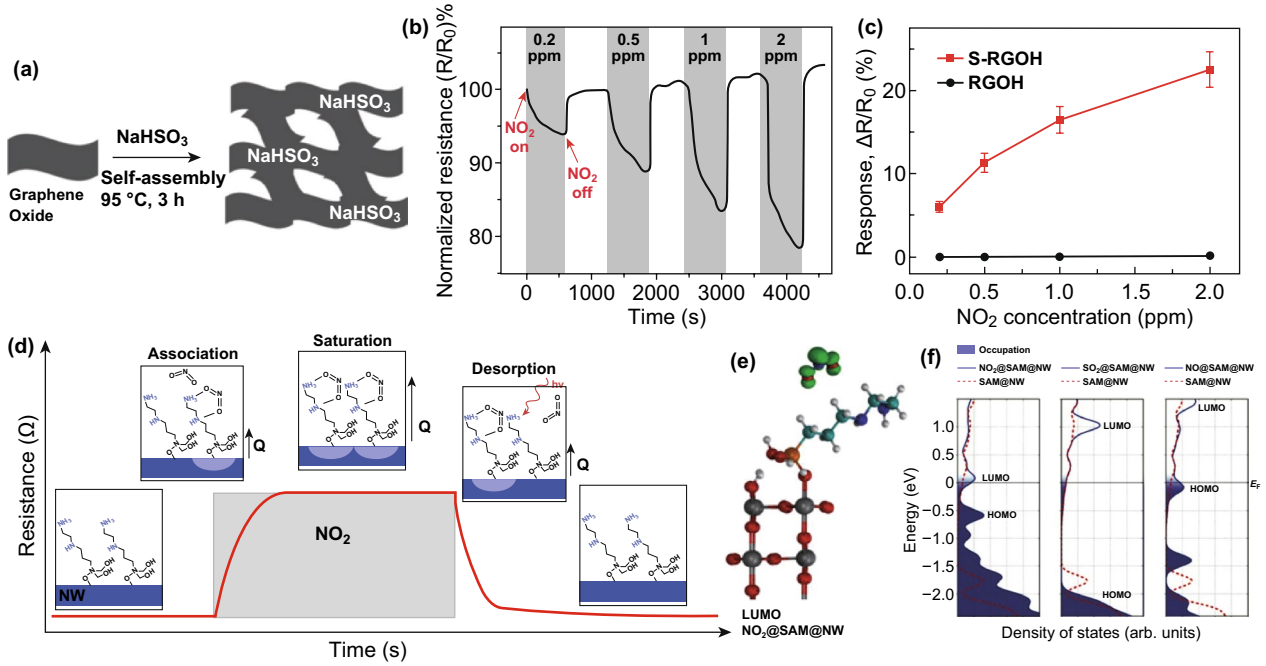

Fig. 14 **a** Schema of the synthesis of 3D chemically modified graphene hydrogel. **b** Dynamic response of the 3D S-RGOH sensor versus time after exposure to 0.2–2 ppm NO_2. **c** Plots of the quantitative responses of the S-RGOH and RGOH sensors versus NO_2 concentration. Reproduced with permission [68]. Copyright 2017, Wiley–VCH. **d, e** Schematic illustration of the NO_2 sensing mechanism by en-APTAS 1-modified NWs. **f** Density of states (DOS) of the en-APTAS 1-modified SnO_2 with adsorbed NO_2, SO_2, and NO. The Fermi levels of the different systems are set at 0 eV. For comparison, the DOS of the en-APTAS 1-modified SnO_2 NW without an adsorbed gas molecule (dashed red line) is shown in each graph. Reproduced with permission [70]. Copyright 2014, Wiley–VCH

A 3D sulfonated rGO hydrogel (S-RGOH)-based gas sensor combining chemical functionalization and porous structures was synthesized in a one-step hydrothermal reaction (Fig. 14a) [68]. Addition of a $NaHSO_3$ probe dramatically enhanced the response (Fig. 14c) of NO_2 with fast recovery (Fig. 14b), assisted by the porous structures of the graphene host. Self-assembled monolayers (SAMs) with suitable alignment of the gas–SAM frontier molecular orbitals (Fig. 14e) with respect to the SAM–NW Fermi level (Fig. 14f); this led to high selectivity and sensitivity to analyte gas [70]. SnO_2 NWs were modified with amine-terminated SAM and applied as light-driven chemi-resistors working at RT, achieving good NO_2 sensing performance, the schematic mechanism of which can be found in Fig. 14d. This concept was extended to porous MOX nanostructures for further enhancements of their sensing properties. APTES-modified porous WO_3 nanotubes (P-WO_3 NTs (10%)@APTES) performed the best sensitivity and selectivity (Fig. 14a), which can be ascribed to the large surface area and high gas diffusion rate provided by P-WO_3, and selective reaction between NO_2 and surface SAM with APTES (Fig. 15b, c). The existence of SAM on the surface of inorganic materials (except 2D nanomaterials) limits the working temperature, which greatly weakens the sensing performance, although it could be resolved by UV irradiation. Using conductive polymer as the host material with surface SAM functionalization by the "1-stone 2 birds" strategy was promising and novel (Fig. 15d, e) [72]. Superb sensing performances were achieved by combining RT sensitivity of CP and good selectivity of SAM (Fig. 15f) [72].

Figure 16a shows the low cross-sensitivity to humidity and other interferon gases by refreshing the regenerative surface involving the interaction between facile redox fair (Tb^{3+}/Tb^{4+}) and surface OH group (or water vapor) on SnO_2. This 5 Tb–SnO_2-based chemi-resistor achieved high response to acetone exposure [128]. The oleic acid SAM also was effective in screening the effect of humidity (< 350 ppm) when it was layered on PANI surface (Fig. 16b, c) [82]. Although it is not enough for practical application, this demonstration is still valuable in pointing to a promising way to eliminate the interferon of humidity.

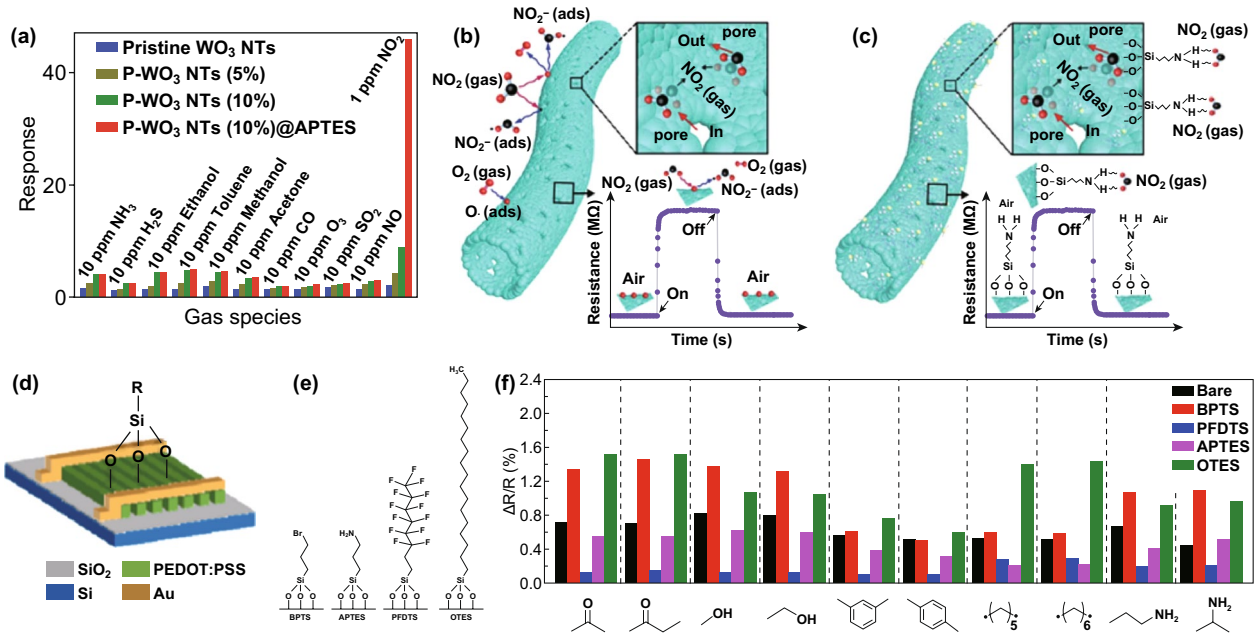

Fig. 15 **a** Selectivity comparison of different gas sensors at the corresponding operating temperature. Schematic illustration of the NO_2 sensing mechanism of sensors based on **b** P-WO_3 NTs (10%) and **c** P-WO_3 NTs (10%)@APTES. Reproduced with permission [71]. Copyright 2018, Royal Society of Chemistry. **d** The schema of silane-coated PEDOT:PSS sensor. **e** The molecular chain of different silane-coated on PEDOT:PSS. **f** Response to VOCs. Reproduced with permission [72]. Copyright 2018, Royal Society of Chemistry

Recently, MOF materials are great opportunity in generating sub-nanometer or nanometer pores with high uniformity. Neat MOFs chemi-resistors were prepared based on hydrophobic MOF (ZIF-67), which showed selective response to VOCs, with slightly interfering effects of humidity (Fig. 17a) [129, 130]. ZnO@ZIF-8 core-sheath NRs powders were synthesized by hydrothermal reaction using a self-template strategy (Fig. 17b) [131]. The chemi-resistive gas sensor based on the thick film of ZnO@ZIF-8 hybrids had satisfactory sensitivity and response time to 100 ppm formaldehyde, even under interfering humidity (Fig. 17c). Mixing the CP with molecularly imprinted polymer (MIP) molecular (Fig. 17d) was another effective approach to improve not only the responsivity, but selectivity (Fig. 17f) [132]. Responses of interferon (2,4,6-TNT) and analyte (2,4-DNT) were suppressed and enhanced, respectively, although they are of very similar molecular structure and functional group [132]. However, the speed of response and recovery showed no obvious change (Fig. 17e) [132]. Instead of using functional MOFs as filter film coating on sensing materials to provide additional selectivity and/or sensitization, EC-MOFs are novel emerging materials with regular porosity and conductivity, which are promising for chemi-resistors with high sensitivity and selectivity [76, 133–158]. Unlike MOX and MOX-MOFs, which still need additional thermal or photonic energy as the trigger source to activate the sensing reaction, EC-MOFs can be directly used as sensitive materials based on their regular micro-porosity, selective frameworks, high electronic conductivity, and RT activity [139, 144–146, 159–166]. Therefore, EC-MOFs are promising components for hybrid gas sensors and will be powerful competitors for the new generation of gas sensors.

As mentioned above, the introduction of molecular probing and sieving effect can effectively overcome the poor selectivity problem of chemi-resistors. Up to date, only a few organic/inorganic probe or porous materials with molecule sieving effects have been applied to chemi-resistors to realize simple guest–matrix interaction (e.g., -NH_2 group with NO_2, –NO_2 group with NH_3, $NaHSO_3$ with NO_2) or molecule rejection (e.g., anti-humidity, gas molecules with large kinetic diameter). Such cases are ultra-small fraction of the state-of-art gas molecule adsorption and separation areas. More guest–matrix interactions (e.g., van der Waals interactions, hydrogen bond, π–π interactions, weak acid–base interactions) and gas separation design (e.g., channel traffic

https://doi.org/10.1007/s40820-020-0407-5

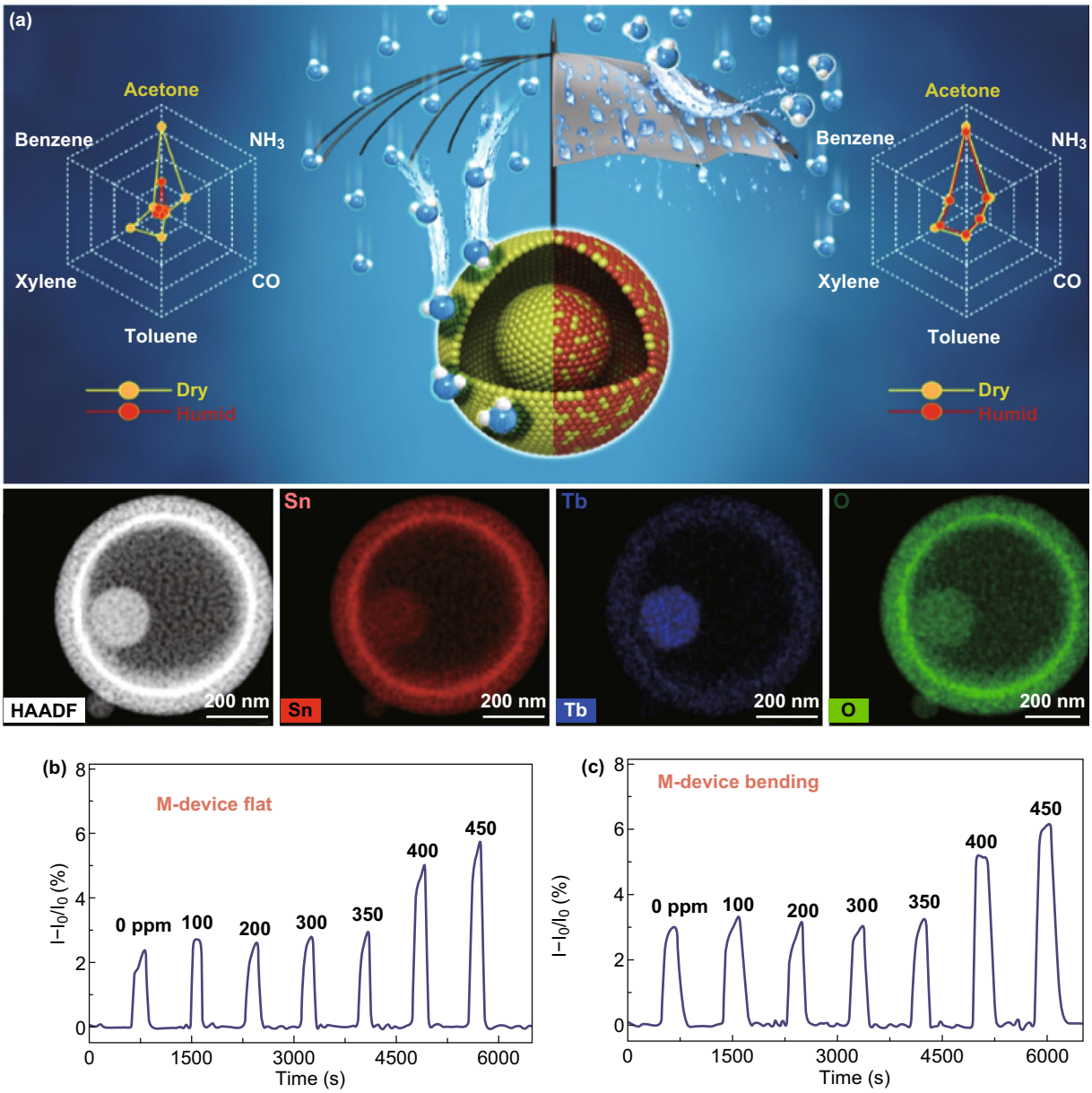

Fig. 16 **a** Polar plots of the gas responses of pure SnO_2 and 5 Tb–SnO_2 sensors exposed to different gases (at 20 ppm) in dry (yellow) and RH 80% (red) atmospheres, and EDS elemental mapping of Sn, Tb, and O in 5 Tb–SnO_2. Reproduced with permission [128]. Copyright 2018, American Chemical Society. **b, c** Response curves to 1-hexanal at different humidity in bending and flat states. Reproduced with permission [82]. Copyright 2018, Wiley–VCH. (Color figure online)

effects, framework flexibility), that have been well studied on rGO, polymers (e.g., metal-induced ordered microporous polymers (MMPs), covalent-organic frameworks (COFs), conjugated mesoporous/microporous polymers (CMPs)), MOFs, can be introduced to chemi-resistors for advanced sensing performances. The representative works are summarized in Table 5.

3.6 Hybrid Gas Sensors Based on Combined Mechanisms

In many cases, multi-forms working on the hybrid materials can simultaneously and dramatically improve sensitivity and responsivity. When the heterojunction barrier (the SnO_2/rGO heterostructure interface) was combined

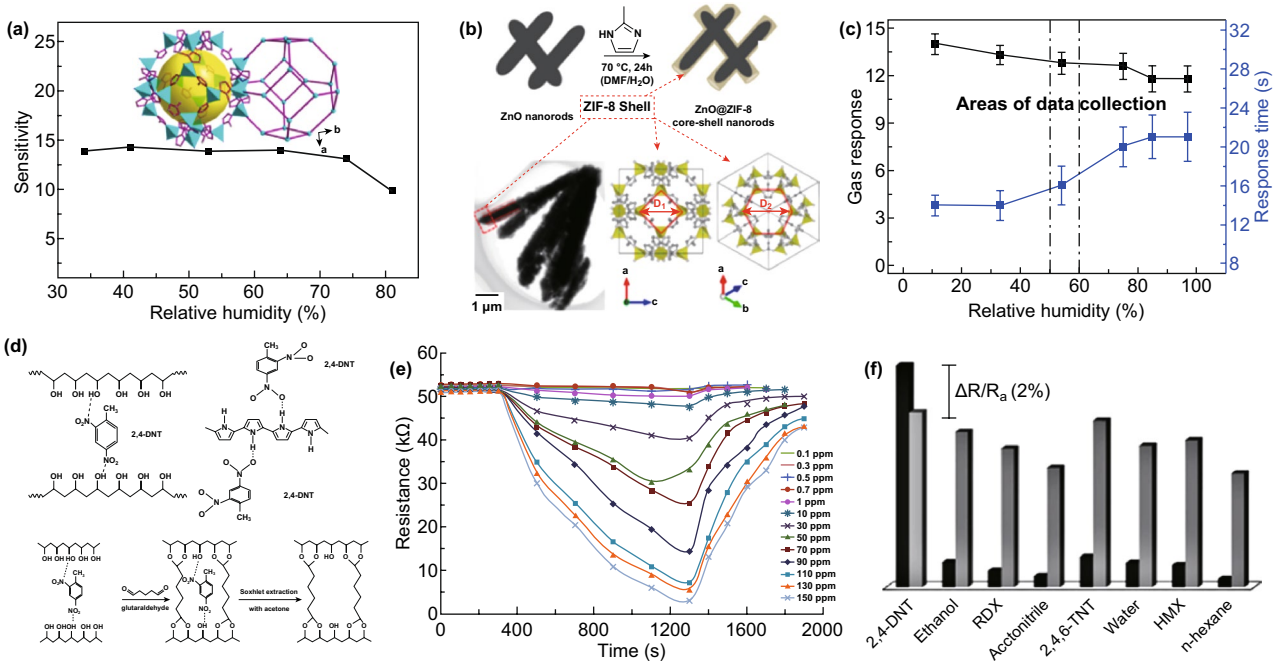

Fig. 17 **a** Effect of environmental humidity on sensitivity of ZIF-67 sensor (inset is the SOD-type structure of ZIF-67). Reproduce with permission [129]. Copyright 2014, American Chemical Society. **b** Schematic diagram of the ZnO@ZIF-8 NRs synthesized with ZnO NRs as a template; and **c** gas response and response time for 100 ppm formaldehyde as a function of the relative humidity. Reproduced with permission [131]. Copyright 2016, American Chemical Society. **d** Schema of the interaction of 2,4-DNT with the hybrid ingredients (PVA, PPy, and MIP). **e** Response of a fabricated chemi-resistor sensor coated with PVA/PPy/MIP hybrids with respect to the 2,4- DNT explosive vapor. **f** Column curves of PVA/PPy/MIP hybrids to different organic compounds. Reproduced with permission [132]. Copyright 2018, Wiley–VCH

Table 5 Representative works based on molecular probing and sieving effect

Materials	Gas detection	Detection range	Work temperature	Refs.
ZnO@ZIF-71	Benzene	10–200 ppm	250 °C	[258]
ZnO@ZIF-CoZn	Acetone	0.25–100 ppm	260 °C	[259]
ZnO@ZIF-8	H_2	5–50 ppm	250 °C	[260]
ZnO@ZIF-8	Propene Ethene	250 ppm	RT	[261]
Polyoxometalate @ZIF-8@ZnO	HCHO	25–200 ppm	RT	[262]
ZnO@ZIF-8	HCHO	10–200 ppm	300 °C	[263]
ZnO@ZIF-8	H_2	10–50 ppm	300 °C	[264]

with catalytic Pt, sensitivity of the SnO_2/rGO hybrids to H_2 was greatly enhanced (Fig. 18a–e) [74]. Hydrogen ranging from 0.5 to 3% in air could be quantitatively detected at near RT with response and recovery times of 3–7 and 2–6 s, respectively. Furthermore, when the catalytic effect was co-working with the p-n heterojunctions and porous structure (Fig. 19a), Co_3O_4–PdO loaded on n-SnO_2 hybrid hollow nanocubes (Fig. 19b) reached selectivity and response amplitudes for the detection of acetone superior to those MOF-derived metal oxide sensing layers previously reported. Accordingly, the sensor arrays (Co_3O_4-loaded n-SnO_2 HNCs and Co_3O_4–PdO-loaded n-SnO_2 HNCs) can clearly distinguish 1 ppm humid acetone molecules among the seven interfering analytes (Fig. 19c). The reason is electron migration from n-SnO_2 to PdO or p-Co_3O_4 in the multi-junctions significantly influencing the electron depletion regions, which leads to the superb sensitivity (Fig. 19d, e).

https://doi.org/10.1007/s40820-020-0407-5

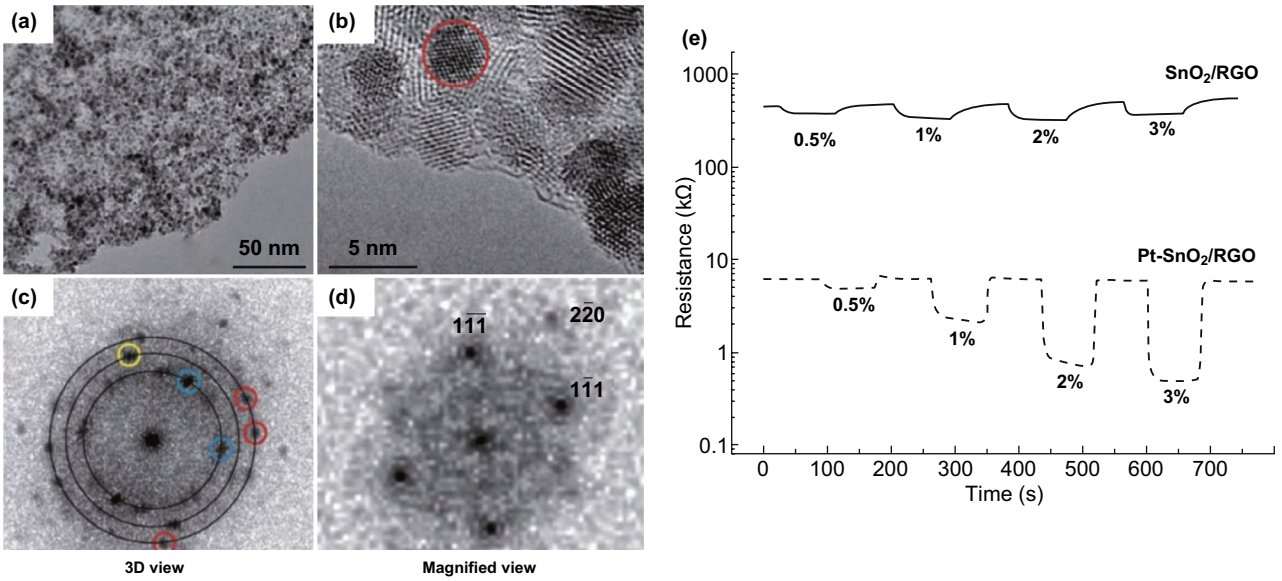

Fig. 18 **a** TEM and **b** HRTEM images of Pt-SnO_2/rGO. Power spectrum of **c** the whole HRTEM image and **d** the region of the HRTEM image indicated by the red circle. **e** Hydrogen-sensing performance at 50 °C of the materials under investigation: variation in the resistance of the rGO/SnO_2 (solid line) and rGO/SnO_2/Pt sensors (dashed line) with pulses of hydrogen at 0.5, 1, 2, and 3%. Reproduced with permission [74]. Copyright 2012, Wiley–VCH

When the catalytic effect co-worked with the molecular sieving effect, improved selectivity (anti-interferon) with enhanced sensitivity can be achieved by coating a layer of hydrophobic and thermally catalytic bimetallic ZIF-CoZn thin film on ZnO to form core-sheath MOX@MOFs nanowire arrays (NWAs) (Fig. 20a) [76]. The bimetallic ZIF-CoZn MOF sheathes gave good thermal stability (ZIF-8(Zn)) and excellent thermal catalytic ability on ZnO (ZIF-67(Co)), as well as hydrophobic channels. By combining their advantages, the ZnO@ZIF-CoZn preparation showed greatly enhanced performance on selectivity (good anti-humidity, Fig. 20b) and also on its response, response and recovery behavior and working temperature (Fig. 20c). More complicated hybrid nanostructures containing MOX, plasmonic/catalytic NMs, and hydrophobic MOFs, i.e., the dual-functional Au@ZnO@ZIF-8 Janus structure (Fig. 20d, e), have been fabricated [77]. Au@ZnO@ZIF-8 hybrids had enhanced selective adsorption, detection and oxidation of HCHO and prevented interference from gases such as H_2O and toluene (Fig. 20f), where Au NRs helped to generate charge carriers on a ZnO surface under visible-light irradiation. The representative works are summarized in Table 6.

4 Summary and Perspective

4.1 Summary of Hybrid Gas-Sensitive Materials

The current progress report reviews advances and the advantages of the chemi-resistive hybrid nanomaterials compared with the single constituent, according to five main sensing mechanisms: manipulating/constructing heterojunctions, catalytic reaction, charge transfer, charge transport, molecular binding/sieving, and their combinations. Table 7 lists typical chemi-resistive materials for hybrid gas sensors categorized by types of materials and conductivity.

4.2 Applications of Chemi-Resistive Sensor-Based e-nose

As the first commercial gas sensor, metal oxide-based chemi-resistors still occupy a leading role in both fundamental researches and commercial devices. Various commercial chemi-resistive gas sensors based on single or hybrid materials have been developed for the detection toward target gases (toxic, flammable, VOCs, explosive, H_2, etc.) ranging from sub-ppm to saturated vapor, which are widely used in fields including environment monitoring, medical care,

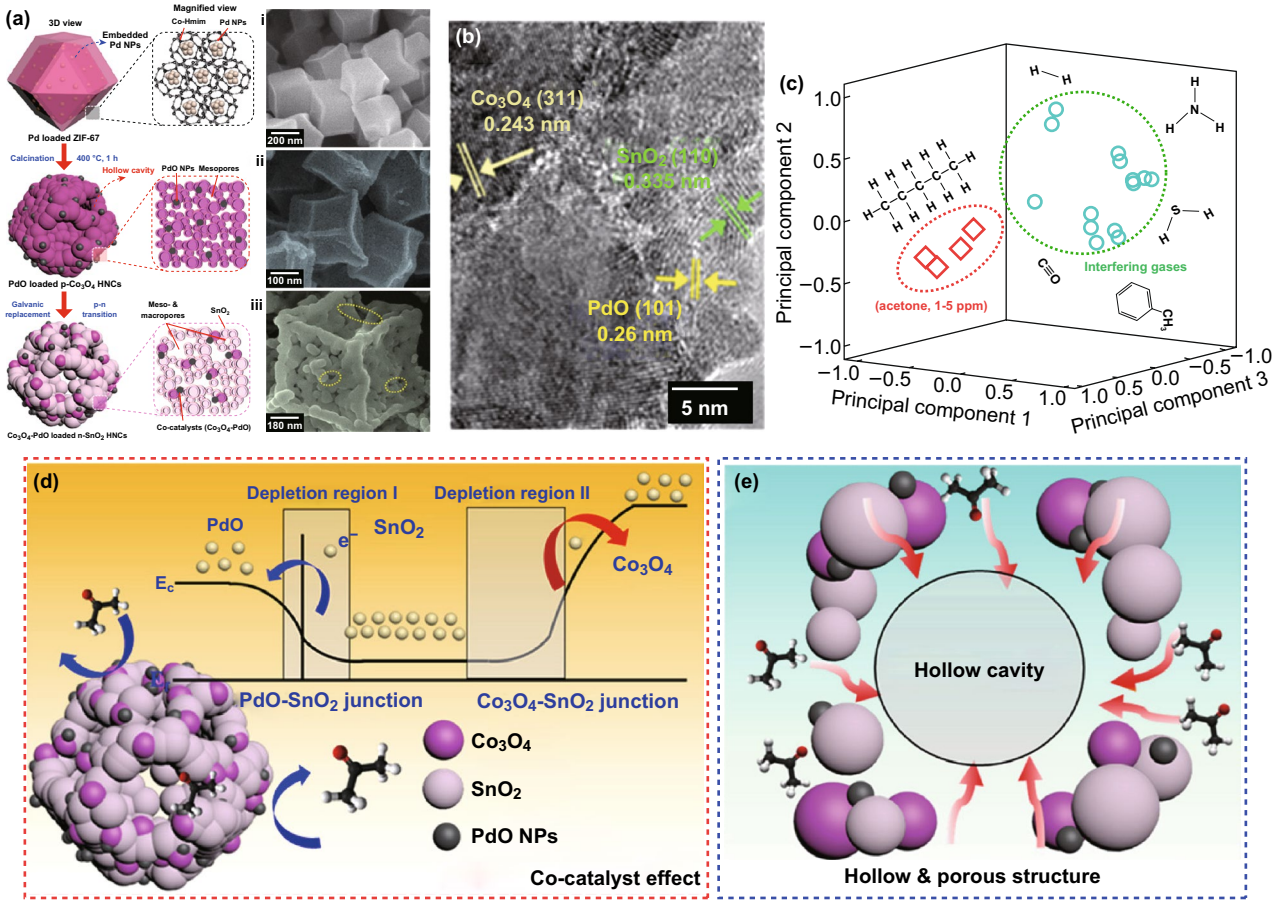

Fig. 19 **a** Schematic illustration and SEM images of synthetic process for the n-SnO_2 HNCs functionalized with Co_3O_4 and PdO. **b** HRTEM lattice spacing image of SnO_2–PdO-loaded p-Co_3O_4 HNCs. **c** Pattern recognition based on PCA using sensor arrays (Co_3O_4-loaded n-SnO_2 HNCs and Co_3O_4–PdO-loaded n-SnO_2 HNCs). Schematic diagrams of **d** gas-sensing reaction derived from co-catalyst effect, and **e** magnified sensing mechanism on the porous surface of HNC. Reproduced with permission [75]. Copyright 2017, Wiley–VCH

food industry, agriculture production, and public security. The versatile commercial chemi-resistive gas sensors are introduced but not limited as follows.

Some e-nose systems comprised of chemi-resistive sensor arrays have succeeded in the application of medical care. Commercial e-nose PEN3 (Airsense Analytics GmbH, Schwerin, Germany) made up of a gas sampling unit and a sensor array (10 different metal oxide thick film sensors (MOS)) can screen colorectal cancer (CRC) and polyps [167]. Another 14 commercial gas sensor-integrated e-nose system could generate characteristic "breath fingerprints" by exhalation components and could diagnose the lung disease through pattern recognition of a "breath fingerprint." Those sensors categorized as MOS, hot wire gas, catalytic combustion gas, and electrochemical gas sensors are produced by the manufacturers, Hanwei (Fig. 21a), Figaro (Fig. 21b) [168], Winsen, Nemoto and Alphasense [169]. Aeonose in (Fig. 21c) [170] is a CE-certified, handheld, and battery-powered e-nose device designed by a Zutphen Company in Netherlands. The aeonose comprises three micro-hotplate metal oxide sensors and a pump to detect gastric cancer from exhaled breath [171]. Sunshine Haick Ltd. have successfully designed the sensor arrays to diagnose lung and gastric cancer via pattern analysis of exhaled VOCs, which has made great and has a perfect perspective. Other representative commercial e-nose in clinical diagnosis of complex regional pain, diabetics, head and neck cancer, dyskinesia, and prostate cancer are summarized in Table 8.

Commercial e-nose has acted as an indispensable instrument for the rapid, accurate, and overall-process assessments of food health and quality aim at adulterated counterpart, contamination and spoilage [172]. An PEN-2 e-nose (WMA

https://doi.org/10.1007/s40820-020-0407-5

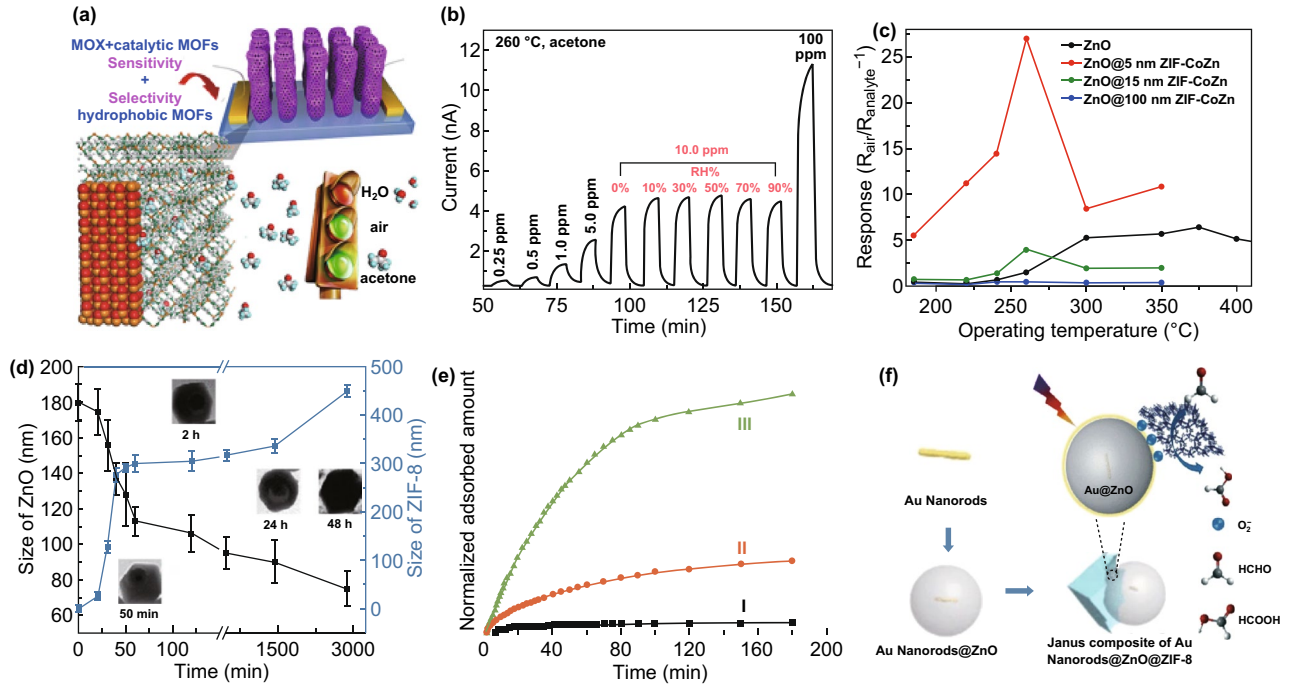

Fig. 20 **a** Schematic illustration of ZnO@ZIF-CoZn core-sheath NWAs sensor; **b** Response-recovery curves to acetone at different concentrations in dry air and in 10 ppm acetone with different relative humidity and at 260 °C; and **c** temperature-dependent responses of ZnO@5 nm ZIF-CoZn. Reproduced with permission [76]. Copyright 2016, Wiley–VCH. **d** Plots of Au@ZnO and Au@ZnO@ZIF-8 size versus time; insets are the representative TEM images of the products at specific times. **e** Kinetics of HCHO adsorption (solid symbols). **f** Proposed mechanism of oxidation of HCHO into HCOOH. Reproduced with permission [77]. Copyright 2018, Springer

Table 6 Representative works based on combined mechanisms

Materials	Gas detection	Detection range	Work temperature	Refs.
Co_3O_4/PEI-CNTs	CO	5–1000 ppm	RT	[265]
$HC(NH_2)_2SnI_3/SnO_2$/Pt	HCHO	5–100 ppm	80 °C	[266]
PdO/SnO_2/CuO	CO	100–2000 ppm	200 °C	[267]
Pd/ZnO/In_2O_3	H_2	50–172 ppb	350 °C	[268]
rGO/ZnO/Pd	CH_4	25–500 ppm	RT	[269]
Pt/ZnO/g-C_3N_4	Ethanol	0.5–50 ppm	250 °C	[270]
	NO_2	0.5–15 ppm	150 °C	
Au/Cu_2O/ZnO	NO_2	5–1000 ppb	RT	[271]
Ag/SnO_2/rGO	Ethanol	100–2000 ppm	280 °C	[272]
TiO_2/$InVO_4$	NH_3	10–1000 ppm	250 °C	[273]
Pd–SnO_2/rGO	CH_4	800–1200 ppm	RT	[274]
Au@In_2O_3@PANI	NH_3	0.5–100 ppm	RT	[275]
Au–ZnO@ZIF-DMBIM	Acetone	0.0001–1000 ppm	RT	[203]
SnO_2/α-Fe_2O_3/Pt	Styrene	0.25–1.25 ppm	206 °C	[276]

Airsense Analysentechnik GmbH, Schwerin, Germany) composed of 10 different metal oxide sensors was utilized to monitor the adulteration of milk with water or reconstituted milk powder [173]. Also, the PEN-2 is used to monitoring the change in volatile production of mandarin during different picking-date [174]. Meanwhile, PEN-2 is used to characterize espresso coffees brewed with different thermal profiles [13]. MOS sensors manufactured by Figaro (Figaro

Table 7 Typical chemi-resistive materials for hybrid gas sensors

Types of chemi-resistive materials	Types of conductivity		
	n	*p*	*n*/*p*
Inorganic compounds	ZnO, SnO_2,TiO_2, MoO_3, WO_3, In_2O_3, V_2O_5, Ta_2O_5, Nb_2O_5, RuO_2, MoS_2, $ZnSnO_3$	NiO, Co_3O_4, TeO_2, CuS, Cr_2O_3, Sb_2O_3, CuO, Cu_2O, Mn_2O_3, CeO_2, PdO, Ag_2O, Bi_2O_3, CoPc. WS_2, $MoSe_2$, $LaFeO_3$ [277]	Fe_2O_3
Organic compounds	PTCDI-Ph	PPy, PEDOT, PANI, p-6P, $Ti_3C_2T_x$ [278] PADS [279]	Polyphenylene [280]
MOFs	CuHITP	Cu-HHTP, NiHITP, NH_2-UiO-66 [281],Cu-HHTP-THQ [204]	
Others			CNTs, BP, rGO

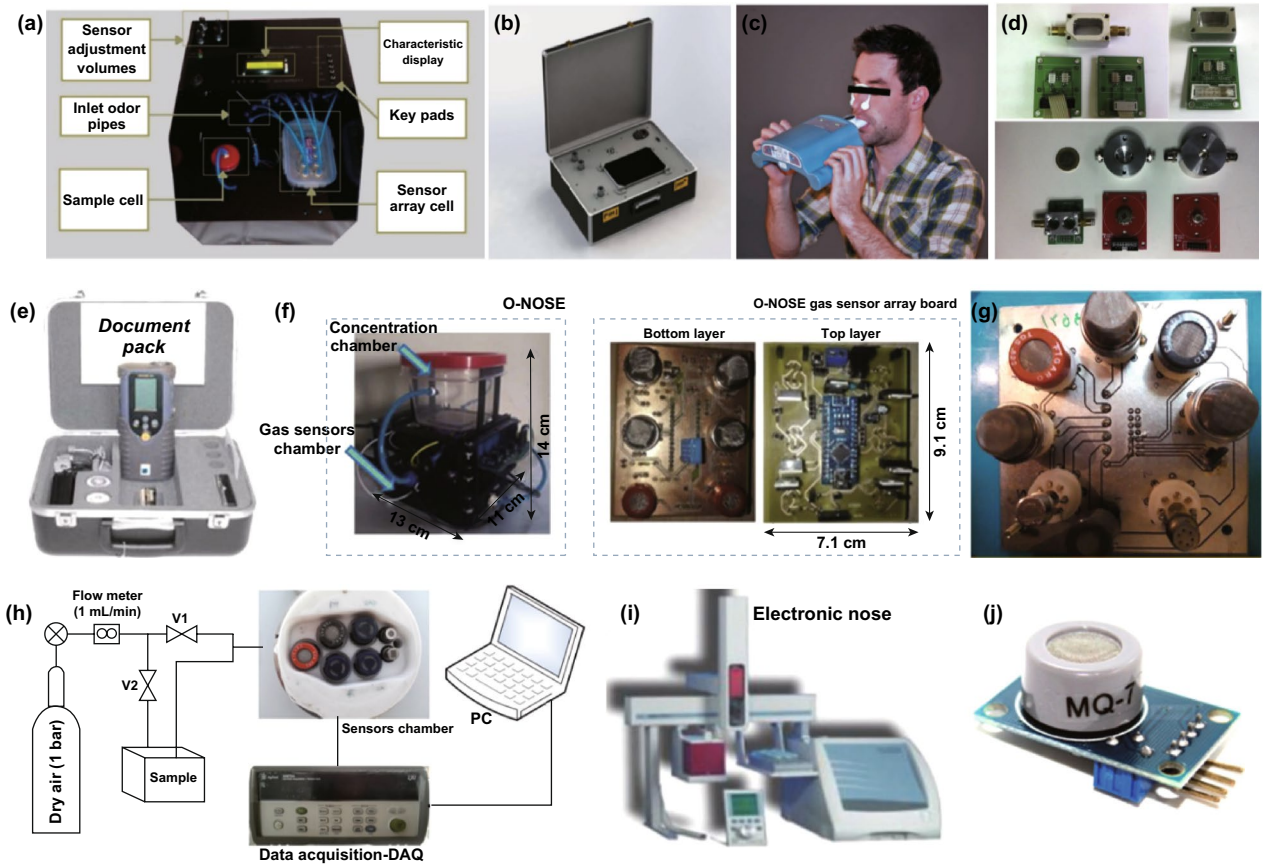

Fig. 21 Schematic of the diffferent commercial e-nose. **a** Photographic image of Hanwei e-nose. Reproduced with permission [212]. Copyright 2017, Springer. **b** E-nose system "NOS.E" produced by Figaro Engineering Inc. [168]. Copyright 2018, IEEE. **c** Aeonose to diagnosis prostate cancer. Reproduced with permission [170]. Copyright 2018, European Association of Urology. **d** E-nose produced by institute of Physics Technology and Information, Spanish Council for Scientific Research. Reproduce with permission [213]. Copyright 2018, Elsevier Ltd. **e** The picture of Cyranose 320. Reproduce with permission [214]. From Chang and Heinemann, Copyright 2018, ASABE. **f** The sensors manufactured by Hanwei Sensors. Reproduced with permission [215]. Copyright 2019, Elsevier Ltd. **g** E-nose produced by Figaro Engineering, Inc., Hanwei company and FIS Inc. Reproduced with permission [216]. Copyright 2018, Elsevier Ltd. **h** E-nose based on MOS TGS and FIS sensors. Reproduced with permission [217]. Copyright 2018, sensors. **I** Fox 3000 electronic nose system. Reproduced with permission [218]. Copyright 2017, Elsevier Ltd. **j** MQ-7 (TORO) sensor model [219]

https://doi.org/10.1007/s40820-020-0407-5

Table 8 Applications of electronic nose instruments for disease diagnosis

Diseases	Objective	E-nose configuration	Sensor type	Sensor arrays	Multivariate data analysis	Refs.
Armpit body odor	Detection and classification of human body odor	Tagushi (TGS) gas sensor from Figaro Engineering Inc.	MOS	5	PCA	[282]
Bile acid diarrhea (BAD)	Identify BAD in volatile organic compounds	The FOX 4000 e-nose from Alpha MOS, Toulouse, France	MOS	18	LDA	[283]
Lung cancer	Diagnosing lung cancer in exhaled breath	Cyranose 320 from Smiths Detection Inc., Edgewood, MD, USA	CP	32	LDA,KNN, PNN, NB, and SVM	[284]
Head/neck and lung carcinomas	Discriminating head and neck carcinoma from lung carcinoma	Aeonose from Zutphen, the Netherlands	MOS	3	PARAFAC and TUCKER	[285]
Prostate Cancer	The detection of prostate cancer from exhaled breath	Aeonose from Zutphen, the Netherlands	MOS	3	ANN	[170]
Complex Regional Pain	Diagnosing complex regional pain syndrome	Aeonose from Zutphen, the Netherlands	MOS	3	ANN	[286]
Mycobacterium tuberculosis	The detection of mycobacterium tuberculosis	ModelBH114-Bloodhound sensors from Leeds, UK	CP	14	PCA	[287]
Patients breath	The VOCs from breath	E-nose from Sunshine Haick medical Co.	GNPs capped with thiols	8–20	PCA, LDA	[112, 288]

MOS metal oxide semiconductor, *CP* conducting polymer, *GNPs* gold nanoparticles

Inc., Japan) were used to recognize odors emitted from different stages in a waste water treatment plant [175]. Tagushi gas sensor based on metal oxide semiconductor from Figaro Engineering Inc. is used to classify the tea aroma [176]. Cyranose 320 in Fig. 21e that consists of an array of 32 thin-film carbon-black conducting polymer sensors was used to identify odor emitted from dairy operations. The portable e-nose based on thin-film semiconductor (SnO_2) sensors (Hanwei Sensors) in Fig. 21f can perform early detection of wine spoilage thresholds in routine tasks of wine quality control. An e-nose system (Fig. 21g) was used to detect detergent powder in raw milk. Representative applications are summarized in Table 9.

The application of commercial e-nose to monitor volatile compounds in the environment both indoor and outdoor provides a reliable solution. Single semiconductor gas sensor GGS 10331 (produced by Umwelt Sensor Technik) was made with a semiconductor sensing layer on Al2O3 substrate to predict the concentration of ammonia under humidity interference [177]. Tagushi (TGS) gas sensor (Figaro Engineering Inc.) was applied to detect NH_3, CO, H_2, C_2H_6O, C_4H_{10}, C_3H_8, CH_4, alcohol, and solvent vapors and the accuracy was 100% [178]. MQ-7 (Fig. 21j) is a commercial electronic nose for monitoring CO. Portable electronic noses in Fig. 21d were used to classify pollutants in water. Similarly, the commercial e-nose is widely used to identify the toxic wastes, soil/water pollution, indoor volatile organic compounds, etc. Table 10 summarizes the recent applications of e-nose for monitoring environment.

E-nose is widely used in agricultural to analyze growth, classify seeds, detect the maturity, monitor quality, which promoted agricultural modernization and saved labor [2]. Eight MOS sensors produced by FIS (Osaka, Japan), MQ (Hanwei, China), and TGS (Figaro Engineering Inc.) were applied for classifying cumin, caraway, and other seeds [179]. Similarly, e-nose based on MOS TGS and FIS sensors (Fig. 21h) were distinguished Iranian Rosa damascena essential oils. An e-nose FOX 4000 (Alpha MOS, Toulouse, France) was chosen to analyze ginseng at different stages [180]. An e-nose FOX 3000 (Fig. 21i) was applied

Table 9 Applications of electronic nose for monitoring foods and beverage

Product	Objective	E-nose configuration	Sensor type	Sensor arrays	Multivariate data analysis	Refs.
Black tea	Monitoring of black tea fermentation process	Tagushi (TGS) gas sensor from Figaro Engineering Inc.	MOS	8	PCA, 2NM MDM	[289]
Pork	Measurement of total volatile basic nitrogen (TVB-N) in pork meat	Tagushi (TGS) gas sensor from Figaro Engineering Inc.	MOS	11	PCA and BP-ANN	[290]
Green tea	Identification of coumarin-enriched Japanese green teas and their particular flavor	E-nose device (FF-2A Fragrance & Flavor Analyzer, Shimadzu, Japan)	OSS	10	PCA, CA	[14]
Milk	Aroma profiling of milk adulteration	A PEN-2 e-nose from Win Muster Airsense Analytics Inc., Schwerin, Germany	MOS	10	PCA, LDA and 4ANN	[291]
Meat	Analysis adulteration of minced mutton with pork	A PEN-2 e-nose from Win Muster Airsense Analytics Inc., Schwerin, Germany	MOS	10	CDA, BDA, PLS, MLR, BPNN	[292]
Ham	Differentiation of hams marked	A PEN-2 e-nose from Win Muster Airsense Analytics Inc., Schwerin, Germany	MOS	10	PCA	[293]
Cherry tomato Juice	Classification with overripe tomato juice	A PEN-2 e-nose from Win Muster Airsense Analytics Inc., Schwerin, Germany	MOS	10	PCA, CA	[294]
Tea	Characterizing the degree of invasion of tea trees	A PEN-2 e-nose from Win Muster Airsense Analytics Inc., Schwerin, Germany	MOS	10	PCA and MLP	[295]
Sausage	Evaluation of lipid oxidation of Chinese-style sausage	A PEN-3 e-nose from Win Muster Airsense Analytics Inc., Schwerin, Germany	MOS	10	SVM, ANN, PLSDA, MLR	[296]
Mango	Quality rapid determination of mango	E-nose from HANWEI Electronics Co.	MOS	8	PCA and SR	[297]
Chicken fat	Rapid measuring of oxidized chicken fat	The FOX 4000 e-nose from Alpha MOS, Toulouse, France	MOS	18	APLSR and ANOVA	[298]
Honey	Identify the botanical origin of honeys	The FOX 3000 e-nose from Alpha MOS, Toulouse, France	MOS	18	PCA, DFA, LS-SVM and PLS	[299]
Orange juice	Classification of Valencia orange juices	The FOX 3000 e-nose from Alpha MOS, Toulouse, France	MOS	12	PCA, FDA	[300]
Wine	Geographical origin confirmation	The FOX 3000 e-nose from Alpha MOS, Toulouse, France	MOS	12	LDA	[301]
Coffee	Study the aromatic profile of espresso coffee as a function of the grinding grade and extraction time	αFOX from Alpha MOS, Toulouse, France	MOS	6	PCA	[302]
Cheese	Authenticity of cheese marked with Picorino	EOS 507 from Sacmi Imola S.C., Imola, Bologna, Italy	MOS	6	PCA, ANN	[303]

https://doi.org/10.1007/s40820-020-0407-5

Table 9 (continued)

Product	Objective	E-nose configuration	Sensor type	Sensor arrays	Multivariate data analysis	Refs.
Tea	Classification of pure Sri Lanka tea	Model 3320 applied sensor lab emission analyzer from applied Sensor Co., Linkoping, Sweden	MOSFET MOS	10 12	PCA, PLS	[304]
Honey	Botanical origin and adulteration with cane sugar	Cyranose 320 from Intelligent Optical Systems Inc., CA, USA	CP	32	PCA, LDA	[305]

OSS oxide semiconductor sensors, *MOSFET* metal oxide semiconductor field-effect transistor

Table 10 Applications of electronic nose in environmental monitoring

Target gases	Objective	E-nose configuration	Sensor type	Sensor arrays	Multivariate data analysis	Refs.
Ethanol, acetone	The detection of ethanol and acetone in outdoor courtyard	Tagushi (TGS) gas sensor from Figaro Engineering Inc. (TGS2600, TGS2602,TGS2611TGS2620)	MOS	4	MoGC and K-NNC	[306]
Air	The quantification of VOC at indoor environments	Figaro TGS2602 air contaminant sensor	MOS	14	PLS-2 calibration models	[307]
Air	The detection of NH_3, CO, H_2, C_2H_6O, C_4H_{10}, C_3H_8, CH_4, Alcohol	A sensor array composed of TGS826,TGS2442,TGS2600, TGS2602TGS2610,TGS2611, TGS2620	MOS	7	LDA, PCA, DT, KNN	[178]
Air	The detection of xylene	TGS2620	MOS	1	N/A	[308]
Air	The detection of n-hexane, acetone, and toluene	e-nose consists of TGS813, TGS2106, TGS2444, TGS244, TGS822, TGS2602, TGS2201, TGS2201	MOS	8	PLS and PCR	[309]
Air	The detection of methane, hydrogen, carbon monoxide	A gas e-nose system based on TGS2611, TGS821, TGS2442	MOS	3	ANNs	[310]
Inorganic analytes emissions	Analysis in landfill and industrial area chemical emissions monitoring	E-nose from Alphasense Inc.	MOS	7	LDA	[311]
Toxic wastes	The detection of ammonia	GGS10331 from Umwelt Sensor Technik	MOS	1	PCA and PLS	[177]
Air	The detection of NO_2	MiCS-2714 produced by SGX Sensortech	MOS	1	N/A	[312]
Odorless gases	The detection of CO and CH_4	MQ sensors from Hanwei Electronics Co.	MOS	6	ANN and LSR	[219]

to characterize and classify seven Chinese robusta coffee cultivars. Commercially available chemical sensors intended for agriculture are summarized in Table 11.

Some commercial e-noses are attempted to detect explosives with ultra-low saturated concentration (parts-per-billion or below) [181]. Figaro Engineering Inc. produce an e-nose comprised of eight MOS sensors to discriminate and quantify different chemical warfare agents mimics [182]. More expectations in applications are also possible in the future.

Table 11 Applications of electronic nose in agriculture

Product	Objective	E-nose configuration	Sensor type	Sensor arrays	Multivariate data analysis	Refs.
Sesame oil	Detection adulteration in sesame oil	A PEN-2 e-nose from Win Muster Airsense Analytics Inc., Schwerin, Germany	MOS	10	PCA, FLT, Step-LDA, SFW, PNN, BPNN, GRNN	[313]
Olive oils	The detection of olive oils	A PEN-2 e-nose from Win Muster Airsense Analytics Inc., Schwerin, Germany	MOS	10	PCA	[314]
Red raspberries	The aromatic characteristics of red raspberries	A PEN-2 e-nose from Win Muster Airsense Analytics Inc., Schwerin, Germany	MOS	10	PCA	[315]
Compost maturity	The monitoring of composting process produces	A PEN-3 e-nose from Win Muster Airsense Analytics Inc., Schwerin, Germany	MOS	10	PCA	[316]
Hyssopus officinalis	Discriminate the accessions	A PEN-3 e-nose from Win Muster Airsense Analytics Inc., Schwerin, Germany	MOS	10	PCA and HCA	[317]
Rice	Estimation of the age and amount of brown rice plant	A PEN-3 e-nose from Win Muster Airsense Analytics Inc., Schwerin, Germany	MOS	10	PCA, LDA, PNN, and BPNN	[318]
Jujubes	Characterization of different varieties of Chinese jujubes	A PEN-3.5 e-nose from Win Muster Airsense Analytics Inc., Schwerin, Germany	MOS	10	PCA and LDA	[319]
Virgin olive oil	Adulteration with hazelnut oil	The FOX 4000 e-nose from Alpha MOS, Toulouse, France	MOS	18	PCA and PLS	[320]
Ginseng	Discrimination of American ginseng and Asian ginseng	The FOX 4000 e-nose from Alpha MOS, Toulouse, France	MOS	18	PCA and PLS	[321]
Flax seed oil	Differently processed oils for fraud detection	The FOX 3000 e-nose from Alpha MOS, Toulouse, France	MOS	18	PCA	[322]
Lonicera japonica	Quality control of Lonicera Japonica stored for different period of time	The FOX 3000 e-nose from Alpha MOS, Toulouse, France	MOS	12	LDA, PCA, and RBF-ANN	[323]
Tomato	Comparison of different stages of tomato	The FOX 4000 e-nose from Alpha MOS, Toulouse, France	MOS	18	PCA and ANOVA	[324]
White pepper	The chemical and flavor qualities of white pepper	α-Gemini from Alpha M.O.S. SA, Toulouse, France	MOS	6	PCA	[325]
Virgin olive oil	Confirmation of geographical origin and authentication	Model 3320 applied sensor lab emission analyzer from applied Sensor Co., Linkoping, Sweden	MOSFET MOS	10 12	PCA, CP-ANN	[326]
Asphalt odor	Asphalt odor patterns in hot mix asphalt production	Cyranose 320 from Intelligent Optical Systems Inc., CA, USA	CP	32	Polar plots, PCA	[327]
Plant Pest and Disease	The discrimination of plant pest and disease	Model ST214 from Scensive Technologies Ltd., Normanton, UK	OCP	13	PCA, DFA, CA	[328]
Odors emissions	Monitoring of odors from a composting plan	EOS from Sacmi Group, Imola, Italy	MOS	6	kNN	[329]

OCP organic conducting polymer

4.3 Challenges and Perspectives

Although excellent advances in both e-nose system and chemi-resistive sensory unit have been reached in the field during the last few years, there is still room for improvements. Below is a summary of the main rules for improving the performance of hybrid material-based gas sensors (details see the summary paragraph of each section):

https://doi.org/10.1007/s40820-020-0407-5

For sensors based on heterojunctions (potential energy barrier manipulation), the more uniform and the larger the contact area of heterojunctions and charge transfer hybrids, the higher the response, resulting in faster speed/lower operating temperature, e.g., Fe_2O_3/TiO_2 tube-like quasi-1D nanostructures (n–n) [114], n-ZnO/p-CoPc [119], CeO_2–In_2O_3 hollow spheres with anti-humidity properties [113], and CdS–ZnO [123, 124].

For sensors based on catalytic effect assistance, the higher the potential energy barrier tuning, the higher the response, e.g., Pd/Sb–SnO_2 [89, 90].

For sensors based on charge transfer, the more dispersion uniformity and the smaller size of catalysts on host-sensing materials, the higher the response, giving faster speed and lower operating temperatures, e.g., SnO_2 QDs/rGO hybrids [109], rGO/MoS_2 aerogel [61], and PANI/rGO [63].

For sensors based on regulation of charge carrier transport, the thinner and the more defect-rich of the hybrid film (e.g., suppression of original gas-off current in current-increased gas sensor), the higher and faster the responses obtained, e.g., PTCDI-Ph/p-6P ultrathin film [64], sandwiched PMMA/Pd/PMMA [110], and MSP-covered CNTs [80].

For sensors based on molecular binding/sieving, the more selective and uniform dispersion of molecular binding/sieving guests, the higher the selectivity, e.g., APTES-modified porous WO_3 nanotubes [72], the oleic acid SAM-modified PANI [82], the ZnO@ZIF-CoZn NWAs [76] P-O3 NTs (10%)@APTES [71].

Improving the performance requires better understanding of the mechanism. Recently, most sensing mechanism represented in the research articles is "possible mechanism" based on the results of comparative tests instead of direct observations. Exactly, the latter one is more trustable and solid results to support the mechanism study, e.g., in situ FTIR [183, 184], in situ Kelvin probe [185], in situ STM [186, 187], in situ TEM [188, 189]). In addition, Theoretically studies (such as DFT simulation) [190], are also helpful for researchers to understand the interaction between the gas analyte and sensitive materials, the succedent electronic structure changes, or band gap regulation in heterojunction, or charge transfer, etc., which can guide the orientation of materials design [70, 190–195]. Otherwise, learning theoretical studies toward hybrid catalyst designs can inspire the further researches on hybrid gas sensing due to the similar surface physical/chemical science, band gap theories, and charge transfer process [196–201].

Controlling the fluidic behavior of gas [202], enhancing the anti-interferon ability by loading novel porous sieving materials (e.g., MOF, COF) [203–206], screening the cross-talk (such as deformation [207, 208]) by special micro-/nanostructures, deeply mining the features of sensing signal [209] (e.g., response, area of peak, and speed), and enhancing catalysis effect using small NPs, clusters, or even single-atom catalyst [108] are the long-term challenges of hybrid gas-sensing materials to adapt the applications under real-world conditions [210, 211]. The advances in knowledge in all our endeavors can be a foundation and useful experience for sensing technology, surface science, catalysis, fluidic mechanics, and microelectronics.

Acknowledgements This research was funded by the Phase-II Grand Challenges Explorations award from the Bill, Melinda Gates Foundation (Grant ID: OPP1109493), International Research Fellow of the Japan Society of the Promotion of Science (JSPS, Postdoctoral Fellowships for Research in Japan (Standard), P18334), the National Natural Science Foundation of China (21801243), and the Natural Science Foundation of Shaanxi province (2018JM6045, 2018JM1046). Research funding was received from Shanghai Key Lab for Urban Ecological Processes and Eco-Restoration (SHUES2019A02).

References

1. H.D. Kotha, V.M. Gupta, IoT application: a survey. Int. J. Eng. Technol. **7**(2.7), 891–896 (2018). https://doi.org/10.14419/ijet.v7i2.7.11089
2. W. Hu, L. Wan, Y. Jian, C. Ren, K. Jin et al., Electronic noses: from advanced materials to sensors aided with data processing. Adv. Mater. Technol. **4**(2), 1800488 (2018). https://doi.org/10.1002/admt.201800488
3. T.T. Dung, Y. Oh, S.-J. Choi, I.-D. Kim, M.-K. Oh, M. Kim, Applications and advances in bioelectronic noses for odour

sensing. Sensors **18**(1), 103 (2018). https://doi.org/10.3390/s18010103

4. J. Zhang, X. Liu, G. Neri, N. Pinna, Nanostructured materials for room-temperature gas sensors. Adv. Mater. **28**(5), 795–831 (2015). https://doi.org/10.1002/adma.201503825
5. I.-D. Kim, A. Rothschild, H.L. Tuller, Advances and new directions in gas-sensing devices. Acta Mater. **61**(3), 974–1000 (2013). https://doi.org/10.1016/j.actamat.2012.10.041
6. J.F. Fennell, S.F. Liu, J.M. Azzarelli, J.G. Weis, S. Rochat, K.A. Mirica, J.B. Ravnsbæk, T.M. Swager, Nanowire chemical/biological sensors: status and a roadmap for the future. Angew. Chem. Int. Ed. **55**(4), 1266–1281 (2015). https://doi.org/10.1002/anie.201505308
7. K. Ihokura, J. Watson, *The Stannic Oxide Gas Sensor principles and Applications* (CRC Press, London, 2017). https://doi.org/10.1201/9780203735893
8. G. Korotcenkov, B.K. Cho, Metal oxide composites in conductometric gas sensors: achievements and challenges. Sens. Actuat. B: Chem. **244**, 182–210 (2017). https://doi.org/10.1016/j.snb.2016.12.117
9. A. Kaushik, R. Kumar, S.K. Arya, M. Nair, B.D. Malhotra, S. Bhansali, Organic-inorganic hybrid nanocomposite-based gas sensors for environmental monitoring. Chem. Rev. **115**(11), 4571–4606 (2015). https://doi.org/10.1021/cr400659h
10. I. Stassen, N. Burtch, A. Talin, P. Falcaro, M. Allendorf, R. Ameloot, An updated roadmap for the integration of metal–organic frameworks with electronic devices and chemical sensors. Chem. Soc. Rev. **46**(11), 3185–3241 (2017). https://doi.org/10.1039/C7CS00122C
11. Y. Li, A.-S. Xiao, B. Zou, H.-X. Zhang, K.-L. Yan, Y. Lin, Advances of metal–organic frameworks for gas sensing. Polyhedron **154**, 83–97 (2018). https://doi.org/10.1016/j.poly.2018.07.028
12. R.S. Andre, R.C. Sanfelice, A. Pavinatto, L.H.C. Mattoso, D.S. Correa, Hybrid nanomaterials designed for volatile organic compounds sensors: a review. Mater. Des. **156**, 154–166 (2018). https://doi.org/10.1016/j.matdes.2018.06.041
13. S. Buratti, S. Benedetti, G. Giovanelli, Application of electronic senses to characterize espresso coffees brewed with different thermal profiles. Eur. Food Res. Technol. **243**(3), 511–520 (2017). https://doi.org/10.1007/s00217-016-2769-y
14. Z. Yang, F. Dong, K. Shimizu, T. Kinoshita, M. Kanamori, A. Morita, N. Watanabe, Identification of coumarin-enriched Japanese green teas and their particular flavor using electronic nose. J. Food Eng. **92**(3), 312–316 (2009). https://doi.org/10.1016/j.jfoodeng.2008.11.014
15. R. Dutta, E.L. Hines, J.W. Gardner, K.R. Kashwan, M. Bhuyan, Tea quality prediction using a tin oxide-based electronic nose: an artificial intelligence approach. Sens. Actuat. B: Chem. **94**(2), 228–237 (2003). https://doi.org/10.1016/S0925-4005(03)00367-8
16. G.J.A.A. Soler-Illia, O. Azzaroni, Multifunctional hybrids by combining ordered mesoporous materials and macromolecular building blocks. Chem. Soc. Rev. **40**(2), 1107–1150 (2011). https://doi.org/10.1039/C0CS00208A
17. J.C. Tan, A.K. Cheetham, Mechanical properties of hybrid inorganic–organic framework materials: establishing fundamental structure–property relationships. Chem. Soc. Rev. **40**(2), 1059–1080 (2011). https://doi.org/10.1039/C0CS00163E
18. G. Rogez, C. Massobrio, P. Rabu, M. Drillon, Layered hydroxide hybrid nanostructures: a route to multifunctionality. Chem. Soc. Rev. **40**(2), 1031–1058 (2011). https://doi.org/10.1039/C0CS00159G
19. C. Laberty-Robert, K. Vallé, F. Pereira, C. Sanchez, Design and properties of functional hybrid organic–inorganic membranes for fuel cells. Chem. Soc. Rev. **40**(2), 961–1005 (2011). https://doi.org/10.1039/C0CS00144A
20. J. Le Bideau, L. Viau, A. Vioux, Ionogels, ionic liquid based hybrid materials. Chem. Soc. Rev. **40**(2), 907–925 (2011). https://doi.org/10.1039/C0CS00059K
21. B. Lebeau, P. Innocenzi, Hybrid materials for optics and photonics. Chem. Soc. Rev. **40**(2), 886–906 (2011). https://doi.org/10.1039/C0CS00106F
22. N. Brun, S. Ungureanu, H. Deleuze, R. Backov, Hybrid foams, colloids and beyond: from design to applications. Chem. Soc. Rev. **40**(2), 771–788 (2011). https://doi.org/10.1039/B920518G
23. K. Kanamori, K. Nakanishi, Controlled pore formation in organotrialkoxysilane-derived hybrids: from aerogels to hierarchically porous monoliths. Chem. Soc. Rev. **40**(2), 754–770 (2011). https://doi.org/10.1039/C0CS00068J
24. C. Sanchez, P. Belleville, M. Popall, L. Nicole, Applications of advanced hybrid organic–inorganic nanomaterials: from laboratory to market. Chem. Soc. Rev. **40**(2), 696–753 (2011). https://doi.org/10.1039/C0CS00136H
25. L.-C. Hu, K.J. Shea, Organo–silica hybrid functional nanomaterials: how do organic bridging groups and silsesquioxane moieties work hand-in-hand? Chem. Soc. Rev. **40**(2), 688–695 (2011). https://doi.org/10.1039/C0CS00219D
26. R. Pardo, M. Zayat, D. Levy, Photochromic organic–inorganic hybrid materials. Chem. Soc. Rev. **40**(2), 672–687 (2011). https://doi.org/10.1039/C0CS00065E
27. J. Yuan, Y. Xu, A.H.E. Müller, One-dimensional magnetic inorganic–organic hybrid nanomaterials. Chem. Soc. Rev. **40**(2), 640–655 (2011). https://doi.org/10.1039/C0CS00087F
28. T.-H. Tran-Thi, R. Dagnelie, S. Crunaire, L. Nicole, Optical chemical sensors based on hybrid organic–inorganic solgel nanoreactors. Chem. Soc. Rev. **40**(2), 621–639 (2011). https://doi.org/10.1039/C0CS00021C
29. F. Hoffmann, M. Fröba, Vitalising porous inorganic silica networks with organic functions: PMOs and related hybrid materials. Chem. Soc. Rev. **40**(2), 608–620 (2011). https://doi.org/10.1039/C0CS00076K
30. M. Vallet-Regí, M. Colilla, B. González, Medical applications of organic–inorganic hybrid materials within the field of silica-based bioceramics. Chem. Soc. Rev. **40**(2), 596–607 (2011). https://doi.org/10.1039/C0CS00025F

 https://doi.org/10.1007/s40820-020-0407-5

31. J.-M. Oh, D.-H. Park, J.-H. Choy, Integrated bio-inorganic hybrid systems for nano-forensics. Chem. Soc. Rev. **40**(2), 583–595 (2011). https://doi.org/10.1039/C0CS00051E
32. U. Schubert, Cluster-based inorganic–organic hybrid materials. Chem. Soc. Rev. **40**(2), 575–582 (2011). https://doi.org/10.1039/C0CS00009D
33. A. Mehdi, C. Reye, R. Corriu, From molecular chemistry to hybrid nanomaterials. Design and functionalization. Chem. Soc. Rev. **40**(2), 563–574 (2011). https://doi.org/10.1039/B920516K
34. L.D. Carlos, R.A.S. Ferreira, V. de Zea Bermudez, B. Julián-López, P. Escribano, Progress on lanthanide-based organic–inorganic hybrid phosphors. Chem. Soc. Rev. **40**(2), 536–549 (2011). https://doi.org/10.1039/C0CS00069H
35. M. Clemente-León, E. Coronado, C. Martí-Gastaldo, F.M. Romero, Multifunctionality in hybrid magnetic materials based on bimetallic oxalate complexes. Chem. Soc. Rev. **40**(2), 473–497 (2011). https://doi.org/10.1039/C0CS00111B
36. C. Sanchez, K.J. Shea, S. Kitagawa, Recent progress in hybrid materials science. Chem. Soc. Rev. **40**(2), 471–472 (2011). https://doi.org/10.1039/C1CS90001C
37. M. Yao, P. Hu, Y. Cao, W. Xiang, X. Zhang, F. Yuan, Y. Chen, Morphology-controlled ZnO spherical nanobelt-flower arrays and their sensing properties. Sens. Actuat. B: Chem. **117**, 562–569 (2013). https://doi.org/10.1016/j.snb.2012.11.088
38. N. Yamazoe, K. Shimanoe, New perspectives of gas sensor technology. Sens. Actuat. B: Chem. **138**(1), 100–107 (2009). https://doi.org/10.1016/j.snb.2009.01.023
39. D.R. Miller, S.A. Akbar, P.A. Morris, Nanoscale metal oxide-based heterojunctions for gas sensing: a review. Sens. Actuat. B: Chem. **204**, 250–272 (2014). https://doi.org/10.1016/j.snb.2014.07.074
40. H.-J. Kim, J.-H. Lee, Highly sensitive and selective gas sensors using p-type oxide semiconductors: overview. Sens. Actuat. B: Chem. **192**, 607–627 (2014). https://doi.org/10.1016/j.snb.2013.11.005
41. T. Li, W. Zeng, Z. Wang, Quasi-one-dimensional metal-oxide-based heterostructural gas-sensing materials: a review. Sens. Actuat. B: Chem. **221**, 1570–1585 (2015). https://doi.org/10.1016/j.snb.2015.08.003
42. Z. Zhao, J. Tian, Y. Sang, A. Cabot, H. Liu, Structure, synthesis, and applications of TiO_2 nanobelts. Adv. Mater. **27**(16), 2557–2582 (2015). https://doi.org/10.1002/adma.201405589
43. T. Wagner, S. Haffer, C. Weinberger, D. Klaus, M. Tiemann, Mesoporous materials as gas sensors. Chem. Soc. Rev. **42**(9), 4036–4053 (2013). https://doi.org/10.1039/C2CS35379B
44. J. Zhang, X. Liu, G. Neri, N. Pinna, Nanostructured materials for room-temperature gas sensors. Adv. Mater. **28**(5), 795–831 (2016). https://doi.org/10.1002/adma.201503825
45. S.-J. Choi, I.-D. Kim, Recent developments in 2D nanomaterials for chemiresistive-type gas sensors. Electron. Mater. Lett. **14**(3), 221–260 (2018). https://doi.org/10.1007/s13391-018-0044-z
46. L. Senesac, T.G. Thundat, Nanosensors for trace explosive detection. Mater. Today **11**(3), 28–36 (2008). https://doi.org/10.1016/s1369-7021(08)70017-8
47. C.N. Xu, J. Tamaki, N. Miura, N. Yamazoe, Grain-size effects on gas sensitivity of porous SnO_2-based elements. Sens. Actuat. B: Chem. **3**(2), 147–155 (1991). https://doi.org/10.1016/0925-4005(91)80207-z
48. J.Q. Xu, Q.Y. Pan, Y.A. Shun, Z.Z. Tian, Grain size control and gas sensing properties of ZnO gas sensor. Sens. Actuat. B: Chem. **66**(1–3), 277–279 (2000). https://doi.org/10.1016/s0925-4005(00)00381-6
49. N. Hongsith, E. Wongrat, T. Kerdcharoen, S. Choopun, Sensor response formula for sensor based on ZnO nanostructures. Sens. Actuat. B: Chem. **144**(1), 67–72 (2010). https://doi.org/10.1021/am5081277
50. M. Yao, Q. Li, G. Hou, C. Lu, B. Cheng et al., Dopant-controlled morphology evolution of WO_3 polyhedra synthesized by RF thermal plasma and their sensing properties. ACS Appl. Mater. Interfaces. **7**(4), 2856–2866 (2015). https://doi.org/10.1021/am5081277
51. I.-S. Hwang, J.-K. Choi, H.-S. Woo, S.-J. Kim, S.-Y. Jung, T.-Y. Seong, I.-D. Kim, J.-H. Lee, Facile control of C_2H_5OH sensing characteristics by decorating discrete Ag nanoclusters on SnO_2 nanowire networks. ACS Appl. Mater. Interfaces. **3**(8), 3140–3145 (2011). https://doi.org/10.1021/am200647f
52. J.-S. Jang, S.-J. Choi, S.-J. Kim, M. Hakim, I.-D. Kim, Rational design of highly porous SnO_2 nanotubes functionalized with biomimetic nanocatalysts for direct observation of simulated diabetes. Adv. Funct. Mater. **26**(26), 4740–4748 (2016). https://doi.org/10.1002/adfm.201600797
53. S.-J. Kim, S.-J. Choi, J.-S. Jang, H.-J. Cho, W.-T. Koo, H.L. Tuller, I.-D. Kim, Exceptional high-performance of Pt-based bimetallic catalysts for exclusive detection of exhaled biomarkers. Adv. Mater. **29**(36), 1700737 (2017). https://doi.org/10.1002/adma.201700737
54. Y. Xiao, L. Lu, A. Zhang, Y. Zhang, L. Sun, L. Huo, F. Li, Highly enhanced acetone sensing performances of porous and single crystalline ZnO nanosheets: high percentage of exposed (100) facets working together with surface modification with Pd nanoparticles. ACS Appl. Mater. Interfaces. **4**(8), 3797–3804 (2012). https://doi.org/10.1021/am3010303
55. S.-Y. Cho, H.-J. Koh, H.-W. Yoo, H.-T. Jung, Tunable chemical sensing performance of black phosphorus by controlled functionalization with noble metals. Chem. Mater. **29**(17), 7197–7205 (2017). https://doi.org/10.1021/acs.chemmater.7b01353
56. J. Ma, Y. Ren, X. Zhou, L. Liu, Y. Zhu et al., Pt nanoparticles sensitized ordered mesoporous WO_3 semiconductor: gas sensing performance and mechanism study. Adv. Funct. Mater. **28**(6), 1705268 (2018). https://doi.org/10.1002/adfm.201705268
57. Y.J. Hong, J.-W. Yoon, J.-H. Lee, Y.C. Kang, One-pot synthesis of Pd-loaded SnO_2 yolk-shell nanostructures for ultraselective methyl benzene sensors. Chem. Eur. J. **20**(10), 2737–2741 (2014). https://doi.org/10.1002/chem.201304502

58. X. Chen, Z. Guo, W.-H. Xu, H.-B. Yao, M.-Q. Li et al., Templating synthesis of SnO_2 nanotubes loaded with Ag_2O nanoparticles and their enhanced gas sensing properties. Adv. Funct. Mater. **21**(11), 2049–2056 (2011). https://doi.org/10.1002/adfm.201002701
59. G. Lu, L.E. Ocola, J. Chen, Room-temperature gas sensing based on electron transfer between discrete tin oxide nanocrystals and multiwalled carbon nanotubes. Adv. Mater. **21**(24), 2487–2491 (2009). https://doi.org/10.1002/adma.200803536
60. L. Guan, S. Wang, W. Gu, J. Zhuang, H. Jin, W. Zhang, T. Zhang, J. Wang, Ultrasensitive room-temperature detection of NO_2 with tellurium nanotube based chemiresistive sensor. Sens. Actuat. B: Chem. **196**, 321–327 (2014). https://doi.org/10.1016/j.snb.2014.02.014
61. H. Long, A. Harley-Trochimczyk, T. Pham, Z. Tang, T. Shi, A. Zettl, C. Carraro, M.A. Worsley, R. Maboudian, High surface area MoS_2/graphene hybrid aerogel for ultrasensitive NO_2 detection. Adv. Funct. Mater. **26**(28), 5158–5165 (2016). https://doi.org/10.1002/adfm.201601562
62. S. Deng, V. Tjoa, H.M. Fan, H.R. Tan, D.C. Sayle, M. Olivo, S. Mhaisalkar, J. Wei, C.H. Sow, Reduced graphene oxide conjugated Cu_2O nanowire mesocrystals for high-performance NO_2 gas sensor. J. Am. Chem. Soc. **134**(10), 4905–4917 (2012). https://doi.org/10.1021/ja211683m
63. Y. Guo, T. Wang, F. Chen, X. Sun, X. Li, Z. Yu, P. Wan, X. Chen, Hierarchical graphene–polyaniline nanocomposite films for high-performance flexible electronic gas sensors. Nanoscale **8**(23), 12073–12080 (2016). https://doi.org/10.1039/C6NR02540D
64. Z. Wang, L. Huang, X. Zhu, X. Zhou, L. Chi, An ultrasensitive organic semiconductor NO_2 sensor based on crystalline TIPS-pentacene films. Adv. Mater. **29**(38), 1703192 (2017). https://doi.org/10.1002/adma.201703192
65. A.R. Jalil, H. Chang, V.K. Bandari, P. Robaschik, J. Zhang et al., Fully integrated organic nanocrystal diode as high performance room temperature NO_2 sensor. Adv. Mater. **28**(15), 2971–2977 (2016). https://doi.org/10.1002/adma.201506293
66. S. Ji, H. Wang, T. Wang, D. Yan, A high-performance room-temperature NO_2 sensor based on an ultrathin heterojunction film. Adv. Mater. **25**(12), 1755–1760 (2013). https://doi.org/10.1002/adma.201204134
67. F. Shao, M.W.G. Hoffmann, J.D. Prades, R. Zamani, J. Arbiol et al., Heterostructured p-CuO (nanoparticle)/n-SnO_2 (nanowire) devices for selective H_2S detection. Sens. Actuat. B: Chem. **181**, 130–135 (2013). https://doi.org/10.1016/j.snb.2013.01.067
68. J. Wu, K. Tao, Y. Guo, Z. Li, X. Wang et al., A 3D chemically modified graphene hydrogel for fast, highly sensitive, and selective gas sensor. Adv. Sci. **4**(3), 1600319 (2017). https://doi.org/10.1002/advs.201600319
69. H. Jin, T.-P. Huynh, H. Haick, Self-healable sensors based nanoparticles for detecting physiological markers via skin and breath: toward disease prevention via wearable devices. Nano Lett. **16**(7), 4194–4202 (2016). https://doi.org/10.1021/acs.nanolett.6b01066
70. M.W.G. Hoffmann, J. Daniel Prades, L. Mayrhofer, F. Hernandez-Ramirez, T.T. Jaervi, M. Moseler, A. Waag, H. Shen, Highly selective SAM-nanowire hybrid NO_2 sensor: insight into charge transfer dynamics and alignment of frontier molecular orbitals. Adv. Funct. Mater. **24**(5), 595–602 (2014). https://doi.org/10.1002/adfm.201301478
71. W. Liu, L. Xu, K. Sheng, C. Chen, X. Zhou et al., APTES-functionalized thin-walled porous WO_3 nanotubes for highly selective sensing of NO_2 in a polluted environment. J. Mater. Chem. A **6**(23), 10976–10989 (2018). https://doi.org/10.1039/c8ta02452a
72. Y. Jiang, N. Tang, C. Zhou, Z. Han, H. Qu, X. Duan, A chemiresistive sensor array from conductive polymer nanowires fabricated by nanoscale soft lithography. Nanoscale **10**(44), 20578–20586 (2018). https://doi.org/10.1039/C8NR04198A
73. B. Esser, J.M. Schnorr, T.M. Swager, Selective detection of ethylene gas using carbon nanotube-based devices: utility in determination of fruit ripeness. Angew. Chem. Int. Ed. **51**(23), 5752–5756 (2012). https://doi.org/10.1002/anie.201201042
74. P.A. Russo, N. Donato, S.G. Leonardi, S. Baek, D.E. Conte, G. Neri, N. Pinna, Room-temperature hydrogen sensing with heteronanostructures based on reduced graphene oxide and tin oxide. Angew. Chem. Int. Ed. **51**(44), 11053–11057 (2012). https://doi.org/10.1002/anie.201204373
75. J.-S. Jang, W.-T. Koo, S.-J. Choi, I.-D. Kim, Metal organic framework-templated chemiresistor: sensing type transition from p-to-n using hollow metal oxide polyhedron via galvanic replacement. J. Am. Chem. Soc. **139**(34), 11868–11876 (2017). https://doi.org/10.1021/jacs.7b05246
76. M.S. Yao, W.X. Tang, G.E. Wang, B. Nath, G. Xu, MOF thin film-coated metal oxide nanowire array: significantly improved chemiresistor sensor performance. Adv. Mater. **28**, 5229–5234 (2016). https://doi.org/10.1002/adma.201506457
77. D. Wang, Z. Li, J. Zhou, H. Fang, X. He, P. Jena, J.-B. Zeng, W.-N. Wang, Simultaneous detection and removal of formaldehyde at room temperature: Janus Au@ZnO@ZIF-8 nanoparticles. Nano-Micro Lett. **10**(1), 4 (2018). https://doi.org/10.1007/s40820-017-0158-0
78. J. Fu, C. Zhao, J. Zhang, Y. Peng, E. Xie, Enhanced gas sensing performance of electrospun Pt-functionalized NiO nanotubes with chemical and electronic sensitization. ACS Appl. Mater. Interfaces. **5**(15), 7410–7416 (2013). https://doi.org/10.1021/am4017347
79. L. Xiao, S. Xu, G. Yu, S. Liu, Efficient hierarchical mixed Pd/SnO_2 porous architecture deposited microheater for low power ethanol gas sensor. Sens. Actuat. B: Chem. **255**, 2002–2010 (2018). https://doi.org/10.1016/j.snb.2017.08.216
80. S. Ishihara, J.M. Azzarelli, M. Krikorian, T.M. Swager, Ultratrace detection of toxic chemicals: triggered disassembly of supramolecular nanotube wrappers. J. Am. Chem. Soc. **138**(26), 8221–8227 (2016). https://doi.org/10.1021/jacs.6b03869
81. M.K. Nakhleh, H. Amal, H. Awad, A.L. Gharra, N. Abu-Saleh, R. Jeries, H. Haick, Z. Abassi, Sensor arrays based on

 https://doi.org/10.1007/s40820-020-0407-5

nanoparticles for early detection of kidney injury by breath samples. Nanomed. Nanotechnol. **10**(8), 1767–1776 (2014). https://doi.org/10.1016/j.nano.2014.06.007

82. Y. Deng, J. Sun, H. Jin, M. Khatib, X. Li et al., Chemically modified polyaniline for the detection of volatile biomarkers of minimal sensitivity to humidity and bending. Adv. Healthc. Mater. **7**(15), 1800232 (2018). https://doi.org/10.1002/adhm.201800232
83. X.M. Sun, Y.D. Li, Colloidal carbon spheres and their core/shell structures with noble-metal nanoparticles. Angew. Chem. Int. Ed. **43**(5), 597–601 (2004). https://doi.org/10.1002/anie.200352386
84. L. Wang, Z. Lou, T. Fei, T. Zhang, Zinc oxide core-shell hollow microspheres with multi-shelled architecture for gas sensor applications. J. Mater. Chem. **21**(48), 19331–19336 (2011). https://doi.org/10.1039/C1JM13354C
85. P. Rai, J.-W. Yoon, H.-M. Jeong, S.-J. Hwang, C.-H. Kwak, J.-H. Lee, Design of highly sensitive and selective Au@NiO yolk-shell nanoreactors for gas sensor applications. Nanoscale **6**(14), 8292–8299 (2014). https://doi.org/10.1039/c4nr01906g
86. P. Rai, J.-W. Yoon, C.-H. Kwak, J.-H. Lee, Role of Pd nanoparticles in gas sensing behaviour of Pd@In_2O_3 yolk-shell nanoreactors. J. Mater. Chem. A **4**(1), 264–269 (2016). https://doi.org/10.1039/c5ta08873a
87. X. Han, M. Jin, S. Xie, Q. Kuang, Z. Jiang, Y. Jiang, Z. Xie, L. Zheng, Synthesis of tin dioxide octahedral nanoparticles with exposed high-energy 221 facets and enhanced gas-sensing properties. Angew. Chem. Int. Ed. **48**(48), 9180–9183 (2009). https://doi.org/10.1002/anie.200903926
88. X.-G. Han, H.-Z. He, Q. Kuang, X. Zhou, X.-H. Zhang, T. Xu, Z.-X. Xie, L.-S. Zheng, Controlling morphologies and tuning the related properties of nano/microstructured ZnO crystallites. J. Phys. Chem. C **113**(2), 584–589 (2009). https://doi.org/10.1021/jp808233e
89. K. Suematsu, M. Sasaki, N. Ma, M. Yuasa, K. Shimanoe, Antimony-doped tin dioxide gas sensors exhibiting high stability in the sensitivity to humidity changes. ACS Sensor **1**(7), 913–920 (2016). https://doi.org/10.1021/acssensors.6b00323
90. N. Ma, K. Suematsu, M. Yuasa, K. Shimanoe, Pd size effect on the gas sensing properties of Pd-loaded SnO_2 in humid atmosphere. ACS Appl. Mater. Interfaces. **7**(28), 15618–15625 (2015). https://doi.org/10.1021/acsami.5b04380
91. Y. Lin, P. Deng, Y. Nie, Y. Hu, L. Xing, Y. Zhang, X. Xue, Room-temperature self-powered ethanol sensing of a Pd/ZnO nanoarray nanogenerator driven by human finger movement. Nanoscale **6**(9), 4604–4610 (2014). https://doi.org/10.1039/c3nr06809a
92. L. Guo, F. Chen, N. Xie, X. Kou, C. Wang et al., Ultrasensitive sensing platform based on Pt–ZnO–In_2O_3 nanofibers for detection of acetone. Sens. Actuat. B: Chem. **272**, 185–194 (2018). https://doi.org/10.1016/j.snb.2018.05.161
93. Z. Wang, Z. Li, T. Jiang, X. Xu, C. Wang, Ultrasensitive hydrogen sensor based on Pd^0-loaded SnO_2 electrospun nanofibers at room temperature. ACS Appl. Mater. Interfaces. **5**(6), 2013–2021 (2013). https://doi.org/10.1021/am3028553
94. S.-J. Choi, W.-T. Koo, S.-J. Kim, J.-S. Jang, H.L. Tuller, I.-D. Kim, Heterogeneous sensitization of metal-organic framework driven metal@metal oxide complex catalysts on oxide nanofiber scaffold toward superior gas sensors. J. Am. Chem. Soc. **138**(40), 13431–13437 (2016). https://doi.org/10.1021/jacs.6b09167
95. M. Yao, P. Hu, N. Han, F. Ding, C. Yin, F. Yuan, J. Yang, Y. Chen, ZnO micro-windbreak for enhanced gas diffusion. Sens. Actuat. B: Chem. **186**, 614–621 (2013). https://doi.org/10.1016/j.snb.2013.06.057
96. Z. Jing, J. Zhan, Fabrication and gas-sensing properties of porous ZnO nanoplates. Adv. Mater. **20**(23), 4547–4551 (2008). https://doi.org/10.1002/adma.200800243
97. X. Lai, J. Li, B.A. Korgel, Z. Dong, Z. Li, F. Su, J. Du, D. Wang, General synthesis and gas-sensing properties of multiple-shell metal oxide hollow microspheres. Angew. Chem. Int. Ed. **50**(12), 2738–2741 (2011). https://doi.org/10.1002/anie.201004900
98. Y. Shimizu, T. Hyodo, M. Egashira, Meso-to macro-porous oxides as semiconductor gas sensors. Catal. Surv. Asia **8**(2), 127–135 (2004). https://doi.org/10.1023/b:cats.0000027014.79515.87
99. F. Sun, W. Cai, Y. Li, L. Jia, F. Lu, Direct growth of mono- and multilayer nanostructured porous films on curved surfaces and their application as gas sensors. Adv. Mater. **17**(23), 2872–2877 (2005). https://doi.org/10.1002/adma.200500936
100. F. Song, H. Su, J. Han, W.M. Lau, W.-J. Moon, D. Zhang, Bioinspired hierarchical tin oxide scaffolds for enhanced gas sensing properties. J. Phys. Chem. C **116**(18), 10274–10281 (2012). https://doi.org/10.1021/jp2118136
101. T. Waitz, T. Wagner, T. Sauerwald, C.-D. Kohl, M. Tiemann, Ordered mesoporous In_2O_3: synthesis by structure replication and application as a methane gas sensor. Adv. Funct. Mater. **19**(4), 653–661 (2009). https://doi.org/10.1002/adfm.200801458
102. E. Rossinyol, A. Prim, E. Pellicer, J. Arbiol, F. Hernandez-Ramirez et al., Synthesis and characterization of chromium-doped mesoporous tungsten oxide for gas-sensing applications. Adv. Funct. Mater. **17**(11), 1801–1806 (2007). https://doi.org/10.1002/adfm.200600722
103. M. D'Arienzo, L. Armelao, A. Cacciamani, C.M. Mari, S. Polizzi et al., One-step preparation of SnO_2 and Pt-doped SnO_2 as inverse opal thin films for gas sensing. Chem. Mater. **22**(13), 4083–4089 (2010). https://doi.org/10.1021/cm100866g
104. M. D'Arienzo, L. Armelao, C.M. Mari, S. Polizzi, R. Ruffo, R. Scotti, F. Morazzoni, Macroporous WO_3 thin films active in NH_3 sensing: role of the hosted Cr isolated centers and Pt nanoclusters. J. Am. Chem. Soc. **133**(14), 5296–5304 (2011). https://doi.org/10.1021/ja109511a
105. J. Jones, H. Xiong, A.T. DeLaRiva, E.J. Peterson, H. Pham et al., Thermally stable single-atom platinum-on-ceria catalysts via atom trapping. Science **353**(6295), 150–154 (2016). https://doi.org/10.1126/science.aaf8800

106. P. Liu, Y. Zhao, R. Qin, S. Mo, G. Chen et al., Photochemical route for synthesizing atomically dispersed palladium catalysts. Science **352**(6287), 797–800 (2016). https://doi.org/10.1126/science.aaf5251
107. A.J. Therrien, A.J. Hensley, M.D. Marcinkowski, R. Zhang, F.R. Lucci et al., An atomic-scale view of single-site Pt catalysis for low-temperature CO oxidation. Nat. Catal. **1**(3), 192 (2018). https://doi.org/10.1038/s41929-018-0028-2
108. A. Wang, J. Li, T. Zhang, Heterogeneous single-atom catalysis. Nat. Rev. Chem. **2**, 65–81 (2018). https://doi.org/10.1038/s41570-018-0010-1
109. Z. Song, Z. Wei, B. Wang, Z. Luo, S. Xu et al., Sensitive room-temperature H_2S gas sensors employing SnO_2 quantum wire/reduced graphene oxide nanocomposites. Chem. Mater. **28**(4), 1205–1212 (2016). https://doi.org/10.1021/acs.chemmater.5b04850
110. B. Jang, K.Y. Lee, J.-S. Noh, W. Lee, Nanogap-based electrical hydrogen sensors fabricated from Pd-PMMA hybrid thin films. Sens. Actuator. B: Chem. **193**, 530–535 (2014). https://doi.org/10.1016/j.snb.2013.11.080
111. G. Peng, U. Tisch, O. Adams, M. Hakim, N. Shehada et al., Diagnosing lung cancer in exhaled breath using gold nanoparticles. Nat. Nanotechnol. **4**, 669 (2009). https://doi.org/10.1038/nnano.2009.235
112. N. Kahn, O. Lavie, M. Paz, Y. Segev, H. Haick, Dynamic nanoparticle-based flexible sensors: diagnosis of ovarian carcinoma from exhaled breath. Nano Lett. **15**(10), 7023–7028 (2015). https://doi.org/10.1021/acs.nanolett.5b03052
113. J.-W. Yoon, J.-S. Kim, T.-H. Kim, Y.J. Hong, Y.C. Kang, J.-H. Lee, A new strategy for humidity independent oxide chemiresistors: dynamic self-refreshing of In_2O_3 sensing surface assisted by layer-by-layer coated CeO_2 nanoclusters. Small **12**(31), 4229–4240 (2016). https://doi.org/10.1002/smll.201601507
114. C.-L. Zhu, H.-L. Yu, Y. Zhang, T.-S. Wang, Q.-Y. Ouyang et al., Fe_2O_3/TiO_2 tube-like nanostructures: synthesis, structural transformation and the enhanced sensing properties. ACS Appl. Mater. Interfaces. **4**(2), 665–671 (2012). https://doi.org/10.1021/am201689x
115. S. Park, S. An, Y. Mun, C. Lee, UV-enhanced NO_2 gas sensing properties of SnO_2-Core/ZnO-shell nanowires at room temperature. ACS Appl. Mater. Interfaces. **5**(10), 4285–4292 (2013). https://doi.org/10.1021/am400500a
116. S. Cui, Z. Wen, X. Huang, J. Chang, J. Chen, Stabilizing MoS_2 nanosheets through SnO_2 nanocrystal decoration for high-performance gas sensing in air. Small **11**(19), 2305–2313 (2015). https://doi.org/10.1002/smll.201402923
117. T. Kida, A. Nishiyama, Z. Hua, K. Suematsu, M. Yuasa, K. Shimanoe, WO_3 nano lamella gas sensor: porosity control using SnO_2 nanoparticles for enhanced NO_2 sensing. Langmuir **30**(9), 2571–2579 (2014). https://doi.org/10.1021/la4049105
118. Y.-C. Her, B.-Y. Yeh, S.-L. Huang, Vapor-solid growth of p-Te/n-SnO_2 hierarchical heterostructures and their enhanced room-temperature gas sensing properties. ACS Appl. Mater. Interfaces. **6**(12), 9150–9159 (2014). https://doi.org/10.1021/am5012518
119. A. Kumar, S. Samanta, A. Singh, M. Roy, S. Singh et al., Fast response and high sensitivity of ZnO nanowires—cobalt phthalocyanine heterojunction based H_2S sensor. ACS Appl. Mater. Interfaces. **7**(32), 17713–17724 (2015). https://doi.org/10.1021/acsami.5b03652
120. J.H. Kim, A. Katoch, S.H. Kim, S.K. Sang, Chemiresistive sensing behavior of SnO_2 (n)–Cu_2O (p) core-shell nanowires. ACS Appl. Mater. Interfaces. **7**(28), 15351–15358 (2015). https://doi.org/10.1021/acsami.5b03224
121. D. Zhang, Z. Wu, X. Zong, Y. Zhang, Fabrication of polypyrrole/Zn_2SnO_4 nanofilm for ultra-highly sensitive ammonia sensing application. Sens. Actuat. B: Chem. **274**, 575–586 (2018). https://doi.org/10.1016/j.snb.2018.08.001
122. Z. Pang, Q. Nie, A. Wei, J. Yang, F. Huang, Q. Wei, Effect of In_2O_3 nanofiber structure on the ammonia sensing performances of In_2O_3/PANI composite nanofibers. J. Mater. Sci. **52**(2), 686–695 (2017). https://doi.org/10.1007/s10853-016-0362-1
123. M. Villani, D. Calestani, L. Lazzarini, L. Zanotti, R. Mosca, A. Zappettini, Extended functionality of ZnO nanotetrapods by solution-based coupling with CdS nanoparticles. J. Mater. Chem. **22**(12), 5694–5699 (2012). https://doi.org/10.1039/C2JM16164H
124. J. Zhai, D. Wang, L. Peng, Y. Lin, X. Li, T. Xie, Visible-light-induced photoelectric gas sensing to formaldehyde based on CdS nanoparticles/ZnO heterostructures. Sens. Actuat. B: Chem. **147**(1), 234–240 (2010). https://doi.org/10.1016/j.snb.2010.03.003
125. J. Zhai, L. Wang, D. Wang, H. Li, Y. Zhang, D.Q. He, T. Xie, Enhancement of gas sensing properties of CdS nanowire/ZnO nanosphere composite materials at room temperature by visible-light activation. ACS Appl. Mater. Interfaces. **3**(7), 2253–2258 (2011). https://doi.org/10.1021/am200008y
126. A. Chizhov, M. Rumyantseva, R. Vasiliev, D. Filatova, K. Drozdov, I. Krylov, A. Abakumov, A. Gaskov, Visible light activated room temperature gas sensors based on nanocrystalline ZnO sensitized with CdSe quantum dots. Sens. Actuat. B: Chem. **205**, 305–312 (2014). https://doi.org/10.1016/j.snb.2014.08.091
127. L. Huo, X. Yang, Z. Liu, X. Tian, T. Qi, X. Wang, K. Yu, J. Sun, M. Fan, Modulation of potential barrier heights in Co_3O_4/SnO_2 heterojunctions for highly H2-selective sensors. Sens. Actuat. B: Chem. **244**, 694–700 (2017). https://doi.org/10.1016/j.snb.2017.01.061
128. C.-H. Kwak, T.-H. Kim, S.-Y. Jeong, J.-W. Yoon, J.-S. Kim, J.-H. Lee, Humidity-independent oxide semiconductor chemiresistors using terbium-doped SnO_2 yolk-shell spheres for real-time breath analysis. ACS Appl. Mater. Interfaces. **10**(22), 18886–18894 (2018). https://doi.org/10.1021/acsami.8b04245
129. E.-X. Chen, H. Yang, J. Zhang, Zeolitic imidazolate framework as formaldehyde gas sensor. Inorg. Chem. **53**(11), 5411–5413 (2014). https://doi.org/10.1021/ic500474j

 https://doi.org/10.1007/s40820-020-0407-5

130. E.-X. Chen, H.-R. Fu, R. Lin, Y.-X. Tan, J. Zhang, Highly selective and sensitive trimethylamine gas sensor based on cobalt imidazolate framework material. ACS Appl. Mater. Interfaces. **6**(24), 22871–22875 (2014). https://doi.org/10.1021/am5071317
131. H. Tian, H. Fan, M. Li, L. Ma, Zeolitic imidazolate framework coated ZnO nanorods as molecular sieving to improve selectivity of formaldehyde gas sensor. ACS Sensor **1**(3), 243–250 (2016). https://doi.org/10.1021/acssensors.5b00236
132. M.F. Koudehi, S.M. Pourmortazavi, Polyvinyl alcohol/polypyrrole/molecularly imprinted polymer nanocomposite as highly selective chemiresistor sensor for 2,4-DNT vapor recognition. Electroanalysis **30**(10), 2302–2310 (2018). https://doi.org/10.1002/elan.201700751
133. K. Tan, S. Zuluaga, E. Fuentes, E.C. Mattson, J.F. Veyan, H. Wang, J. Li, T. Thonhauser, Y.J. Chabal, Trapping gases in metal-organic frameworks with a selective surface molecular barrier layer. Nat. Commun. **7**, 13871 (2016). https://doi.org/10.1038/ncomms13871
134. H. Li, M.M. Sadiq, K. Suzuki, R. Ricco, C. Doblin et al., Magnetic metal-organic frameworks for efficient carbon dioxide capture and remote trigger release. Adv. Mater. **28**(9), 1839–1844 (2016). https://doi.org/10.1002/adma.201505320
135. P.-Q. Liao, N.-Y. Huang, W.-X. Zhang, J.-P. Zhang, X.-M. Chen, Controlling guest conformation for efficient purification of butadiene. Science **356**(6343), 1193–1196 (2017). https://doi.org/10.1126/science.aam7232
136. F. Vermoortele, M. Maes, P.Z. Moghadam, M.J. Lennox, F. Ragon et al., p-Xylene-selective metal-organic frameworks: a case of topology-directed selectivity. J. Am. Chem. Soc. **133**(46), 18526–18529 (2011). https://doi.org/10.1021/ja207287h
137. L. Zhang, P. Cui, H. Yang, J. Chen, F. Xiao et al., Metal–organic frameworks as promising photosensitizers for photoelectrochemical water splitting. Adv. Sci. **3**(1), 1500243 (2016). https://doi.org/10.1002/advs.201500243
138. M. Zhao, K. Yuan, W. Yun, G. Li, J. Guo, G. Lin, W. Hu, H. Zhao, Z. Tang, Metal–organic frameworks as selectivity regulators for hydrogenation reactions. Nature **539**(7627), 76 (2016). https://doi.org/10.1038/nature19763
139. M.G. Campbell, D. Sheberla, S.F. Liu, T.M. Swager, M. Dincă, Cu3(hexaiminotriphenylene)2: an electrically conductive 2D metal–organic framework for chemiresistive sensing. Angew. Chem. Int. Ed. **127**(14), 4423–4426 (2015). https://doi.org/10.1002/anie.201411854
140. D. Sheberla, J.C. Bachman, J.S. Elias, C.J. Sun, Y. Shao-Horn, M. Dinca, Conductive MOF electrodes for stable supercapacitors with high areal capacitance. Nat. Mater. **16**(2), 220–224 (2017). https://doi.org/10.1038/nmat4766
141. T. Yamada, M. Sadakiyo, H. Kitagawa, High proton conductivity of one-dimensional ferrous oxalate dihydrate. J. Am. Chem. Soc. **131**(9), 3144–3145 (2009). https://doi.org/10.1021/ja808681m
142. G. Xu, K. Otsubo, T. Yamada, S. Sakaida, H. Kitagawa, Superprotonic conductivity in a highly oriented crystalline metal-organic framework nanofilm. J. Am. Chem. Soc. **135**(20), 7438–7441 (2013). https://doi.org/10.1021/ja402727d
143. L. Sun, M.G. Campbell, M. Dincă, Electrically conductive porous metal–organic frameworks. Angew. Chem. Int. Ed. **55**(11), 3566–3579 (2016). https://doi.org/10.1002/anie.201506219
144. G. Xu, G.C. Guo, M.S. Yao, Z.H. Fu, G.E. Wang, *The Chemistry of Metal-Organic Frameworks: Synthesis, Characterization, and Applications: 14*, vol. 1 (Wiley, Weinheim, 2016), pp. 421–462. https://doi.org/10.1002/9783527693078.ch1
145. M. Hmadeh, Z. Lu, Z. Liu, F. Gándara, H. Furukawa, S. Wan et al., New porous crystals of extended metal-catecholates. Chem. Mater. **24**(18), 3511–3513 (2012). https://doi.org/10.1021/cm301194a
146. A.A. Talin, A. Centrone, A.C. Ford, M.E. Foster, V. Stavila et al., Tunable electrical conductivity in metal-organic framework thin-film devices. Science **343**(6166), 66–69 (2014). https://doi.org/10.1126/science.1246738
147. X. Huang, P. Sheng, Z.Y. Tu, F.J. Zhang, J.H. Wang et al., A two-dimensional π–d conjugated coordination polymer with extremely high electrical conductivity and ambipolar transport behaviour. Nat. Commun. **6**, 7408 (2015). https://doi.org/10.1038/ncomms8408
148. S. Takaishi, M. Hosoda, T. Kajiwara, H. Miyasaka, M. Yamashita et al., Electroconductive porous coordination polymer $Cu[Cu(pdt)_2]$ composed of donor and acceptor building units. Inorg. Chem. **48**(19), 9048–9050 (2009). https://doi.org/10.1021/ic802117q
149. T. Kambe, R. Sakamoto, K. Hoshiko, K. Takada, M. Miyachi et al., π-Conjugated nickel bis(dithiolene) complex nanosheet. J. Am. Chem. Soc. **135**, 2462–2465 (2013). https://doi.org/10.1021/ja312380b
150. S. Takaishi, M. Hosoda, T. Kajiwara, H. Miyasaka, M. Yamashita et al., Electroconductive porous coordination polymer $Cu[Cu(pdt)_2]$ composed of donor and acceptor building units. Inorg. Chem. **48**(19), 9048–9050 (2008). https://doi.org/10.1021/ic802117q
151. X. Ribas, J.C. Dias, J. Morgado, K. Wurst, I.C. Santos et al., Alkaline side-coordination strategy for the design of nickel (II) and nickel (III) bis (1, 2-diselenolene) complex based materials. Inorg. Chem. **43**(12), 3631–3641 (2004). https://doi.org/10.1021/ic049860x
152. K.J. Erickson, F. Leonard, V. Stavila, M.E. Foster, C.D. Spataru et al., Thin film thermoelectric metal-organic framework with high Seebeck coefficient and low thermal conductivity. Adv. Mater. **27**(22), 3453–3459 (2015). https://doi.org/10.1002/adma.201501078
153. S.S. Park, E.R. Hontz, L. Sun, C.H. Hendon, A. Walsh, T. Van Voorhis, M. Dinca, Cation-dependent intrinsic electrical conductivity in isostructural tetrathiafulvalene-based microporous metal-organic frameworks. J. Am. Chem. Soc. **137**(5), 1774–1777 (2015). https://doi.org/10.1021/ic049860x

154. J. Cui, Z. Xu, An electroactive porous network from covalent metal-dithiolene links. Chem. Commun. **50**(30), 3986–3988 (2014). https://doi.org/10.1039/c4cc00408f
155. T. Panda, R. Banerjee, High Charge Carrier Mobility in two dimensional indium (III) isophthalic acid based frameworks. Proc. Natl. Acad. Sci. India Sect. A Phys. Sci. **84**(2), 331–336 (2014). https://doi.org/10.1007/s40010-014-0152-6
156. D. Chen, H. Xing, Z. Su, C. Wang, Electrical conductivity and electroluminescence of a new anthracene-based metal-organic framework with π-conjugated zigzag chains. Chem. Commun. **52**(10), 2019–2022 (2016). https://doi.org/10.1039/C5CC09065B
157. L.E. Darago, M.L. Aubrey, C.J. Yu, M.I. Gonzalez, J.R. Long, Electronic conductivity, ferrimagnetic ordering, and reductive insertion mediated by organic mixed-valence in a ferric semiquinoid metal–organic framework. J. Am. Chem. Soc. **137**(50), 15703–15711 (2015). https://doi.org/10.1021/jacs.5b10385
158. L. Sun, C.H. Hendon, M.A. Minier, A. Walsh, M. Dincă, Million-fold electrical conductivity enhancement in Fe_2(DEBDC) versus Mn_2(DEBDC) (E = S, O). J. Am. Chem. Soc. **137**(19), 6164–6167 (2015). https://doi.org/10.1021/jacs.5b02897
159. D. Sheberla, L. Sun, M.A. Blood-Forsythe, S.L. Er, C.R. Wade, C.K. Brozek, A.N. Aspuru-Guzik, M. Dincă, High electrical conductivity in Ni_3(2,3,6,7,10,11-hexaiminotriphenylene)$_2$, a semiconducting metal-organic graphene analogue. J. Am. Chem. Soc. **136**, 8859–8862 (2014). https://doi.org/10.1021/ja502765n
160. T. Kambe, R. Sakamoto, T. Kusamoto, T. Pal, N. Fukui et al., Redox control and high conductivity of nickel bis(dithiolene) complex π-nanosheet: a potential organic two-dimensional topological insulator. J. Am. Chem. Soc. **136**, 14357–14360 (2014). https://doi.org/10.1021/ja507619d
161. C. Hermosa, J.V. Alvarez, M.R. Azani, C.J. Gomez-Garcia, M. Fritz et al., Intrinsic electrical conductivity of nanostructured metal-organic polymer chains. Nat. Commun. **4**, 1709 (2013). https://doi.org/10.1038/ncomms2696
162. S. Takaishi, Y. Tobu, H. Kitagawa, A. Goto, T. Shimizu, T. Okubo, T. Mitani, R. Ikeda, The NOR observation of Spin-Peierls transition in an antiferromagnetic MX-chain complex NiBr(chxn) (2) Br-2. J. Am. Chem. Soc. **126**(6), 1614–1615 (2004). https://doi.org/10.1021/ja039857x
163. R.A. Heintz, H. Zhao, X. Ouyang, G. Grandinetti, J. Cowen, K.R. Dunbar, New insight into the nature of Cu (TCNQ): solution routes to two distinct polymorphs and their relationship to crystalline films that display bistable switching behavior. Inorg. Chem. **38**(1), 144–156 (1999). https://doi.org/10.1021/ic9812095
164. M.G. Campbell, S.F. Liu, T.M. Swager, M. Dinca, Chemiresistive sensor arrays from conductive 2D metal-organic frameworks. J. Am. Chem. Soc. **137**(43), 13780–13783 (2015). https://doi.org/10.1021/jacs.5b09600
165. M.K. Smith, K.E. Jensen, P.A. Pivak, K.A. Mirica, Direct self-assembly of conductive nanorods of metal–organic frameworks into chemiresistive devices on shrinkable polymer films. Chem. Mater. **28**(15), 5264–5268 (2016). https://doi.org/10.1021/acs.chemmater.6b02528
166. M.K. Smith, K.A. Mirica, Self-organized frameworks on textiles (SOFT): conductive fabrics for simultaneous sensing, capture, and filtration of gases. J. Am. Chem. Soc. **139**(46), 16759–16767 (2017). https://doi.org/10.1021/jacs.7b08840
167. D.F. Altomare, F. Porcelli, A. Picciariello, M. Pinto, M. Di Lena et al., The use of the PEN3 e-nose in the screening of colorectal cancer and polyps. Tech. Coloproctol. **20**(6), 405–409 (2016). https://doi.org/10.1007/s10151-016-1457-z
168. T.W. Zhang, T.Liu, M. Zhang, Y. Zhang, H. Li et al., NOS.E: a new fast response electronic nose health monitoring system, in *2018 40th Annual International Conference of the IEEE Engineering in Medicine and Biology Society (EMBC)* **2018**, pp. 4977–4980 (2018). http://doi.org/10.1109/EMBC.2018.8513416
169. W. Li, H. Liu, D. Xie, Z. He, X. Pi, Lung cancer screening based on type-different sensor arrays. Sci. Rep. **7**(1), 1969 (2017). https://doi.org/10.1038/s41598-017-02154-9
170. C.G. Waltman, T.A.T. Marcelissen, J.G.H. van Roermund, Exhaled-breath testing for prostate cancer based on volatile organic compound profiling using an electronic nose device (aeonose): a preliminary report. Eur. Urol. Focus (2018). https://doi.org/10.1016/j.euf.2018.11.006
171. V.N.E. Schuermans, Z. Li, A. Jongen, Z. Wu, J. Shi, J. Ji, N.D. Bouvy, Pilot study: detection of gastric cancer from exhaled air analyzed with an electronic nose in Chinese patients. Surg. Innov. **25**(5), 429–434 (2018). https://doi.org/10.1177/1553350618781267
172. A. Sanaeifar, H. ZakiDizaji, A. Jafari, M.D.L. Guardia, Early detection of contamination and defect in foodstuffs by electronic nose: A review. TrAC Trend. Anal. Chem. **97**, 257–271 (2017). https://doi.org/10.1016/j.trac.2017.09.014
173. H. Yu, J. Wang, Y. Xu, Identification of adulterated milk using electronic nose. Sens. Mater. **19**, 275–285 (2007). https://doi.org/10.1007/978-0-387-71720-3_15
174. A.H. Gómez, J. Wang, G. Hu, A.G. Pereira, Electronic nose technique potential monitoring mandarin maturity. Sens. Actuat. B: Chem. **113**(1), 347–353 (2006). https://doi.org/10.1016/j.snb.2005.03.090
175. A. Blanco-Rodriguez, V.F. Camara, F. Campo, L. Becheran, A. Duran et al., Development of an electronic nose to characterize odours emitted from different stages in a wastewater treatment plant. Water Res. **134**, 92–100 (2018). https://doi.org/10.1016/j.watres.2018.01.067
176. S. Borah, E.L. Hines, M.S. Leeson, D.D. Iliescu, M. Bhuyan, J.W. Gardner, Neural network based electronic nose for classification of tea aroma. Sens. Instrum. Food Qual. Saf. **2**(1), 7–14 (2007). https://doi.org/10.1007/s11694-007-9028-7
177. L. Wozniak, P. Kalinowski, G. Jasinski, P. Jasinski, FFT analysis of temperature modulated semiconductor gas sensor response for the prediction of ammonia concentration under

 https://doi.org/10.1007/s40820-020-0407-5

humidity interference. Microelectron. Reliab. **84**, 163–169 (2018). https://doi.org/10.1016/j.microrel.2018.03.034

178. A.A.S. Ali, A. Farhat, S. Mohamad, A. Amira, F. Bensaali, M. Benammar, A. Bermak, Embedded platform for gas applications using hardware/software co-design and RFID. IEEE Sens. J. **18**(11), 4633–4642 (2018). https://doi.org/10.1109/jsen.2018.2822711
179. M. Ghasemi-Varnamkhasti, Z.S. Amiri, M. Tohidi, M. Dowlati, S.S. Mohtasebi, A.C. Silva, D.D.S. Fernandes, M.C.U. Araujo, Differentiation of cumin seeds using a metal-oxide based gas sensor array in tandem with chemometric tools. Talanta **176**, 221–226 (2018). https://doi.org/10.1016/j.talanta.2017.08.024
180. S. Cui, J. Wang, L. Yang, J. Wu, X. Wang, Qualitative and quantitative analysis on aroma characteristics of ginseng at different ages using E-nose and GC-MS combined with chemometrics. J. Pharm. Biomed. Anal. **102**, 64–77 (2015). https://doi.org/10.1016/j.jpba.2014.08.030
181. J. Gardner, J. Yinon, *Electronic Noses and Sensors for the Detection of Explosives* (Springer, Netherlands, 2004). https://doi.org/10.1007/1-4020-2319-7
182. C. Olguín, N. Laguarda-Miró, L. Pascual, E. García-Breijo, R. Martínez-Mañez, J. Soto, An electronic nose for the detection of Sarin, Soman and Tabun mimics and interfering agents. Sens. Actuat. B: Chem. **202**, 31–37 (2014). https://doi.org/10.1016/j.snb.2014.05.060
183. B. Wang, T.-P. Huynh, W. Wu, N. Hayek, T.T. Do et al., A highly sensitive diketopyrrolopyrrole-based ambipolar transistor for selective detection and discrimination of xylene isomers. Adv. Mater. **28**(21), 4012–4018 (2016). https://doi.org/10.1002/adma.201505641
184. R.G. Pavelko, H. Daly, M. Hübner, C. Hardacre, E. Llobet, Time-resolved DRIFTS, MS, and resistance study of SnO_2 materials: the role of surface hydroxyl groups in formation of donor states. J. Phys. Chem. C **117**(8), 4158–4167 (2013). https://doi.org/10.1021/jp312532u
185. A. Oprea, N. Bârsan, U. Weimar, Work function changes in gas sensitive materials: fundamentals and applications. Sens. Actuat. B: Chem. **142**(2), 470–493 (2009). https://doi.org/10.1016/j.snb.2009.06.043
186. H. Feng, S. Tan, H. Tang, Q. Zheng, Y. Shi et al., Temperature- and coverage-dependent kinetics of photocatalytic reaction of methanol on TiO_2 (110) – (1 × 1) surface. J. Phys. Chem. C **120**(10), 5503–5514 (2016). https://doi.org/10.1021/acs.jpcc.5b12010
187. K.R. Phillips, S.C. Jensen, M. Baron, S.-C. Li, C.M. Friend, Sequential photo-oxidation of methanol to methyl formate on TiO_2(110). J. Am. Chem. Soc. **135**(2), 574–577 (2013). https://doi.org/10.1021/ja3106797
188. J. Wu, H. Shan, W. Chen, X. Gu, P. Tao, C. Song, W. Shang, T. Deng, In situ environmental TEM in imaging gas and liquid phase chemical reactions for materials research. Adv. Mater. **28**(44), 9686–9712 (2016). https://doi.org/10.1002/adma.201602519
189. K. Kishita, T. Kamino, A. Watabe, K. Kuroda, H. Saka, In situ TEM observation of solid-gas reactions. J. Phys: Conf. Ser. **126**(1), 012085 (2008). https://doi.org/10.1088/1742-6596/126/1/012085
190. M. Yoosefian, H. Raissi, A. Mola, The hybrid of Pd and SWCNT (Pd loaded on SWCNT) as an efficient sensor for the formaldehyde molecule detection: a DFT study. Sens. Actuat. B: Chem. **212**, 55–62 (2015). https://doi.org/10.1016/j.snb.2015.02.004
191. V.V. Dobrokhotov, D.N. McIlroy, M.G. Norton, C.A. Berven, Transport properties of hybrid nanoparticle-nanowire systems and their application to gas sensing. Nanotechnology **17**(16), 4135–4142 (2006). https://doi.org/10.1088/0957-4484/17/16/024
192. L. Wang, R. Chai, Z. Lou, G. Shen, Highly sensitive hybrid nanofiber-based room-temperature CO sensors: experiments and density functional theory simulations. Nano Res. **11**(2), 1029–1037 (2017). https://doi.org/10.1007/s12274-017-1718-9
193. A. Omidvar, M. Anafcheh, N.L. Hadipour, Computational studies on carbon nanotube-graphene nanoribbon hybrids by density functional theory calculations. Sci. Iran. **20**(3), 1014–1017 (2013). https://doi.org/10.1016/j.scient.2013.05.018
194. Z. Guo, N. Liao, M. Zhang, W. Xue, Theoretical approach to evaluate graphene/PANI composite as highly selective ammonia sensor. Appl. Surf. Sci. **453**, 336–340 (2018). https://doi.org/10.1016/j.apsusc.2018.05.108
195. H. Fu, X. Yang, X. An, W. Fan, X. Jiang, A. Yu, Experimental and theoretical studies of V_2O_5@TiO_2 core-shell hybrid composites with high gas sensing performance towards ammonia. Sens. Actuat. B: Chem. **252**, 103–115 (2017). https://doi.org/10.1016/j.snb.2017.05.027
196. J. Tian, Z. Zhao, A. Kumar, R.I. Boughton, H. Liu, Recent progress in design, synthesis, and applications of one-dimensional TiO_2 nanostructured surface heterostructures: a review. Chem. Soc. Rev. **43**(20), 6920–6937 (2014). https://doi.org/10.1039/c4cs00180j
197. D. Friedmann, A. Hakki, H. Kim, W. Choi, D. Bahnemann, Heterogeneous photocatalytic organic synthesis: state-of-the-art and future perspectives. Green Chem. **18**(20), 5391–5411 (2016). https://doi.org/10.1039/c6gc01582d
198. C. Gao, J. Wang, H. Xu, Y. Xiong, Coordination chemistry in the design of heterogeneous photocatalysts. Chem. Soc. Rev. **46**(10), 2799–2823 (2017). https://doi.org/10.1039/c6cs00727a
199. K. Rajeshwar, M.E. Osugi, W. Chanmanee, C.R. Chenthamarakshan, M.V.B. Zanoni, P. Kajitvichyanukul, R. Krishnan-Ayer, Heterogeneous photocatalytic treatment of organic dyes in air and aqueous media. J. Photochem. Photobiol., C **9**(4), 171–192 (2008). https://doi.org/10.1016/j.jphotochemrev.2008.09.001
200. Y. Qu, X. Duan, Progress, challenge and perspective of heterogeneous photocatalysts. Chem. Soc. Rev. **42**(7), 2568–2580 (2013). https://doi.org/10.1039/c2cs35355e
201. A. Kudo, Y. Miseki, Heterogeneous photocatalyst materials for water splitting. Chem. Soc. Rev. **38**(1), 253–278 (2009). https://doi.org/10.1039/b800489g

202. Y.Y. Broza, X. Zhou, M. Yuan, D. Qu, Y. Zheng et al., Disease detection with molecular biomarkers: from chemistry of body fluids to nature-inspired chemical sensors. Chem. Rev. **119**(22), 11761–11817 (2019). https://doi.org/10.1021/acs.chemrev.9b00437
203. M.-S. Yao, L.-A. Cao, Y.-X. Tang, G.-E. Wang, R.-H. Liu et al., Gas transport regulation in a MO/MOF interface for enhanced selective gas detection. J. Mater. Chem. A **7**(31), 18397–18403 (2019). https://doi.org/10.1039/C9TA05226G
204. M. Yao, J.-J. Zheng, A.-Q. Wu, G. Xu, S.S. Nagarkar, G. Zhang, M. Tsujimoto, S. Sakaki, S. Horike, K.-I. Otake, Dual-ligand porous coordination polymer chemiresistor with modulated conductivity and porosity. Angew. Chem. Int. Ed. **59**(1), 172–176 (2020). https://doi.org/10.1002/anie.201909096
205. M.S. Yao, J.W. Xiu, Q.Q. Huang, W.-H. Li, W.W. Wu et al., Van der Waals heterostructured MOF-on-MOF thin films: cascading functionality to realize advanced chemiresistive sensing. Angew. Chem. Int. Ed. **58**(42), 14915–14919 (2019). https://doi.org/10.1002/anie.201907772
206. X. Fang, B. Zong, S. Mao, Metal-organic framework-based sensors for environmental contaminant sensing. Nano-Micro Lett. **10**(4), 64 (2018). https://doi.org/10.1007/s40820-018-0218-0
207. W. Wu, B. Wang, M. Segev-Bar, W. Dou, F. Niu et al., Free-standing and eco-friendly polyaniline thin films for multifunctional sensing of physical and chemical stimuli. Adv. Funct. Mater. **27**(40), 1703147 (2017). https://doi.org/10.1002/adfm.201703147
208. O.S. Kwon, S.J. Park, J.S. Lee, E. Park, T. Kim et al., Multidimensional conducting polymer nanotubes for ultrasensitive chemical nerve agent sensing. Nano Lett. **12**(6), 2797–2802 (2012). https://doi.org/10.1021/nl204587t
209. K. Yan, D. Zhang, Feature selection and analysis on correlated gas sensor data with recursive feature elimination. Sens. Actuat. B: Chem. **212**, 353–363 (2015). https://doi.org/10.1016/j.snb.2015.02.025
210. S. Cui, S. Mao, G. Lu, J. Chen, Graphene coupled with nanocrystals: opportunities and challenges for energy and sensing applications. J. Phys. Chem. Lett. **4**(15), 2441–2454 (2013). https://doi.org/10.1021/jz400976a31d
211. S. Mao, G. Lu, J. Chen, Nanocarbon-based gas sensors: progress and challenges. J. Mater. Chem. A **2**(16), 5573–5579 (2014). https://doi.org/10.1039/c3ta13823b
212. H.R. Estakhroyeh, E. Rashedi, M. Mehran, Design and construction of electronic nose for multi-purpose applications by sensor array arrangement using IBGSA. J. Intell. Robot. Syst. **92**(2), 205–221 (2017). https://doi.org/10.1007/s10846-017-0759-3
213. J.L. Herrero, J. Lozano, J.P. Santos, J.I. Suarez, On-line classification of pollutants in water using wireless portable electronic noses. Chemosphere **152**, 107–116 (2016). https://doi.org/10.1016/j.chemosphere.2016.02.106
214. F. Chang, P. Heinemann, Prediction of human responses to dairy odor using an electronic nose and neural networks. Trans. ASABE **61**(2), 399–409 (2018). https://doi.org/10.13031/trans.12177
215. J.C. Rodriguez Gamboa, E.S. Albarracin E, A.J. da Silva, L.L. de Andrade-Lima, T.A.E. Ferreira, Wine quality rapid detection using a compact electronic nose system: application focused on spoilage thresholds by acetic acid. **Lwt 108**, 377–384 (2019). https://doi.org/10.1016/j.lwt.2019.03.074
216. M. Tohidi, M. Ghasemi-Varnamkhasti, V. Ghafarinia, S. Saeid Mohtasebi, M. Bonyadian, Identification of trace amounts of detergent powder in raw milk using a customized low-cost artificial olfactory system: a novel method. Measurement **124**, 120–129 (2018). https://doi.org/10.1016/j.measurement.2018.04.006
217. A. Gorji-Chakespari, A.M. Nikbakht, F. Sefidkon, M. Ghasemi-Varnamkhasti, J. Brezmes, E. Llobet, Performance comparison of fuzzy ARTMAP and LDA in qualitative classification of iranian rosa damascena essential oils by an electronic nose. Sensors (Basel) **16**(5), 636 (2016). https://doi.org/10.3390/s16050636
218. W. Dong, J. Zhao, R. Hu, Y. Dong, L. Tan, Differentiation of Chinese robusta coffees according to species, using a combined electronic nose and tongue, with the aid of chemometrics. Food Chem. **229**, 743–751 (2017). https://doi.org/10.1016/j.foodchem.2017.02.149
219. A. Shahid, J.H. Choi, A. Rana, H.S. Kim, Least squares neural network-based wireless E-Nose system using an SnO_2 sensor array. Sensors (Basel) **18**(5), 1446 (2018). https://doi.org/10.3390/s18051446
220. L. Yao, K. Kan, Y. Lin, J. Song, J. Wang, J. Gao, P. Shen, L. Li, K. Shi, Si doped highly crystalline mesoporous In_2O_3 nanowires: synthesis, characterization and ultra-high response to NOx at room temperature. RSC Adv. **5**(20), 15515–15523 (2015). https://doi.org/10.1039/c4ra14354j
221. K. He, Z. Jin, X. Chu, W. Bi, W. Wang, C. Wang, S. Liu, Fast response–recovery time toward acetone by a sensor prepared with Pd doped WO_3 nanosheets. RSC Adv. **9**(49), 28439–28450 (2019). https://doi.org/10.1039/c9ra04429a
222. L. Lv, Y. Wang, P. Cheng, B. Zhang, F. Dang, L. Xu, Ultrasonic spray pyrolysis synthesis of three-dimensional $ZnFe_2O_4$-based macroporous spheres for excellent sensitive acetone gas sensor. Sens. Actuat. B: Chem. **297**, 126755 (2019). https://doi.org/10.1016/j.snb.2019.126755
223. K. Shingange, H. Swart, G.H. Mhlongo, Ultrafast detection of low acetone concentration displayed by Au-loaded $LaFeO_3$ nanobelts owing to synergetic effects of porous 1D morphology and catalytic activity of Au nanoparticles. ACS Omega **4**(21), 19018–19029 (2019). https://doi.org/10.1021/acsomega.9b01989
224. C.-L. Hsu, B.-Y. Jhang, C. Kao, T.-J. Hsueh, UV-illumination and Au-nanoparticles enhanced gas sensing of p-type Na-doped ZnO nanowires operating at room temperature. Sens. Actuat. B: Chem. **274**, 565–574 (2018). https://doi.org/10.1016/j.snb.2018.08.016
225. Y. Zhang, L. Zhou, Y. Liu, D. Liu, F. Liu et al., Gas sensor based on samarium oxide loaded mulberry-shaped tin oxide for highly selective and sub ppm-level acetone detection.

 https://doi.org/10.1007/s40820-020-0407-5

J. Colloid Interface Sci. **531**, 74–82 (2018). https://doi.org/10.1016/j.jcis.2018.07.052

226. Y. Lu, J. Li, J. Han, H.T. Ng, C. Binder, C. Partridge, M. Meyyappan, Room temperature methane detection using palladium loaded single-walled carbon nanotube sensors. Chem. Phys. Lett. **391**(4–6), 344–348 (2004). https://doi.org/10.1016/j.cplett.2004.05.029
227. H. Li, J. Xu, Y. Zhu, X. Chen, Q. Xiang, Enhanced gas sensing by assembling Pd nanoparticles onto the surface of SnO_2 nanowires. Talanta **82**(2), 458–463 (2010). https://doi.org/10.1016/j.talanta.2010.04.053
228. J.-Y. Kim, J.-H. Lee, J.-H. Kim, A. Mirzaei, H.W. Kim, S.S. Kim, Realization of H_2S sensing by Pd-functionalized networked CuO nanowires in self-heating mode. Sens. Actuat. B: Chem. **299**, 126965 (2019). https://doi.org/10.1016/j.snb.2019.126965
229. Y. Yang, C. Tian, J. Wang, L. Sun, K. Shi, W. Zhou, H. Fu, Facile synthesis of novel 3D nanoflower-like Cu(x)O/multilayer graphene composites for room temperature NO(x) gas sensor application. Nanoscale **6**(13), 7369–7378 (2014). https://doi.org/10.1039/c4nr00196f
230. J. Zhang, D. Zeng, S. Zhao, J. Wu, K. Xu, Q. Zhu, G. Zhang, C. Xie, Room temperature NO_2 sensing: what advantage does the rGO-NiO nanocomposite have over pristine NiO? Phys. Chem. Chem. Phys. **17**(22), 14903–14911 (2015). https://doi.org/10.1039/c5cp01987g
231. Q. Huang, D. Zeng, H. Li, C. Xie, Room temperature formaldehyde sensors with enhanced performance, fast response and recovery based on zinc oxide quantum dots/graphene nanocomposites. Nanoscale **4**(18), 5651–5658 (2012). https://doi.org/10.1039/c2nr31131c
232. H. Wang, S. Nie, H. Li, R. Ali, J. Fu et al., 3D hollow quasi-graphite capsules/polyaniline hybrid with a high performance for room-temperature ammonia gas sensors. ACS Sens. **4**(9), 2343–2350 (2019). https://doi.org/10.1021/acssensors.9b00882
233. M. Kooti, S. Keshtkar, M. Askarieh, A. Rashidi, Progress toward a novel methane gas sensor based on SnO_2 nanorods-nanoporous graphene hybrid. Sens. Actuator. B: Chem. **281**, 96–106 (2019). https://doi.org/10.1016/j.snb.2018.10.032
234. H. Liu, W. Zhang, H. Yu, L. Gao, Z. Song et al., Solution-processed gas sensors employing SnO_2 quantum dot/MWCNT nanocomposites. ACS Appl. Mater. Interfaces. **8**(1), 840–846 (2016). https://doi.org/10.1021/acsami.5b10188
235. F. Liang, S. Chen, W. Xie, C. Zou, The decoration of Nb-doped TiO_2 microspheres by reduced graphene oxide for enhanced CO gas sensing. J. Phys. Chem. Solids **114**, 195–200 (2018). https://doi.org/10.1016/j.jpcs.2017.11.001
236. C. Zou, J. Hu, Y. Su, F. Shao, Z. Tao et al., Three-dimensional Fe_3O_4@reduced graphene oxide heterojunctions for high-performance room-temperature NO_2 sensors. Front. Mater. **6**, 00195 (2019). https://doi.org/10.3389/fmats.2019.00195
237. T. Jiang, P. Wan, Z. Ren, S. Yan, Anisotropic polyaniline/SWCNT composite films prepared by in situ electropolymerization on highly oriented polyethylene for high-efficiency ammonia sensor. ACS Appl. Mater. Interfaces. **11**(41), 38169–38176 (2019). https://doi.org/10.1021/acsami.9b13336
238. G.K. Ekaterina Dovgolevsky, U. Tisch, H. Haick, Monolayer-capped cubic platinum nanoparticles for sensing nonpolar analytes in highly umid atmospheres. Am. Chem. Soc. **114**(33), 14042–14049 (2010). https://doi.org/10.1021/jp105810w
239. C.H. Park, V. Schroeder, B.J. Kim, T.M. Swager, Ionic liquid-carbon nanotube sensor arrays for human breath related volatile organic compounds. ACS Sens. **3**(11), 2432–2437 (2018). https://doi.org/10.1021/acssensors.8b00987
240. Y. Zilberman, U. Tisch, G. Shuster, W. Pisula, X. Feng, K. Mullen, H. Haick, Carbon nanotube/hexa-peri-hexabenzocoronene bilayers for discrimination between nonpolar volatile organic compounds of cancer and humid atmospheres. Adv. Mater. **22**(38), 4317–4320 (2010). https://doi.org/10.1002/adma.201001275
241. P. Sun, Y. Cai, S. Du, X. Xu, L. You et al., Hierarchical α-Fe_2O_3/SnO_2 semiconductor composites: hydrothermal synthesis and gas sensing properties. Sens. Actuat. B: Chem. **182**, 336–343 (2013). https://doi.org/10.1016/j.snb.2013.03.019
242. G. Lu, J. Xu, J. Sun, Y. Yu, Y. Zhang, F. Liu, UV-enhanced room temperature NO_2 sensor using ZnO nanorods modified with SnO_2 nanoparticles. Sens. Actuat. B: Chem. **162**(1), 82–88 (2012). https://doi.org/10.1016/j.snb.2011.12.039
243. D. Gu, X. Li, Y. Zhao, J. Wang, Enhanced NO_2 sensing of SnO_2/SnS_2 heterojunction based sensor. Sens. Actuat. B: Chem. **244**, 67–76 (2017). https://doi.org/10.1016/j.snb.2016.12.125
244. C.W. Peng Sun, J. Liu, X. Zhou, X. Li, X. Hu, G. Lu, Hierarchical assembly of α-Fe_2O_3 nanosheets on SnO_2 hollow nanospheres with enhanced ethanol sensing properties. ACS Appl. Mater. Interfaces. **7**(34), 19119–19125 (2015). https://doi.org/10.1021/acsami.5b04751
245. X. Li, C. Wang, H. Guo, P. Sun, F. Liu, X. Liang, G. Lu, Double-shell architectures of $ZnFe_2O_4$ nanosheets on ZnO hollow spheres for high-performance gas sensors. ACS Appl. Mater. Interfaces. **7**(32), 17811–17818 (2015). https://doi.org/10.1021/acsami.5b04118
246. C. Wang, X. Cheng, X. Zhou, P. Sun, X. Hu, K. Shimanoe, G. Lu, N. Yamazoe, Hierarchical α-Fe_2O_3/NiO composites with a hollow structure for a gas sensor. ACS Appl. Mater. Interfaces. **6**(15), 12031–12307 (2014). https://doi.org/10.1021/am501063z
247. K. Xu, N. Li, D. Zeng, S. Tian, S. Zhang, D. Hu, C. Xie, Interface bonds determined gas-sensing of SnO_2–SnS_2 hybrids to ammonia at room temperature. ACS Appl. Mater. Interfaces. **7**(21), 11359–12368 (2015). https://doi.org/10.1021/acsami.5b01856
248. C. Wu, J. Zhang, X. Wang, C. Xie, S. Shi, D. Zeng, Effect of heterointerface on NO_2 sensing properties of in situ formed TiO_2 QDs-decorated NiO nanosheets. Nanomaterials **9**(11), 1628 (2019). https://doi.org/10.3390/nano9111628
249. X. Chang, X. Li, X. Qiao, K. Li, Y. Xiong, X. Li, T. Guo, L. Zhu, Q. Xue, Metal-organic frameworks derived ZnO@MoS

nanosheets core/shell heterojunctions for ppb-level acetone detection: ultra-fast response and recovery. Sens. Actuat. B: Chem. **304**, 127430 (2020). https://doi.org/10.1016/j.snb.2019.127430

250. K.T. Alali, J. Liu, Q. Liu, R. Li, H. Zhang, K. Aljebawi, P. Liu, J. Wang, Enhanced acetone gas sensing response of ZnO/$ZnCo_2O_4$ nanotubes synthesized by single capillary electrospinning technology. Sens. Actuat. B: Chem. **252**, 511–522 (2017). https://doi.org/10.1016/j.snb.2017.06.034
251. J.H. Bang, M.S. Choi, A. Mirzaei, W. Oum, S. Han, S.S. Kim, H.W. Kim, Porous Si/SnO_2 nanowires heterostructures for H_2S gas sensing. Ceram. Int. **46**(1), 604–611 (2020). https://doi.org/10.1016/j.ceramint.2019.09.010
252. S. Li, A. Liu, Z. Yang, J. He, J. Wang et al., Room temperature gas sensor based on tin dioxide@ polyaniline nanocomposite assembled on flexible substrate: ppb-level detection of NH_3. Sens. Actuat. B: Chem. **299**, 126970 (2019). https://doi.org/10.1016/j.snb.2019.126970
253. L. Liu, Y. Wang, Y. Dai, G. Li, S. Wang, T. Li, T. Zhang, S. Qin, In situ growth of NiO@SnO_2 hierarchical nanostructures for high performance H_2S sensing. ACS Appl. Mater. Interfaces. **11**(47), 44829–44836 (2019). https://doi.org/10.1021/acsami.9b13001
254. Q. Sun, J. Wang, J. Hao, S. Zheng, P. Wan, T. Wang, H. Fang, Y. Wang, SnS_2/SnS p–n heterojunctions with an accumulation layer for ultrasensitive room-temperature NO_2 detection. Nanoscale **11**(29), 13741–13749 (2019). https://doi.org/10.1039/c9nr02780g
255. W. Zeng, Y. Liu, J. Mei, C. Tang, K. Luo, S. Li, H. Zhan, Z. He, Hierarchical SnO_2–Sn_3O_4 heterostructural gas sensor with high sensitivity and selectivity to NO_2. Sens. Actuat. B: Chem. **301**, 127010 (2019). https://doi.org/10.1016/j.snb.2019.127010
256. X. Zhou, W. Feng, C. Wang, X. Hu, X. Li, P. Sun, K. Shimanoe, N. Yamazoe, G. Lu, Porous ZnO/$ZnCo_2O_4$ hollow spheres: synthesis, characterization, and applications in gas sensing. J. Mater. Chem. A **2**(41), 17683–17690 (2014). https://doi.org/10.1039/c4ta04386c
257. L. Han, D. Wang, J. Cui, L. Chen, T. Jiang, Y. Lin, Study on formaldehyde gas-sensing of In_2O_3-sensitized ZnO nanoflowers under visible light irradiation at room temperature. J. Mater. Chem. **22**(25), 12915–12920 (2012). https://doi.org/10.1039/c2jm16105b
258. T. Zhou, Y. Sang, X. Wang, C. Wu, D. Zeng, C. Xie, Pore size dependent gas-sensing selectivity based on ZnO@ZIF nanorod arrays. Sens. Actuat. B: Chem. **258**, 1099–1106 (2018). https://doi.org/10.1016/j.snb.2017.12.024
259. M.S. Yao, W.X. Tang, G.E. Wang, B. Nath, G. Xu, MOF thin film-coated metal oxide nanowire array: significantly improved chemiresistor sensor performance. Adv. Mater. **28**(26), 5229–5234 (2016). https://doi.org/10.1002/adma.201506457
260. X. Wu, S. Xiong, Z. Mao, S. Hu, X. Long, A designed ZnO@ZIF-8 core-shell nanorod film as a gas sensor with excellent selectivity for H_2 over CO. Chemistry **23**(33), 7969–7975 (2017). https://doi.org/10.1002/chem.201700320
261. S.S. Nair, N. Illyaskutty, B. Tam, A.O. Yazaydin, K. Emmerich et al., ZnO@ZIF-8: Gas sensitive core-shell hetero-structures show reduced cross-sensitivity to humidity. Sens. Actuat. B: Chem. **304**, 127184 (2020). https://doi.org/10.1016/j.snb.2019.127184
262. P. Wang, X. Zou, H. Tan, S. Wu, L. Jiang, G. Zhu, Ultrathin ZIF-8 film containing polyoxometalate as an enhancer for selective formaldehyde sensing. J. Mater. Chem. C **6**(20), 5412–5419 (2018). https://doi.org/10.1039/c8tc00987b
263. H. Tian, H. Fan, M. Li, L. Ma, Zeolitic imidazolate framework coated ZnO nanorods as molecular sieving to improve selectivity of formaldehyde gas sensor. ACS Sensor **1**(3), 243–250 (2015). https://doi.org/10.1021/acssensors.5b00236
264. M. Drobek, J.H. Kim, M. Bechelany, C. Vallicari, A. Julbe, S.S. Kim, MOF-based membrane encapsulated ZnO nanowires for enhanced gas sensor selectivity. ACS Appl. Mater. Interfaces. **8**(13), 8323–8328 (2016). https://doi.org/10.1021/acsami.5b12062
265. L. Dang, G. Zhang, K. Kan, Y. Lin, F. Bai, L. Jing, P. Shen, L. Li, K. Shi, Heterostructured Co_3O_4/PEI–CNTs composite: fabrication, characterization and CO gas sensors at room temperature. J. Mater. Chem. A **2**(13), 4558–4565 (2014). https://doi.org/10.1039/c3ta15019d
266. X. Zhang, Y. Sun, Y. Fan, Z. Liu, Z. Zeng, H. Zhao, X. Wang, J. Xu, Effects of organotin halide perovskite and Pt nanoparticles in SnO_2-based sensing materials on the detection of formaldehyde. J. Mater. Sci.-Mater. Electron. **30**(23), 20624–20637 (2019). https://doi.org/10.1007/s10854-019-02428-0
267. S. Javanmardi, S. Nasresfahani, M.H. Sheikhi, Facile synthesis of PdO/SnO_2/CuO nanocomposite with enhanced carbon monoxide gas sensing performance at low operating temperature. Mater. Res. Bull. **118**, 110496 (2019). https://doi.org/10.1016/j.materresbull.2019.110496
268. J.H. Lee, J.H. Kim, J.Y. Kim, A. Mirzaei, H.W. Kim, S.S. Kim, ppb-Level selective hydrogen gas detection of Pd-functionalized In_2O_3-loaded ZnO nanofiber gas sensors. Sensors (Basel) **19**(19), 4276 (2019). https://doi.org/10.3390/s19194276
269. Y. Xia, J. Wang, L. Xu, X. Li, S. Huang, A room-temperature methane sensor based on Pd-decorated ZnO/rGO hybrids enhanced by visible light photocatalysis. Sens. Actuat. B: Chem. **304**, 127334 (2020). https://doi.org/10.1016/j.snb.2019.127334
270. H. Tian, H. Fan, J. Ma, Z. Liu, L. Ma, S. Lei, J. Fang, C. Long, Pt-decorated zinc oxide nanorod arrays with graphitic carbon nitride nanosheets for highly efficient dual-functional gas sensing. J. Hazard. Mater. **341**, 102–111 (2018). https://doi.org/10.1016/j.jhazmat.2017.07.056
271. W.-C. Lu, S.S. Kumar, Y.-C. Chen, C.-M. Hsu, H.-N. Lin, Au/Cu_2O/ZnO ternary nanocomposite for low concentration NO_2 gas sensing at room temperature. Mater. Lett. **256**, 126657 (2019). https://doi.org/10.1016/j.matlet.2019.126657
272. Y. Wei, G. Yi, Y. Xu, L. Zhou, X. Wang et al., Synthesis, characterization, and gas-sensing properties of Ag/SnO_2/rGO composite by a hydrothermal method. J. Mater.

 https://doi.org/10.1007/s40820-020-0407-5

Sci.-Mater. Electron. **28**(22), 17049–17057 (2017). https://doi.org/10.1007/s10854-017-7630-y

273. Y. Zhou, Q. Ding, J. Li, Q. Yang, T. Wu et al., TiO_2/$InVO_4$ n–n heterojunctions for efficient ammonia gas detection and their sensing mechanisms. J. Mater. Sci. **54**(21), 13660–13673 (2019). https://doi.org/10.1007/s10853-019-03868-z
274. S. Nasresfahani, M.H. Sheikhi, M. Tohidi, A. Zarifkar, Methane gas sensing properties of Pd-doped SnO_2/reduced graphene oxide synthesized by a facile hydrothermal route. Mater. Res. Bull. **89**, 161–169 (2017). https://doi.org/10.1016/j.materresbull.2017.01.032
275. S. Li, Y. Diao, Z. Yang, J. He, J. Wang et al., Enhanced room temperature gas sensor based on Au-loaded mesoporous In_2O_3 nanospheres@polyaniline core-shell nanohybrid assembled on flexible PET substrate for NH_3 detection. Sens. Actuator. B: Chem. **276**, 526–533 (2018). https://doi.org/10.1016/j.snb.2018.08.120
276. B. Liu, Y. Li, L. Gao, F. Zhou, G. Duan, Ultrafine Pt NPs-decorated SnO_2/α-Fe_2O_3 hollow nanospheres with highly enhanced sensing performances for styrene. J. Hazard. Mater. **358**, 355–365 (2018). https://doi.org/10.1016/j.jhazmat.2018.07.021
277. M. Chen, H. Wang, J. Hu, Y. Zhang, K. Li et al., Near-room-temperature ethanol gas sensor based on mesoporous Ag/Zn–LaFeO3 nanocomposite. Adv. Mater. Interfaces **6**(1), 1801453 (2018). https://doi.org/10.1002/admi.201801453
278. E. Lee, A. VahidMohammadi, B.C. Prorok, Y.S. Yoon, M. Beidaghi, D.-J. Kim, Room temperature gas sensing of two-dimensional titanium carbide (MXene). ACS Appl. Mater. Interfaces. **9**(42), 37184–37190 (2017). https://doi.org/10.1021/acsami.7b11055
279. J. Zhou, H. Lin, X.-F. Cheng, J. Shu, J.-H. He et al., Ultrasensitive and robust organic gas sensors through dual hydrogen bonding. Mater. Horiz. **6**, 554–562 (2019). https://doi.org/10.1039/C8MH01098F
280. T. Vossmeyer, B. Guse, I. Besnard, R.E. Bauer, K. MüLLEN, A. Yasuda, Gold nanoparticle/polyphenylene dendrimer composite films: preparation and vapor-sensing properties. Adv. Mater. **14**(3), 238–242 (2002). https://doi.org/10.1002/1521-4095(20020205)14:3%3C238:AID-ADMA238%3E3.0.CO;2-%23
281. M.E. DMello, N.G. Sundaram, A. Singh, A.K. Singh, S.B. Kalidindi, An amine functionalized zirconium metal–organic framework as an effective chemiresistive sensor for acidic gases. Chem. Commun. **55**(3), 349–352 (2019). https://doi.org/10.1039/C8CC06875E
282. C. Wongchoosuk, M. Lutz, T. Kerdcharoen, Detection and classification of human body odor using an electronic nose. Sensors (Basel) **9**(9), 7234–7249 (2009). https://doi.org/10.3390/s90907234
283. J.A. Covington, E.W. Westenbrink, N. Ouaret, R. Harbord, C. Bailey et al., Application of a novel tool for diagnosing bile acid diarrhoea. Sensors (Basel) **13**(9), 11899–11912 (2013). https://doi.org/10.3390/s130911899
284. R. Thriumani, A. Zakaria, Y.Z.H. Hashim, A.I. Jeffree, K.M. Helmy et al., A study on volatile organic compounds emitted by in vitro lung cancer cultured cells using gas sensor array and SPME-GCMS. BMC Cancer **18**(1), 362 (2018). https://doi.org/10.1186/s12885-018-4235-7
285. M.R. van Hooren, N. Leunis, D.S. Brandsma, A.C. Dingemans, B. Kremer, K.W. Kross, Differentiating head and neck carcinoma from lung carcinoma with an electronic nose: a proof of concept study. Eur. Arch. Otorhinolaryngol. **273**(11), 3897–3903 (2016). https://doi.org/10.1007/s00405-016-4038-x
286. E.J. Bijl, J.G. Groeneweg, D.W. Wesselius, D.L. Stronks, F. Huygen, Diagnosing complex regional pain syndrome using an electronic nose, a pilot study. J. Breath Res. **13**(3), 036004 (2019). https://doi.org/10.1088/1752-7163/aaf9c1
287. A.K. Pavlou, N. Magan, J.M. Jones, J. Brown, P. Klatser, A.P. Turner, Detection of Mycobacterium tuberculosis (TB) in vitro and in situ using an electronic nose in combination with a neural network system. Biosens. Bioelectron. **20**(3), 538–544 (2004). https://doi.org/10.1016/j.bios.2004.03.002
288. H. Amal, M. Leja, K. Funka, R. Skapars, A. Sivins et al., Detection of precancerous gastric lesions and gastric cancer through exhaled breath. Gut **65**(3), 400–407 (2016). https://doi.org/10.1136/gutjnl-2014-308536
289. N. Bhattacharyya, S. Seth, B. Tudu, P. Tamuly, A. Jana, D. Ghosh, R. Bandyopadhyay, M. Bhuyan, Monitoring of black tea fermentation process using electronic nose. J. Food Eng. **80**(4), 1146–1156 (2007). https://doi.org/10.1016/j.jfoodeng.2006.09.006
290. L. Huang, J. Zhao, Q. Chen, Y. Zhang, Nondestructive measurement of total volatile basic nitrogen (TVB-N) in pork meat by integrating near infrared spectroscopy, computer vision and electronic nose techniques. Food Chem. **145**, 228–236 (2014). https://doi.org/10.1016/j.foodchem.2013.06.073
291. M. Tohidi, M. Ghasemi-Varnamkhasti, V. Ghafarinia, M. Bonyadian, S.S. Mohtasebi, Development of a metal oxide semiconductor-based artificial nose as a fast, reliable and non-expensive analytical technique for aroma profiling of milk adulteration. Int. Dairy J. **77**, 38–46 (2018). https://doi.org/10.1016/j.idairyj.2017.09.003
292. X. Tian, J. Wang, S. Cui, Analysis of pork adulteration in minced mutton using electronic nose of metal oxide sensors. J. Food Eng. **119**(4), 744–749 (2013). https://doi.org/10.1016/j.jfoodeng.2013.07.004
293. M. Laureati, S. Buratti, G. Giovanelli, M. Corazzin, D.P. Lo Fiego, E. Pagliarini, Characterization and differentiation of Italian Parma, San Daniele and Toscano dry-cured hams: a multi-disciplinary approach. Meat Sci. **96**(1), 288–294 (2014). https://doi.org/10.1016/j.meatsci.2013.07.014
294. X. Hong, J. Wang, S. Qiu, Authenticating cherry tomato juices: discussion of different data standardization and fusion approaches based on electronic nose and tongue. Food Res. Int. **60**, 173–179 (2014). https://doi.org/10.1016/j.foodres.2013.10.039
295. Y. Sun, J. Wang, S. Cheng, Discrimination among tea plants either with different invasive severities or different invasive times using MOS electronic nose combined with

a new feature extraction method. Comput. Electron. Agric. **143**, 293–301 (2017). https://doi.org/10.1016/j.compag.2017.11.007

296. X. Gu, Y. Sun, K. Tu, L. Pan, Evaluation of lipid oxidation of Chinese-style sausage during processing and storage based on electronic nose. Meat Sci. **133**, 1–9 (2017). https://doi.org/10.1016/j.meatsci.2017.05.017
297. L. Shao, L. Wei, X. Zhang, G. Hui, Z. Zhao, Fabrication of electronic nose system and exploration on its applications in mango fruit (M-indica cv. Datainong) quality rapid determination. J. Food Meas. Charact. **11**(4), 1969–1977 (2017). https://doi.org/10.1007/s11694-017-9579-1
298. S. Song, L. Yuan, X. Zhang, K. Hayat, H. Chen, F. Liu, Z. Xiao, Y. Niu, Rapid measuring and modelling flavour quality changes of oxidised chicken fat by electronic nose profiles through the partial least squares regression analysis. Food Chem. **141**(4), 4278–4288 (2013). https://doi.org/10.1016/j.foodchem.2013.07.009
299. L. Huang, H. Liu, B. Zhang, D. Wu, Application of electronic nose with multivariate analysis and sensor selection for botanical origin identification and quality determination of honey. Food Bioprocess Tech. **8**(2), 359–370 (2014). https://doi.org/10.1007/s11947-014-1407-6
300. C. Steine, F. Beaucousin, C. Siv, G. Peiffer, Potential of semiconductor sensor arrays for the origin authentication of pure Valencia orange juices. J. Agr. Food Chem. **49**(7), 3151–3160 (2001). https://doi.org/10.1021/jf0014664
301. A.Z. Berna, S. Trowell, D. Clifford, W. Cynkar, D. Cozzolino, Geographical origin of Sauvignon Blanc wines predicted by mass spectrometry and metal oxide based electronic nose. Anal. Chim. Acta **648**(2), 146–152 (2009). https://doi.org/10.1016/j.aca.2009.06.056
302. C. Severini, I. Ricci, M. Marone, A. Derossi, T. De Pilli, Changes in the aromatic profile of espresso coffee as a function of the grinding grade and extraction time: a study by the electronic nose system. J. Agric. Food Chem. **63**(8), 2321–2327 (2015). https://doi.org/10.1021/jf505691u
303. C. Cevoli, L. Cerretani, A. Gori, M.F. Caboni, T. Gallina Toschi, A. Fabbri, Classification of Pecorino cheeses using electronic nose combined with artificial neural network and comparison with GC-MS analysis of volatile compounds. Food Chem. **129**(3), 1315–1319 (2011). https://doi.org/10.1016/j.foodchem.2011.05.126
304. Z. Kovács, I. Dalmadi, L. Lukács, L. Sipos, K. Szántai-Kőhegyi, Z. Kókai, A. Fekete, Geographical origin identification of pure Sri Lanka tea infusions with electronic nose, electronic tongue and sensory profile analysis. J. Chemomet. **24**(3–4), 121–130 (2010). https://doi.org/10.1002/cem.1280
305. A. Zakaria, A.Y. Shakaff, M.J. Masnan, M.N. Ahmad, A.H. Adom et al., A biomimetic sensor for the classification of honeys of different floral origin and the detection of adulteration. Sensors (Basel) **11**(8), 7799–7822 (2011). https://doi.org/10.3390/s110807799
306. V.H. Bennetts, E. Schaffernicht, V.P. Sese, A.J. Lilienthal, M. Trincavelli, A novel approach for gas discrimination in natural environments with open sampling systems, in *IEEE Sensors 2014 Proceedings* (2014). http://doi.org/10.1109/icsens.2014.6985437
307. E.J. Wolfrum, R.M. Meglen, D. Peterson, J. Sluiter, Metal oxide sensor arrays for the detection, differentiation, and quantification of volatile organic compounds at sub-parts-per-million concentration levels. Sens. Actuat. B: Chem. **115**(1), 322–329 (2006). https://doi.org/10.1016/j.snb.2005.09.026
308. X. Zhou, Y. Wang, Z. Wang, L. Yang, X. Wu, N. Han, Y. Chen, Synergetic p + n field-effect transistor circuits for ppb-level xylene detection. IEEE Sens. J. **18**(9), 3875–3882 (2018). https://doi.org/10.1109/jsen.2018.2818710
309. B. Szulczyński, J. Gębicki, J. Namieśnik, Monitoring and efficiency assessment of biofilter air deodorization using electronic nose prototype. Chem. Pap. **72**(3), 527–532 (2017). https://doi.org/10.1007/s11696-017-0310-9
310. B. Mumyakmaz, K. Karabacak, An E-Nose-based indoor air quality monitoring system: prediction of combustible and toxic gas concentrations. Turk. J. Electr. Eng. Comput. Sci. **23**, 729–740 (2015). https://doi.org/10.3906/elk-1304-210
311. S. De Vito, E. Massera, G. Di Francia, C. Ambrosino, P. Di Palma, V. Magliulo, *Sensors and Microsystems*, Chapter 59, 373–377 (2011). http://doi.org/10.1007/978-94-007-1324-6_59
312. B. Urasinska-Wojcik, T.A. Vincent, M.F. Chowdhury, J.W. Gardner, Ultrasensitive WO_3 gas sensors for NO_2 detection in air and low oxygen environment. Sens. Actuat. B: Chem. **239**, 1051–1059 (2017). https://doi.org/10.1016/j.snb.2016.08.080
313. Z. Hai, J. Wang, Electronic nose and data analysis for detection of maize oil adulteration in sesame oil. Sens. Actuat. B: Chem. **119**(2), 449–455 (2006). https://doi.org/10.1016/j.snb.2006.01.001
314. O.S. Jolayemi, F. Tokatli, S. Buratti, C. Alamprese, Discriminative capacities of infrared spectroscopy and e-nose on Turkish olive oils. Eur. Food Res. Technol. **243**(11), 2035–2042 (2017). https://doi.org/10.1007/s00217-017-2909-z
315. G. Giovanelli, S. Limbo, S. Buratti, Effects of new packaging solutions on physico-chemical, nutritional and aromatic characteristics of red raspberries (Rubus idaeus L.) in postharvest storage. Postharvest Biol. Technol. **98**, 72–81 (2014). https://doi.org/10.1016/j.postharvbio.2014.07.002
316. R. Lopez, I. Giraldez, A. Palma, M. Jesus Diaz, Assessment of compost maturity by using an electronic nose. Waste Manag **48**, 174–180 (2016). https://doi.org/10.1016/j.wasman.2015.09.039
317. A. Hajdari, A. Giorgi, G. Beretta, F. Gelmini, S. Buratti et al., Phytochemical and sensorial characterization of *Hyssopus officinalis* subsp *aristatus* (godr.) Nyman (*Lamiaceae*) by GC-MS, HPLC-UV-DAD, spectrophotometric assays and e-nose with aid of chemometric techniques. Eur. Food Res. Technol. **244**(7), 1313–1327 (2018). https://doi.org/10.1007/s00217-018-3046-z
318. S. Xu, Z. Zhou, H. Lu, X. Luo, Y. Lan, Y. Zhang, Y. Li, Estimation of the age and amount of brown rice plant hoppers based on bionic electronic nose use. Sensors **14**(10), 18114–81130 (2014). https://doi.org/10.3390/s141018114

319. Q. Chen, J. Song, J. Bi, X. Meng, X. Wu, Characterization of volatile profile from ten different varieties of Chinese jujubes by HS-SPME/GC-MS coupled with E-nose. Food Res. Int. **105**, 605–615 (2018). https://doi.org/10.1016/j.foodres.2017.11.054
320. S. Mildner-Szkudlarz, H.H. Jeleń, The potential of different techniques for volatile compounds analysis coupled with PCA for the detection of the adulteration of olive oil with hazelnut oil. Food Chem. **110**(3), 751–761 (2008). https://doi.org/10.1016/j.foodchem.2008.02.053
321. S. Cui, J. Wu, J. Wang, X. Wang, Discrimination of American ginseng and Asian ginseng using electronic nose and gas chromatography-mass spectrometry coupled with chemometrics. J. Ginseng Res. **41**(1), 85–95 (2017). https://doi.org/10.1016/j.jgr.2016.01.002
322. C.Q. Wei, W.Y. Liu, W.P. Xi, D. Cao, H.J. Zhang et al., Comparison of volatile compounds of hot-pressed, cold-pressed and solvent-extracted flaxseed oils analyzed by SPME-GC/MS combined with electronic nose: major volatiles can be used as markers to distinguish differently processed oils. Eur. J. Lipid Sci. Technol. **117**(3), 320–330 (2015). https://doi.org/10.1002/ejlt.201400244
323. Y. Xiong, X. Xiao, X. Yang, D. Yan, C. Zhang et al., Quality control of *Lonicera japonica* stored for different months by electronic nose. J. Pharm. Biomed. Anal. **91**, 68–72 (2014). https://doi.org/10.1016/j.jpba.2013.12.016
324. T. Liu, W. Zhu, J. Huang, H. Chen, R. Nie, C.-M. Li, Comparison of the nutritional as well as the volatile composition of in-season and off-season Hezuo 903 tomato at red stage. Eur. Food Res. Technol. **243**(2), 203–214 (2016). https://doi.org/10.1007/s00217-016-2736-7
325. H. Liu, F.K. Zeng, Q.H. Wang, H.S. Wu, L.H. Tan, Studies on the chemical and flavor qualities of white pepper (Piper nigrum L.) derived from five new genotypes. Eur. Food Res. Technol. **237**(2), 245–251 (2013). https://doi.org/10.1007/s00217-013-1986-x
326. M.S. Cosio, D. Ballabio, S. Benedetti, C. Gigliotti, Geographical origin and authentication of extra virgin olive oils by an electronic nose in combination with artificial neural networks. Anal. Chim. Acta **567**(2), 202–210 (2006). https://doi.org/10.1016/j.aca.2006.03.035
327. F. Autelitano, F. Giuliani, Analytical assessment of asphalt odor patterns in hot mix asphalt production. J. Clean. Prod. **172**, 1212–1223 (2018). https://doi.org/10.1016/j.jclepro.2017.10.248
328. J. Laothawornkitkul, J.P. Moore, J.E. Taylor, M. Possell, T.D. Gibson, C.N. Hewitt, N.D. Paul, Discrimination of plant volatile signatures by an electronic nose: a potential technology for plant pest and disease monitoring. Environ. Sci. Technol. **42**(22), 8433–8439 (2008). https://doi.org/10.1021/es801738s
329. L. Capelli, S. Sironi, IEEE, Monitoring odour emissions from an oil & gas plant: electronic nose performance testing in the field, in *2017 ISOCS/IEEE International Symposium on Olfaction and Electronic Nose (ISOEN)*. http://doi.org/10.1109/ISOEN.2017.7968862